(2)

Defense Nuclear Agency
Alexandria, VA 22310-3398

Burnout Thresholds and Cross Section of Power MOS Transistors with Heavy Ions

A. E. Waskiewicz
J. W. Groninger
Rockwell International Corporation
P.O. Box 3105
Anaheim, CA 92803-3105

February 1990

Technical Report

CONTRACT No. DNA-MIPR-88-507

Approved for public release;
distribution is unlimited.

DISTRIBUTION LIST UPDATE

This mailer is provided to enable DNA to maintain current distribution lists for reports. We would appreciate your providing the requested information.

☐ Add the individual listed to your distribution list.

☐ Delete the cited organization/individual.

☐ Change of address.

NAME: ______________________________

ORGANIZATION: ______________________________

OLD ADDRESS	**CURRENT ADDRESS**
______________	______________
______________	______________
______________	______________

TELEPHONE NUMBER: (   ) ______________________________

SUBJECT AREA(s) OF INTEREST:

______________ ______________

______________ ______________

______________ ______________

DNA OR OTHER GOVERNMENT CONTRACT NUMBER: ______________

CERTIFICATION OF NEED TO KNOW BY GOVERNMENT SPONSOR (if other than DNA).

SPONSORING ORGANIZATION: ______________________________

CONTRACTING OFFICER OR REPRESENTATIVE: ______________________________

SIGNATURE: ______________________________

CUT HERE AND RETURN

Direc
Defense Nuc ... y
ATTN: TITL
Washington, DC 20305-1000

Director
Defense Nuclear Agency
ATTN: TITL
Washington, DC 20305-1000

UNCLASSIFIED
SECURITY CLASSIFICATION OF THIS PAGE

REPORT DOCUMENTATION PAGE

1a REPORT SECURITY CLASSIFICATION UNCLASSIFIED	1b RESTRICTIVE MARKINGS
2a. SECURITY CLASSIFICATION AUTHORITY N/A since Unclassified	3 DISTRIBUTION/AVAILABILITY OF REPORT Approved for public release; distribution is unlimited.
2b. DECLASSIFICATION/DOWNGRADING SCHEDULE N/A since Unclassified	
4. PERFORMING ORGANIZATION REPORT NUMBER(S)	5 MONITORING ORGANIZATION REPORT NUMBER(S) Unnumbered
6a. NAME OF PERFORMING ORGANIZATION Rockwell International Corporation 6b OFFICE SYMBOL (If applicable)	7a NAME OF MONITORING ORGANIZATION Defense Nuclear Agency
6c. ADDRESS (City, State, and ZIP Code) P.O. Box 3105 Anaheim, CA 92803-3105	7b ADDRESS (City, State, and ZIP Code) 6801 Telegraph Road Alexandria, VA 22310-3398
8a. NAME OF FUNDING/SPONSORING ORGANIZATION 8b OFFICE SYMBOL (If applicable) RAEE/Cohn	9 PROCUREMENT INSTRUMENT IDENTIFICATION NUMBER DNA MIPR-88-507
8c. ADDRESS (City, State, and ZIP Code)	10 SOURCE OF FUNDING NUMBERS PROGRAM ELEMENT NO / PROJECT NO / TASK NO / WORK UNIT ACCESSION NO

11 TITLE (Include Security Classification)

Burnout Thresholds and Cross Sections of Power MOS Transistors with Heavy Ions.

12 PERSONAL AUTHOR(S)

Waskiewicz, A. E. and Groninger, J. W.

13a. TYPE OF REPORT	13b TIME COVERED	14. DATE OF REPORT (Year, Month, Day)	15 PAGE COUNT
Technical	FROM 860501 TO 880430	900201	106

16. SUPPLEMENTARY NOTATION

17. COSATI CODES			18 SUBJECT TERMS (Continue on reverse if necessary and identify by block number)
FIELD	GROUP	SUB-GROUP	
9	1		Power MOSFET; Heavy Ion Burnout Characterization; SEU; Power MOSFET Test Results
13	12		MOSFET; SEU Test Results

19 ABSTRACT (Continue on reverse if necessary and identify by block number)

Power MOSFET heavy ion-induced Single Event Burnout tests were performed jointly by representatives of the Aerospace Corporation, NASA Goddard, NWSC Crane and Rockwell International. For the most part, presented are the results of the burnout threshold and cross section characterizations performed on n-channel power MOSFETs, however a small amount of p-channel data is also included. In addition, data on the effect of temperature, gate bias, total dose and inductive loading on MOSFET Single Event Burnout sensitivity is proferred. At the time of the test effort, radiation hardened devices were being developed by International Rectifier and RCA/GE. The heavy-ion-induced burnout test results on available samples of these devices are also incorporated for comparison to the commercial and JEDEC versions tested. (AU)

20 DISTRIBUTION/AVAILABILITY OF ABSTRACT ☐ UNCLASSIFIED/UNLIMITED ☒ SAME AS RPT ☐ DTIC USERS	21 ABSTRACT SECURITY CLASSIFICATION UNCLASSIFIED
22a NAME OF RESPONSIBLE INDIVIDUAL Bennie F. Maddox	22b TELEPHONE (Include Area Code) (703) 325-7042 / 22c OFFICE SYMBOL

DD Form 1473, JUN 86 Previous editions are obsolete SECURITY CLASSIFICATION OF THIS PAGE

UNCLASSIFIED

CONVERSION TABLE

Conversion factors for U.S. Customary to metric (SI) units of measurement.

MULTIPLY ——————→ BY ——————→ TO GET
TO GET ←—————— BY ←—————— DIVIDE

angstrom	1.000 000 X E -10	meters (m)
atmosphere (normal)	1.013 25 X E +2	kilo pascal (kPa)
bar	1.000 000 X E +2	kilo pascal (kPa)
barn	1.000 000 X E -28	meter^2 (m^2)
British thermal unit (thermochemical)	1.054 350 X E +3	joule (J)
calorie (thermochemical)	4.184 000	joule (J)
cal (thermochemical)/cm^2	4.184 000 X E -2	mega joule/m^2 (MJ/m^2)
curie	3.700 000 X E +1	giga becquerel (GBq)*
degree (angle)	1.745 329 X E -2	radian (rad)
degree Fahrenheit	$t_K = (t°f + 459.67)/1.8$	degree kelvin (K)
electron volt	1.602 19 X E -19	joule (J)
erg	1.000 000 X E -7	joule (J)
erg/second	1.000 000 X E -7	watt (W)
foot	3.048 000 X E -1	meter (m)
foot-pound-force	1.355 818	joule (J)
gallon (U.S. liquid)	3.785 412 X E -3	meter^3 (m^3)
inch	2.540 000 X E -2	meter (m)
jerk	1.000 000 X E +9	joule (J)
joule/kilogram (J/kg) (radiation dose absorbed)	1.000 000	Gray (Gy)**
kilotons	4.183	terajoules
kip (1000 lbf)	4.448 222 X E +3	newton (N)
kip/inch^2 (ksi)	6.894 757 X E +3	kilo pascal (kPa)
ktap	1.000 000 X E +2	newton-second/m^2 ($N\text{-}s/m^2$)
micron	1.000 000 X E -6	meter (m)
mil	2.540 000 X E -5	meter (m)
mile (international)	1.609 344 X E +3	meter (m)
ounce	2.834 952 X E -2	kilogram (kg)
pound-force (lbf avoirdupois)	4.448 222	newton (N)
pound-force inch	1.129 848 X E -1	newton-meter (N·m)
pound-force/inch	1.751 268 X E +2	newton/meter (N/m)
pound-force/foot^2	4.788 026 X E -2	kilo pascal (kPa)
pound-force/inch^2 (psi)	6.894 757	kilo pascal (kPa)
pound-mass (lbm avoirdupois)	4.535 924 X E -1	kilogram (kg)
pound-mass-foot^2 (moment of inertia)	4.214 011 X E -2	kilogram-meter^2 ($kg \cdot m^2$)
pound-mass/foot^3	1.601 846 X E +1	kilogram/meter^3 (kg/m^3)
rad (radiation dose absorbed)	1.000 000 X E -2	Gray (Gy)**
roentgen	2.579 760 X E -4	coulomb/kilogram (C/kg)
shake	1.000 000 X E -8	second (s)
slug	1.459 390 X E +1	kilogram (kg)
torr (mm Hg, 0°C)	1.333 22 X E -1	kilo pascal (kPa)

* The becquerel (Bq) is the SI unit of radioactivity; 1 Bq = 1 event/s.
**The Gray (Gy) is the SI unit of absorbed radiation.

TABLE OF CONTENTS

LIST OF ILLUSTRATIONS

LIST OF ILLUSTRATIONS

LIST OF ILLUSTRATIONS (Continued)

LIST OF TABLES

SECTION 1

INTRODUCTION

Power MOS devices have demonstrated lower on-resistance per unit area for a given breakdown voltage, high input impedances, and high operating frequency capability. These attributes have made power MOSFETs attractive in the design of satellite and missile power conditioning circuits. Commercially available power MOSFETs had indicated a susceptibility to large threshold shifts with total-ionizing dose and burnout in high dose rate ionization environments. However, it was not anticipated that incident heavy ions representative of cosmic rays of interest in space could cause the catastrophic failure of the device -- regardless of manufacturer and device type. Tests performed with fission particles of Californium-252 indicated this to be indeed a possibility[1].

A modest effort principally supported by NASA/Goddard, The Aerospace Corporation, Naval Weapons Support Center/Crane, and Rockwell/Autonetics ICBM Systems Division was initiated to characterize available MOSFETs for susceptibility to heavy-ion-induced burnout. "Available" MOSFETs ranged initially from commercially available devices contributed by manufacturers on a quid pro quo (share the test results) basis, to devices aerospace system designers had an interest in evaluating, and finally, to developmental radiation-hardened devices. The test effort primarily included Berkeley Cyclotron heavy ion destructive Single

Event Burnout (SEB) verification and nondestructive SEB cross section characterization tests. To a lesser degree, the effect of temperature, gate bias, total dose, and inductive loading on SEB sensitivity was also examined. In addition, some testing with protons was performed. It is the intent of this report to document the results of the above test effort.

SECTION 2

HEAVY ION DESTRUCTIVE SINGLE EVENT BURNOUT VERIFICATION

Initial testing was performed to assess the degree to which power MOSFETs were vulnerable to heavy-ion-induced burnout. Several device types were tested, including n-channel and p-channel devices with various package date codes (PDC) from four manufacturers. The tests were performed destructively with no current limiting to avert device failure (see Figure 1). A drain-source voltage was applied to an off device -- V_{GS} a negative quantity for an n-channel device -- and the device exposed to a measured fluence of heavy ions. The drain-source voltage was increased in discrete steps and exposures repeated until failure was observed or an increase in the drain-source voltage was precluded by the rated breakdown voltage BV_{DSS}. Without current limiting, each data point represented the catastrophic failure of a MOSFET.

The devices were tested with monoenergetic ions of copper, argon, neon, and nitrogen from the Lawrence Berkeley 88-inch Cyclotron (see Table 1). The heavy ions ranged in energy between 3 and 4.5 MeV per nucleon with LET values between 3 and 30 MeV/mg/cm^2. The results of the destructive tests are indicated in Tables 2 and 3. During a test sequence, the increment of drain-source bias for the 100-volt devices was no greater than 10 volts and was 5 volts in 50% of the measurements. The V_{DSTH} bias resoluti[illegible]r the 200-volt devices was 10 volts in 85% of the meas[illegible]s performed.

Results, as listed in the tables, included:

1) Heavy ions simulating cosmic rays of interest in space can cause the catastrophic failure of a power MOSFET -- confirming Cf-252 test observations and indicating the Cf-252 test results to be conservative estimates of the SEB susceptibility of the devices.

2) The minimum drain-source bias for burnout (V_{DSTH}) is inversely related to the LET of the incident ion, as illustrated in Figure 2.

3) N-channel devices, when exposed to ions with an LET of 30 MeV/mg/cm^2, can fail with applied drain-source biases less than 50% of BV_{DSS} -- the average percent of BV_{DSS} applied at burnout was 59%, 72%, and 49%, respectively, for the IRF 150, IRF 130, and IRF 250 types of devices tested.

4) With no current limiting, the resultant failures were catastrophic -- manifested by drain-source and source-gate low-impedance current paths.

5) P-channel devices appeared to be relatively insensitive to heavy-ion-induced burnout -- no failures were observed for the 14 devices exposed to copper ions with a bias of BV_{DSS} (see Table 3).

6) V_{DSTH} varied with manufacturers of the same device type and varied within a device type by the same manufacturer.

7) Burnout susceptibility varied over the product line of a manufacturer, and there appeared to be no significant difference in burnout threshold with package date code (PDC). For some device types, PDCs ranged from 1981 to 1986 with no change in V_{DSTH}.

Table 1. Selected LBL 88" cyclotron heavy ions.

ION	ENERGY (MeV)	LET (MeV/mg/cm2)	APPROXIMATE RANGE (um)	FACILITY
KRYPTON	350	38	50	BERKELEY CYCLOTRON
KRYPTON	306	38	45	
COPPER	247	30	40	
ARGON	175	15	40	
NEON	89	6	45	
NITROGEN	67	3	70	

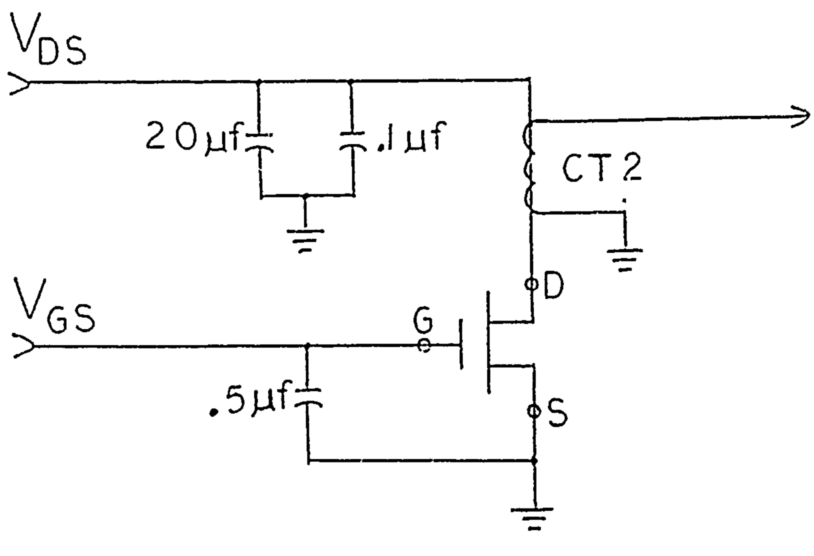

Figure 1. Destructive power MOSFET SEB test circuit.

Table 2. N-channel destructive test results.

PART TYPE	NON-JEDEC P/N	BVdss (Volts)	MFR	PDC	COPPER Vds FAILmin (Volts)	COPPER Vds FAILmax (Volts)	COPPER NO. OF DEV.	ARGON Vds FAILmin (Volts)	ARGON Vds FAILmax (Volts)	ARGON NO. OF DEV.
2N6764	IRF150	100	IR	8315	60	75	3	---	---	-
				8325	60	--	1	---	---	-
				8606	65	70	4	80	100	2
2N6764	IRF150	100	Si	8612	50	75	2	<75	---	1
2N6764	IRF150	100	RCA	8526	65	---	1	---	---	-
				8620	<50	60	2	60	90	2
2N6764	IRF150	100	GE	8612	70	80	3	70	95	2
IRF150	-----	100	GE	8509	---	---	-	70	80	2
2N6782	IRFF110	100	IR	8521	85	---	1	100	---	1
2N6756	IRF130	100	IR	8126	70	---	1	---	---	-
				8214	80	80	2	100	>100	2
				8320	80	---	1	>100	---	2
2N6796	IRFF130	100	IR	8502	75	---	1	---	---	-
				8523	70	---	1	---	---	-
				8547	70	---	1	---	---	-
				8529	70	85	2	100	---	1
				8550	80	---	1	100	>100	2
2N6796	IRFF130	100	Si	8518	60	60	2	80	100	2
				8550	---	---	-	90	>100	2

Table 2. N-channel destructive test results (continued).

PART TYPE	NON-JEDEC P/N	BVdss (Volts)	MFR	PDC	NEON Vds FAILmin (Volts)	NEON Vds FAILmax (Volts)	NEON NO. OF DEV.	NITROGEN Vds FAILmin (Volts)	NITROGEN Vds FAILmax (Volts)	NITROGEN NO. OF DEV.
2N6764	IRF150	100	IR	8315	---	---	-	---	---	-
				8325	---	---		---	---	-
				8606	>100	---	1	---	---	-
2N6764	IRF150	100	Si	8612	90	100	2	---	---	-
2N6764	IRF150	100	RCA	8526	---	---		---	---	-
				8620	>100	---	2	>100	---	1
2N6764	IRF150	100	GE	8612	>95	---	2	---	---	-
IRF150	-----	100	GE	8509	>100	---	2	---	---	-
2N6782	IRFF110	100	IR	8521	---	---	-	---	---	-
2N6756	IRF130	100	IR	8126	---	---	-	---	---	-
				8214	---	---	-	---	---	-
				8320	>100	---	2	>100	---	2
2N6796	IRFF130	100	IR	8502	---	---	-	---	---	-
				8523	---	---	-	---	---	-
				8547	---	---	-	---	---	-
2N6796	IRFF130	100	Si	8529	---	---	-	---	---	-
				8550	>100	---	2	>100	---	2

Table 2. N-channel destructive test results (continued).

PART TYPE	NON-JEDEC P/N	BVdss (Volts)	MFR	PDC	COPPER Vds FAILmin (Volts)	COPPER Vds FAILmax (Volts)	COPPER NO. OF DEV.	ARGON Vds FAILmin (Volts)	ARGON Vds FAILmax (Volts)	ARGON NO. OF DEV.
2N6660	-----	60	Si	8307	35	35	3	45	---	1
2N6766	IRF250	200	IR	8308 8614	120 110	--- 120	2 2	150 130	--- <160	1 2
2N6766	IRF250	200	Si	8548 8606	70 70	<75 75	2 2	60 ---	100 ---	2 -
2N6766	IRF250	200	RCA	8620	90	110		130	---	2
2N6766	IRF250	200	GE	8608	---	---	-	80	90	1
25N20	-----	200	RCA	8410	130	---	1	200	---	1

PART TYPE	NON-JEDEC P/N	BVdss (Volts)	MFR	PDC	NEON Vds FAILmin (Volts)	NEON Vds FAILmax (Volts)	NEON NO. OF DEV.	NITROGEN Vds FAILmin (Volts)	NITROGEN Vds FAILmax (Volts)	NITROGEN NO. OF DEV.
2N6660	-----	60	Si	8307	55	55	2	60	>60 (4)	5
2N6766	IRF250	200	IR	8308 8614	--- >200	--- ---	- 1	200 >200	>210 ---	2 2
2N6766	IRF250	200	Si	8548 8606	--- ---	--- ---	- -	--- 180	--- ---	- 2
2N6766	IRF250	200	RCA	8620	---	---	-	190	200	2
2N6766	IRF250	200	GE	8608	180	---	1	190	>200	2
25N20	-----	200	RCA	8410	>200	---	1	>200	---	2

Table 3. P-channel destructive test results.

PART TYPE	NON-JEDEC P/N	MFR	BVdss (Volts)	PDC	COPPER Vds PASSmax	NO. OF DEV.
IRFF9122	---	IR	100	8511	>100	1
2N6849	IRFF9130	IR	100	8533	>100	1
				8547	>100	1
IRF9130	---	IR	100	8406	>100	2
				8545	>100	2
2N6798	IRF9130	RCA	100	8620	>100	2
12P10	---	RCA	100	8445	>100	2
IRFF9230	---	IR	200	8607	>200	3

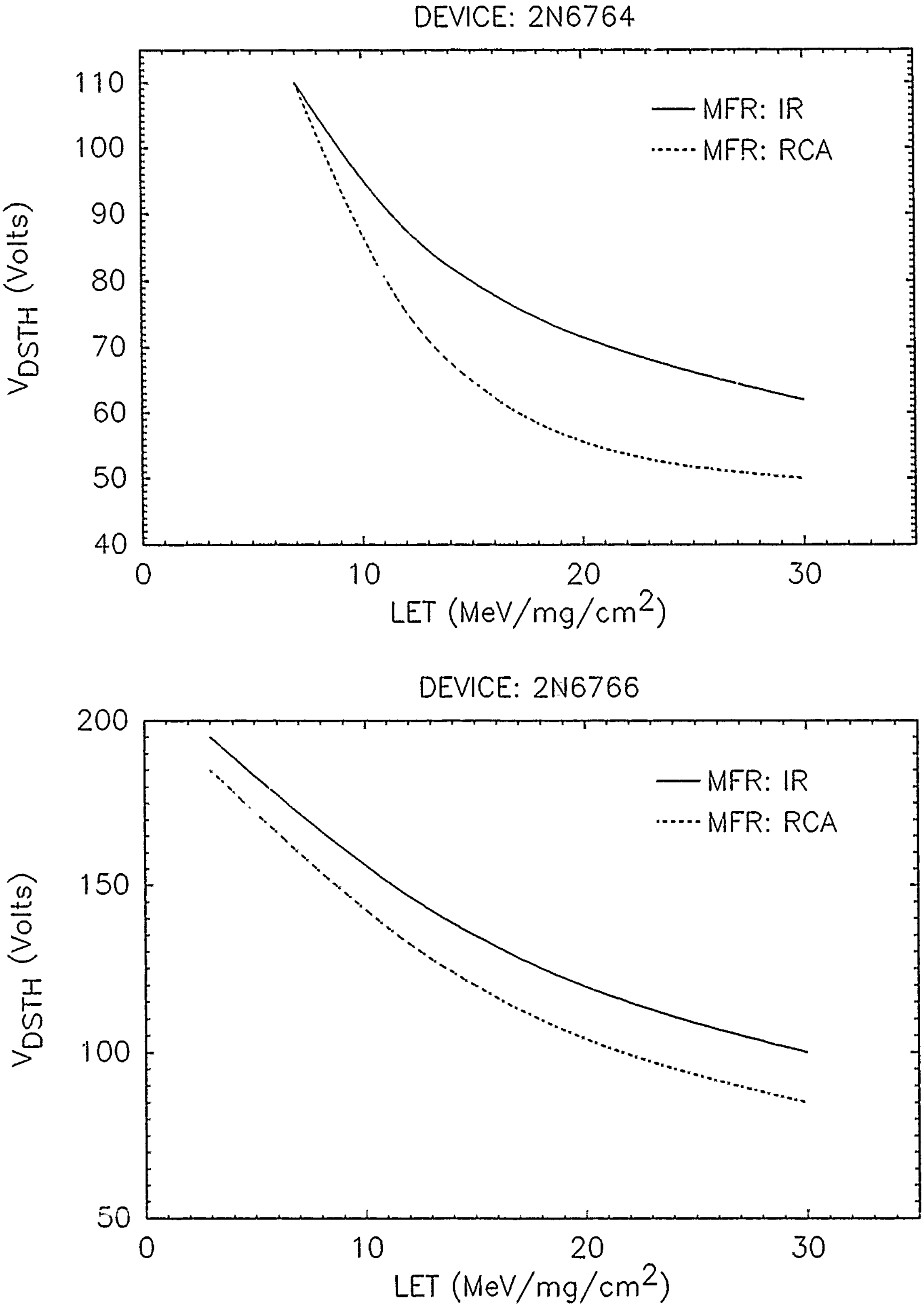

Figure 2. V_{DSTH} **as a function of LET.**

SECTION 3

SINGLE EVENT BURNOUT THRESHOLDS AND CROSS SECTIONS

3.1 BACKGROUND.

The following two sections document the results of the nondestructive power MOSFET tests and present the major portion of the single event burnout characterization effort. Previous testing without current limiting, as reported in Section 2, resulted in each data point representing the catastrophic failure of a device. The number of devices necessary to obtain statistically meaningful data on the ion fluence required for burnout, as a function of applied drain-source bias and ion LET, would have made the effort economically impractical -- especially if the effort were to include several device types. Oberg and Wert developed a method which included counting resistively limited, ion-induced drain-current pulses as a function of ion fluence[2]. This technique was reported to allow the nondestructive measurement of power MOSFET cross sections.

Figure 3 is a typical cross section of a vertical, planar, four-layer, double-diffused MOS (DMOS) transistor and is representative of the technology with which most present-day power MOSFETs are constructed. A power MOSFET device is constructed with thousands of the vertical DMOS transistors effectively connected in parallel. Inherent in the structure is an npn

bipolar parasitic transistor formed by the source and body diffusions and the drain region of the device. It has been theorized that, in the presence of a sufficiently large electric field, ion-induced turn-on of the parasitic transistor with avalanche multiplication of the charge traversing the drain depletion region would result in a regeneratively increasing drain current leading to second breakdown and failure of the device[1,3]. Refer to Section 11 for a more detailed description of the power MOSFET structure and a discussion of possible failure mechanisms. The detection of a drain-source current pulse with amplitude greater than that associated with the photocurrent collected from the back-biased body-drain diode without transistor action would be a precursor of the avalanche condition leading to burnout. Determining the number of pulses as a function of bias and ion LET without degrading the device would allow statistically meaningful burnout characterization of the same device under various exposure conditions -- each data point often representing a large number of device "burnouts."

3.2 TEST METHOD.

The circuit of Figure 4 was implemented to perform the nondestructive power MOSFET SEB threshold and cross-section measurements. The circuit had the effect of limiting the amplitude of the heavy-ion-induced drain-source current pulse, decreasing the drain-source bias as a result of the induced voltage drop across the limiting resistor, and allowing the conditioned pulses to be counted at the end of 75 feet of coaxial cable. The discriminator threshold was set above the signal levels associated with the normal charge collection process of the reverse-biased body-drain junction, but well below the ion-induced pulse amplitude associated with avalanche of the parasitic transistor of the device. The current pulses were counted as a function of applied drain-source bias and the cross section calculated as the number of current pulses divided by the exposure fluence.

A wide range of device types were tested with monoenergetic ions of krypton, copper, argon, neon, and nitrogen from the Lawrence Berkeley 88-inch Cyclotron. The heavy ions ranged in energy between 3 and 4.5 MeV per nucleon with LET values between 3 and 40 MeV/mg/cm^2. Most of the tests were performed with 247-MeV copper ions (LET=30) which closely approximates the worst case particles of interest in space (iron group nucleuses). To a lesser degree, the effects of LET, angle of ion incidence, gate

bias, temperature, and inductive loading on power MOSFET burnout characteristics were investigated.

At the end of a series of nondestructive measurements, the correspondence between the drain-source voltage at the onset of current pulses and the voltage required for burnout was verified. Burnout verification was performed by removing the current limiting resistor and measuring the minimum drain-source bias to cause the device to burnout. The results of the nondestructive and destructive data correlation measurements and SEB cross section measurements are included in Sections 4.1 and 4.2, respectively.

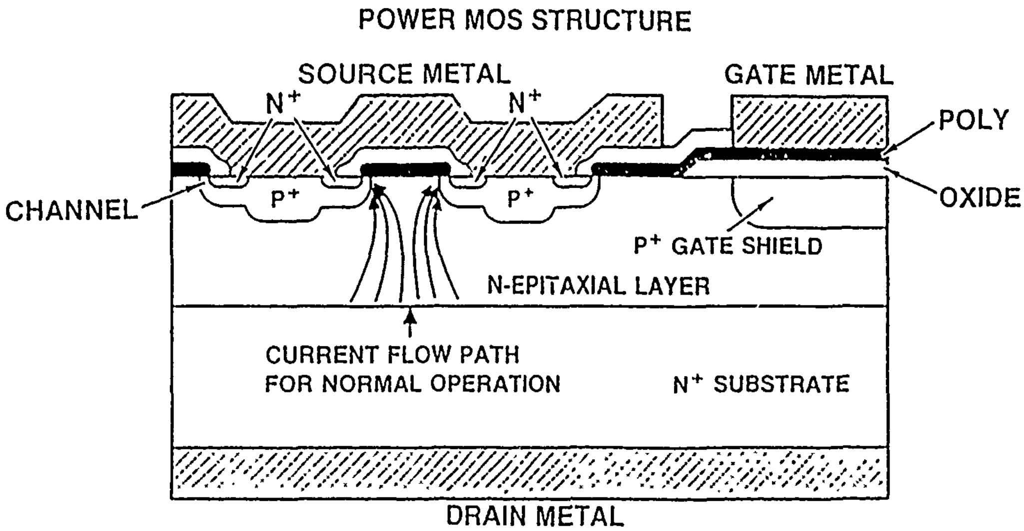

POWER MOSFET TOPOLOGY

SILOX	0.5 microns
SOURCE METAL	5.0 microns
OXIDE	0.8 microns
POLY	0.8 microns
P+ BODY	5.0 microns
N- DRAIN	5.0 - 35.0 microns (BV_{DSS} DEPENDENT)

Figure 3. Power MOSFET structure cross section.

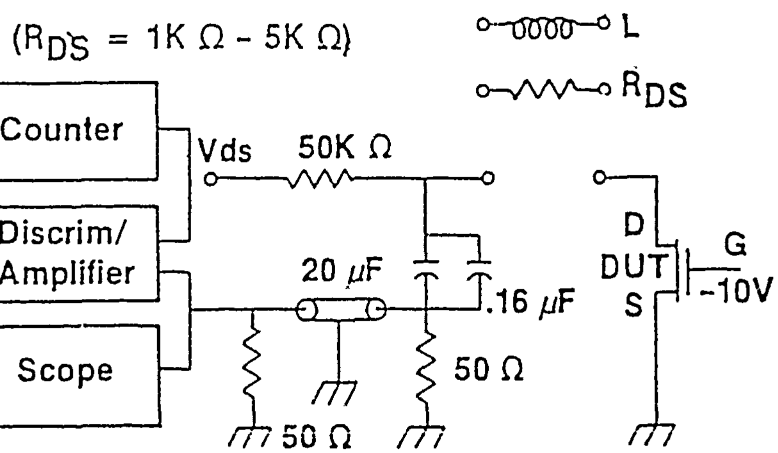

Figure 4. SEB nondestructive test circuit.

SECTION 4

SEE THRESHOLD AND CROSS SECTION TEST RESULTS

4.1 NONDESTRUCTIVE AND DESTRUCTIVE DATA CORRELATION.

Table 4 compares the measured voltage at the onset of drain-source current pulses with resistive current limiting and the failure voltage of the same device with the resistor removed. The table represents the tests of 13 device types with 37 package data codes (PDC). The table includes two questionable 2N6764 data points measured with copper ions incident at 60 degrees to the chip normal. The two devices were part of a four-device set, all of the same type on the same exposure board. The first two devices on the board were exposed with copper ions at zero degrees. The measured failure voltages correlated exactly with the nondestructive voltage measurements. The remaining devices, the two devices in question, were to be tested with 60-degree incident copper ions. The consecutively measured failure voltages appeared to resemble the 0-degree incident ion nondestructive data of these devices. Including the two points in question, 97 percent of the measured failure voltages were within 10 volts of the drain-source voltage at which resistively current-limited pulses were first detected -- in most cases, 10 volts was the incremental increase in the bias between sequential exposures. Excluding the two questionable data points, 100% of the failure voltages were within 10 volts of the nondestructive "burnout" voltage.

Table 4. Nondestructive Vds threshold correlation.

PART TYPE	NON-JEDEC P/N	MFR	PDC	W/ RES. LIMITING THRESHOLD Vds (Volts)	W/ RES. LIMITING THRESHOLD CR.SECT. (cm2)	NO LIMITING PASS Vds (Volts)	NO LIMITING FAIL Vds (Volts)	ION	ANGLE (deg.)	BVdss (Volts
2N6660	-----	Si	8133	39	2.2E-06	35	38	Ne	60	60
				22	3.3E-07	22	24	Cu	0	
				23	5.4E-05	23	25	Cu	0	
			8307	35	3.6E-06	30	40	Cu	45	
				60	1.1E-06	50	60	Ne	0	
2N6764	IRF150	IR	8606	100	PASSED	100	---	Ne	60	100
				85	1.7E-07	80	90	Cu	45	
			8317	60	1.1E-07	60	70	Cu	0	
				100	PASSED	100	---	Ne	0	
				90	3.8E-06	80	90	Cu	60	
			8226	90	1.7E-05	---	70	Cu	60	
			8315	70	5.0E-07	60	70	Cu	0	
				100	7.0E-05	---	90	Cu	60	
IRF150	-----	IR	8704	70	1.3E-06	70	75	Cu	0	100
				90	2.6E-04	80	90	Cu	0	
				100	PASSED	100	---	Cu	0	
IRF150	-----	Si	8644	50	1.7E-07	45	50	Cu	0	100
				45	1.7E-06	45	50	Cu	0	
2N6796	IRFF130	IR	8618	80	5.1E-03	70	80	Cu	0	100
2N6782	IRFF110	IR	8606	90	1.0E-03	80	90	Cu	0	100
				100	PASSED	100	---	Cu	0	
				100	PASSED	100	---	Cu	0	

Table 4. Nondestructive Vds threshold correlation (continued).

PART TYPE	NON-JEDEC P/N	MFR	PDC	W/ RES. LIMITING THRESHOLD Vds (Volts)	CR.SECT. (cm2)	NO LIMITING PASS Vds (Volts)	FAIL Vds (Volts)	ION	ANGLE (deg.)	BVdss (Volts
2N6766	IRF250	IR	8333	80	5.4E-03	70	80	Cu	60	100
		IR	8440	90	1.1E-03	80	90	Cu	0	
				90	7.7E-03	80	90	Cu	0	
2N6798	IRFF230	IR	8334	130	1.1E-06	125	130	Cu	0	200
		IR	8547	145	6.9E-06	145	148	Cu	30	
2N6784	IRFF210	IR	8415	135	9.4E-07	130	135	Cu	0	200
				175	8.2E-07	170	175	Cu	30	
2N6766	IRF250	IR	8617	190	7.9E-05	180	190	Cu	60	200
				140	9.1E-05	140	150	Cu	0	
		IR	8704	130	1.1E-06	125	---	Cu	0	
				135	1.4E-06	130	135	Cu	0	
25N20	-----	RCA	8648	160	1.8E-04	155	165	Cu	60	200
			8431	150	3.6E-04	---	160	Cu	60	
				80	4.9E-02	70	80	Cu	0	
IRH254	-----	IR	8704	200	PASSED	200	---	Cu	0	250
2N6792	IRFF320	IR	8626	210	PASSED	210	---	Cu	0	300
2N6792	IRFF320	Uni	8601	210	PASSED	210	---	Cu	0	300

4.2 SEB THRESHOLD VOLTAGES AND CROSS SECTIONS.

This section presents the data taken with Lawrence Berkeley Cyclotron 88, 247-MeV copper ions, incident at zero degrees to the chip normal, and represents a significant part of the test effort data. The graphs, Figures 5 through 32, are ordered by device voltage rating (BV_{DSS}) and are, for the most part, self-explanatory. Within each device type, the graphs list the manufacturer, the package date code (PDC), and the number of devices tested in parenthesis after the PDC.

Table 5 is an index to the graphs by part type and electrical characteristics. The table also offers a summary of the data, listing the minimum and maximum of the observed SEB threshold voltages and the average measured saturation cross section. The threshold voltage listed in the table was defined as the bias at which 10^5 particles/cm^2 would cause burnout -- a cross section of 10^{-5} cm^2.

Table 5. SEB cross section index.

PART TYPE	MFR	PDC	AVG. BVdssm (Volts)	Vds-th MIN (Volts)	Vds-th MAX (Volts)	AVG.SAT. CR.SECT. (cm2)	NO. OF DEV.	FIGURE
2N6660	Si	8133	69	22	23	9.0E-03	3	5 (a)
		8307	108	28	33	8.2E-03	2	5 (b)
		8624	65	53	60	2.2E-03	3	6
2N6782	IR	8606	116	86	>100	1.3E-02	3	7
2N6788	IR	8333	128	62	---	3.5E-03	1	8 (a)
		8440	130	81	85	2.1E-02	2	8 (b)
IRF120	IR	----	---	57	67	4.1E-02	2	9
2N6796	IR	8253	128	84	---	4.9E-02	1	10 (a)
		8334	114	73	79	6.1E-02	2	11 (a)
		8335	115	88	>110	5.4E-02	2	11 (b)
		8502	122	78	---	5.3E-02	1	10 (b)
		8549	125	77	78	6.5E-02	2	12 (a)
		8618	120	76	>100	5.2E-02	4	12 (b)
2N6796	Si	8518	116	57	61	6.6E-02	2	13
IRF150	IR	8317	131	64	67	1.3E-01	2	14 (a)
		8704	134	73	84	1.9E-01	2	14 (b)
2N6764	IR	8226	125	68	---	8.9E-02	1	15 (a)
		8315	126	72	73	1.6E-01	3	16 (a)
		8317	134	71	78	5.4E-02	2	16 (b)
		8422	121	72	83	1.8E-01	2	15 (b)
		8501	121	75	83	1.0E-01	2	18
		8606	128	69	77	1.3E-01	3	17 (a)
		8638	124	68	---	1.2E-01	1	17 (b)
IRF150	Si	8644	119	52	60	2.1E-01	4	19
IRK150	IR	8704	120	>100	---	-----	1	----
		8704-R	123	>100	---	-----	4	----

Table 5. SEB cross section index (continued).

PART TYPE	MFR	PDC	AVG. BVdssm (Volts)	Vds-th MIN (Volts)	Vds-th MAX (Volts)	AVG.SAT. CR.SECT. (cm2)	NO. OF DEV.	FIGURE
2N6784	IR	8415	232	137	162	1.3E-02	3	20
2N6758	RCA	8622	214	103	118	5.0E-02	2	21
2N6798	RCA	8619	210	92	108	3.6E-02	2	22
2N6798	IR	8334	219	127	153	3.8E-02	3	23 (a)
		8547	220	123	---	3.9E-02	1	23 (b)
2N6766	IR	8614	---	153	---	9.6E-02	1	24 (a)
		8617	217	115	144	1.6E-01	6	24 (b)
		8623	215	118	142	1.8E-01	2	25 (a)
		8704	240	131	148	2.2E-01	3	25 (b)
2N6766	RCA	8601	205	87	120	1.6E-01	4	26 (a)
		8648	205	98	143	1.8E-01	3	26 (b)
2N6766	Si	8548	223	69	72	2.0E-01	2	27 (a)
		8606	224	65	77	1.5E-01	5	27 (b)
25N20	RCA	8431	217	72	86	2.0E-01	2	28 (a)
		8648	211	102	112	1.7E-01	2	28 (b)
IRH254	IR	8704	307	>250	---	------	2	-----
		8729	295	>250	---	------	4	-----
2N6792	IR	8626	420	210	265	2.4E-02	2	29
2N6792	Uni	8601	442	266	274	2.4E-02	2	30
2N6768	Si	8612	458	130	236	1.4E-01	2	31
2N6762	IR	8715	523	316	---	4.0E-02	1	32

Table 6. N-channel devices electrical characteristics.

PART TYPE	NON-JEDEC P/N	BVdss (Volts)	Imax (A)	Rds-on (Ohms)	Pd (Watts)
2N6660	-----	60	1.1	3.0	6.25
2N6782	IRFF110	100	3.5	0.6	15
2N6788	IRFF120	100	6	0.3	20
IRF120	-----	100	9.2	0.3	60
2N6796	IRFF130	100	8	0.18	25
2N6764	IRF150	100	38	0.055	150
IRF150	-----	100	38	0.055	150
IRH150	-----	100	38	0.055	150
2N6784	IRFF210	200	2.25	1.5	15
2N6758	IRF230	200	9	0.4	75
2N6798	IRFF230	200	5.5	0.4	25
2N6766	IRF250	200	30	0.085	150
25N20	-----	200	25	0.15	150
IRH254	-----	250	19	0.19	150
2N6792	IRFF320	400	2.5	1.8	20
2N6768	IRF350	400	14	0.3	150
2N6762	IRF430	500	4.5	1.5	75

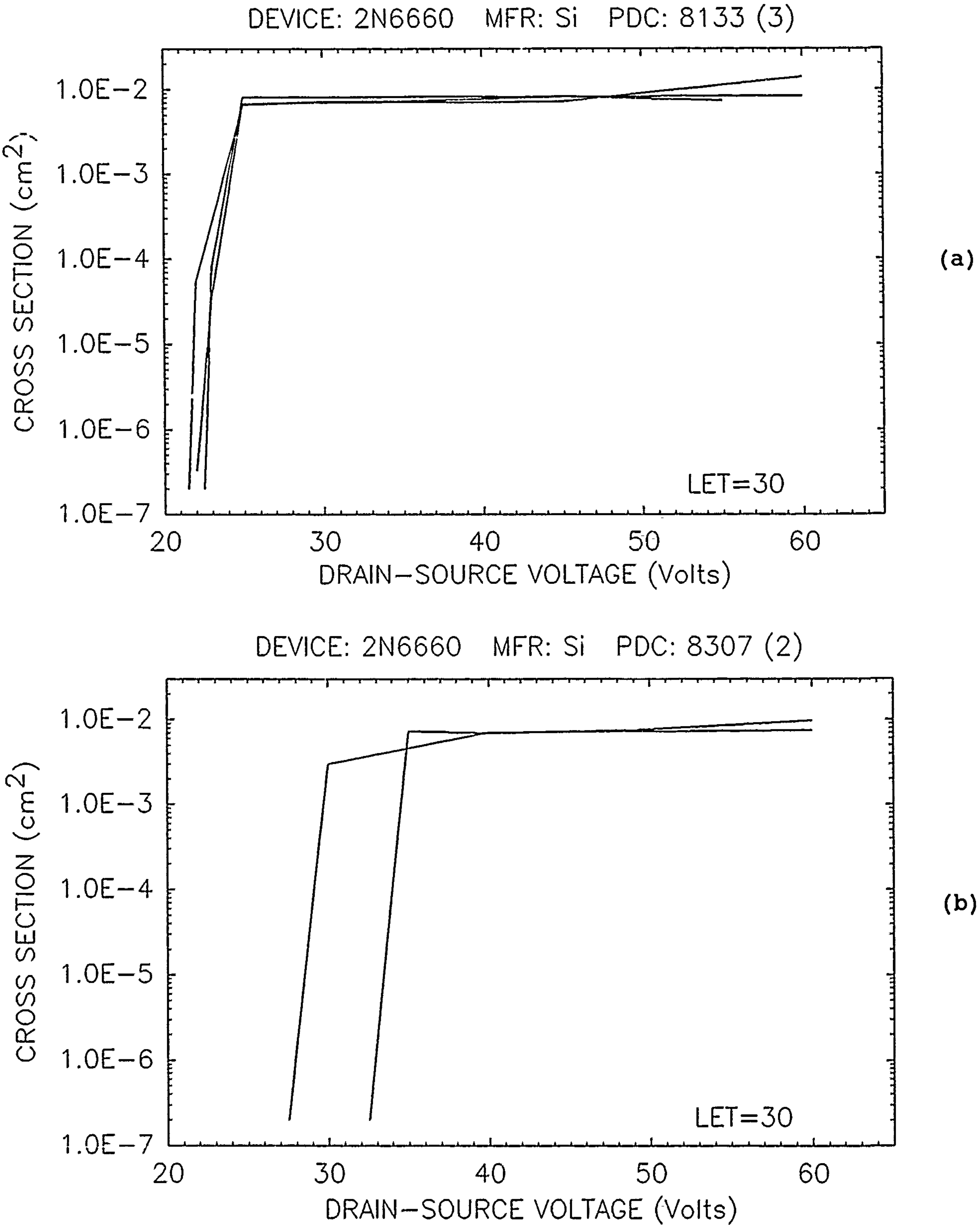

Figure 5. 2N6660 SEB cross section versus V_{DS}.

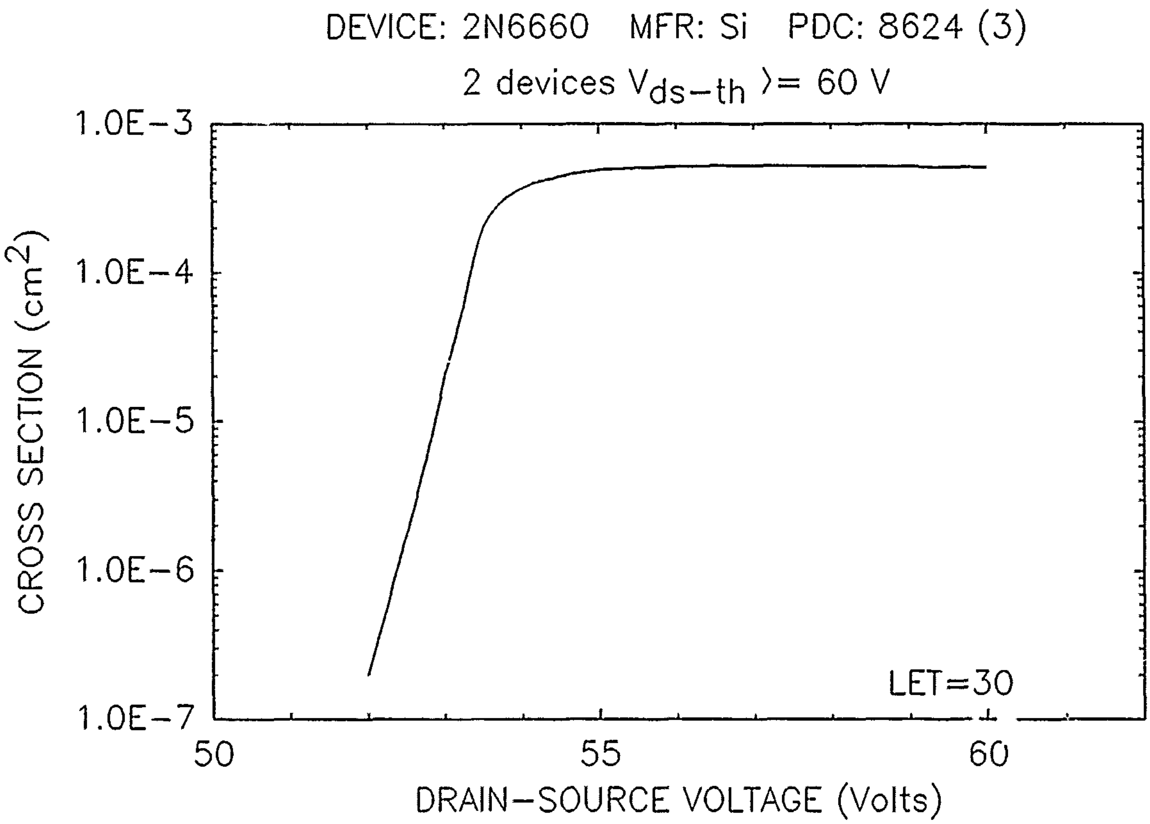

Figure 6. 2N6660 SEB cross section versus V_{DS}.

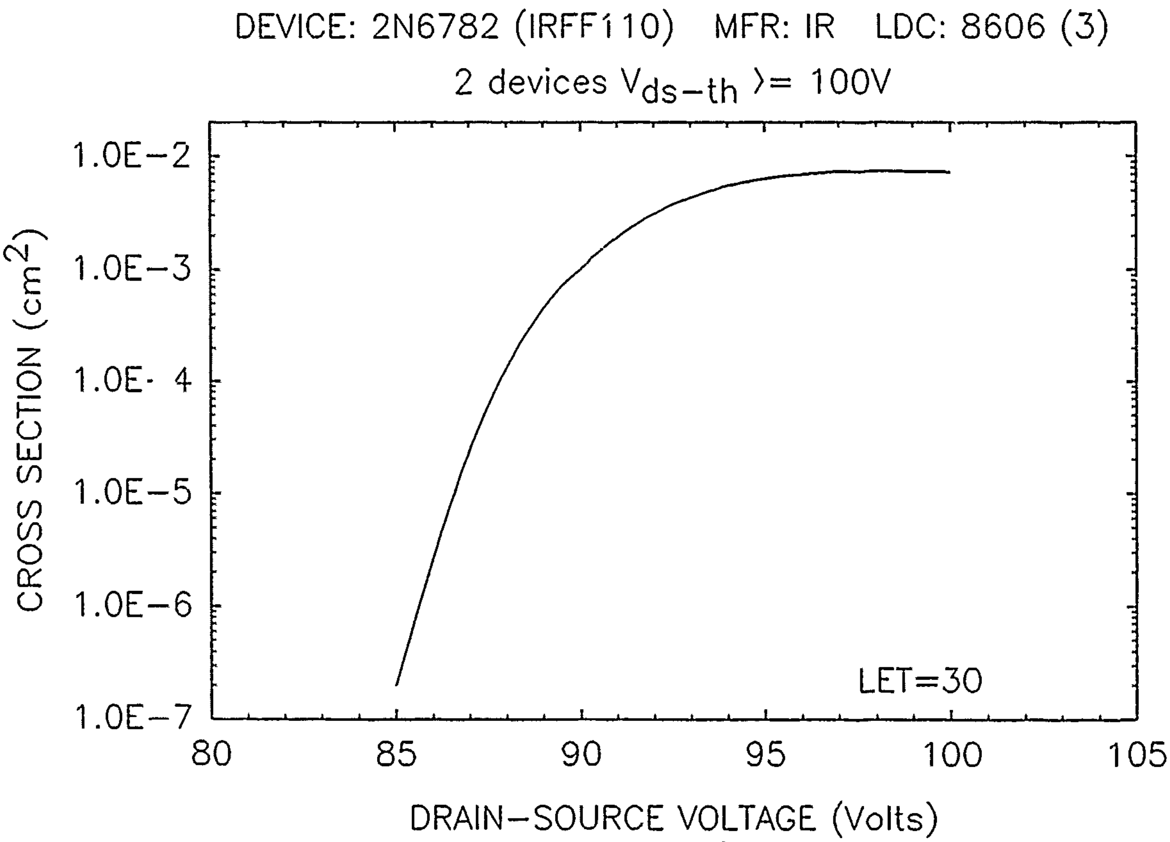

Figure 7. 2N6782 SEB cross section versus V_{DS}.

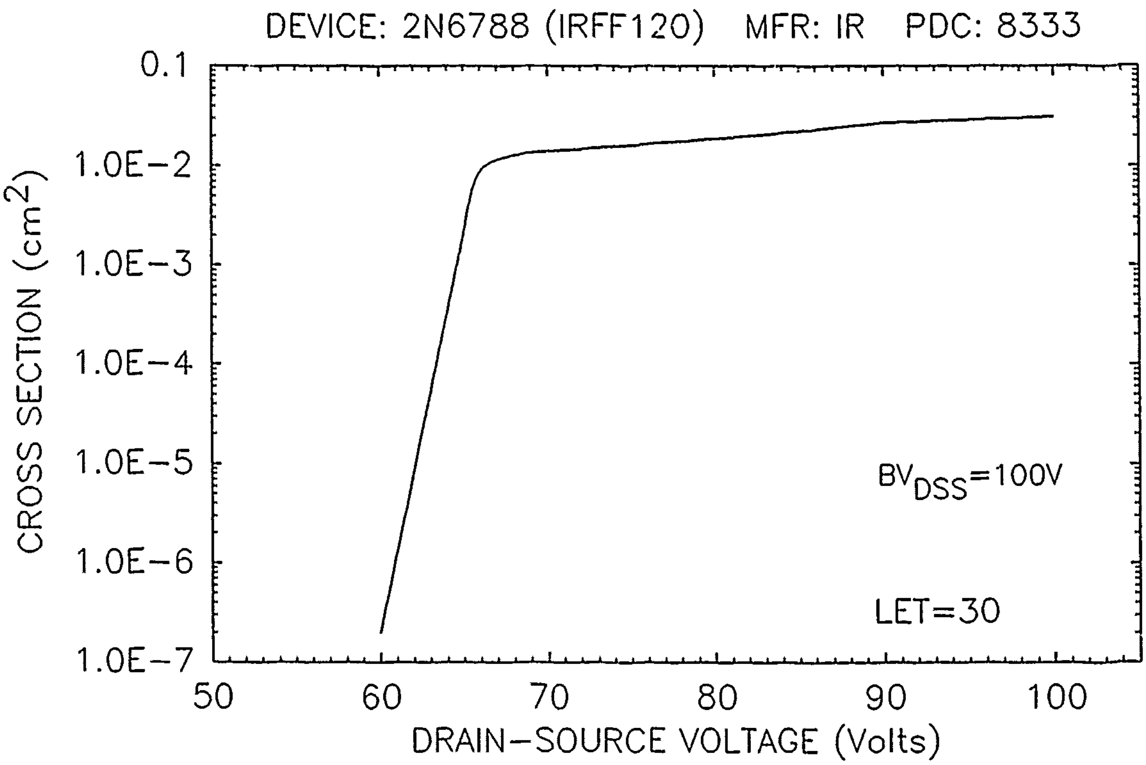

(a)

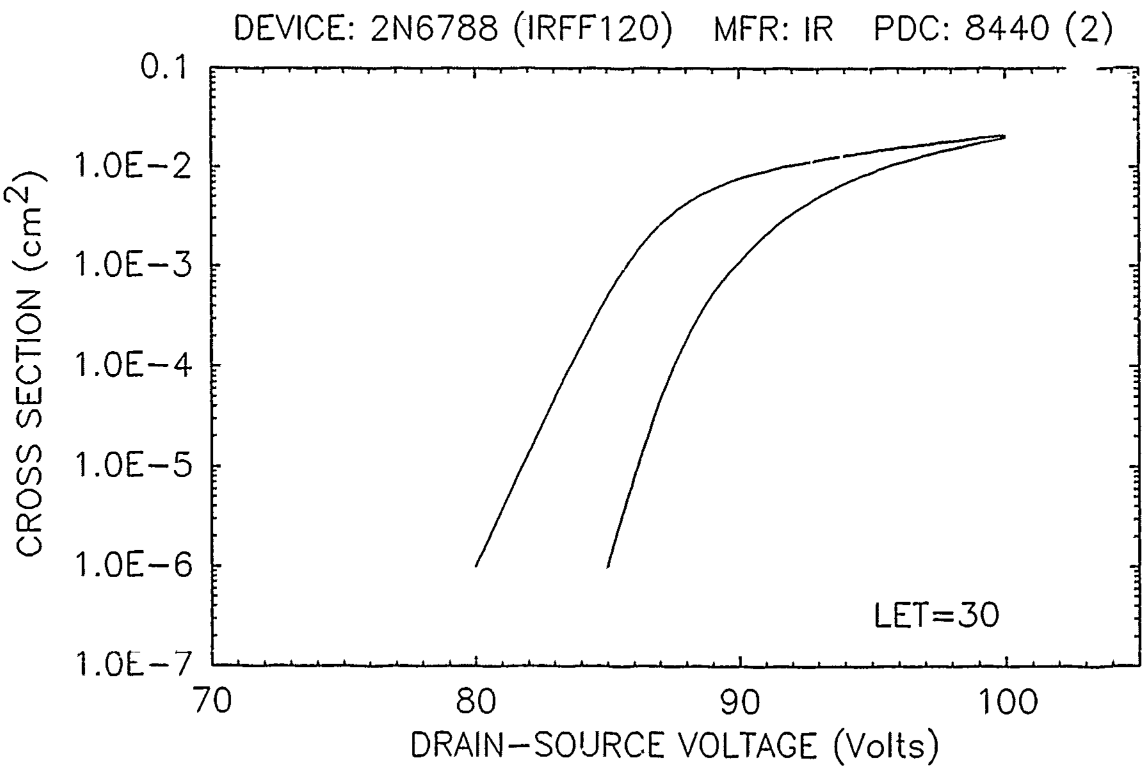

(b)

Figure 8. 2N6788 SEB cross section versus V_{DS}.

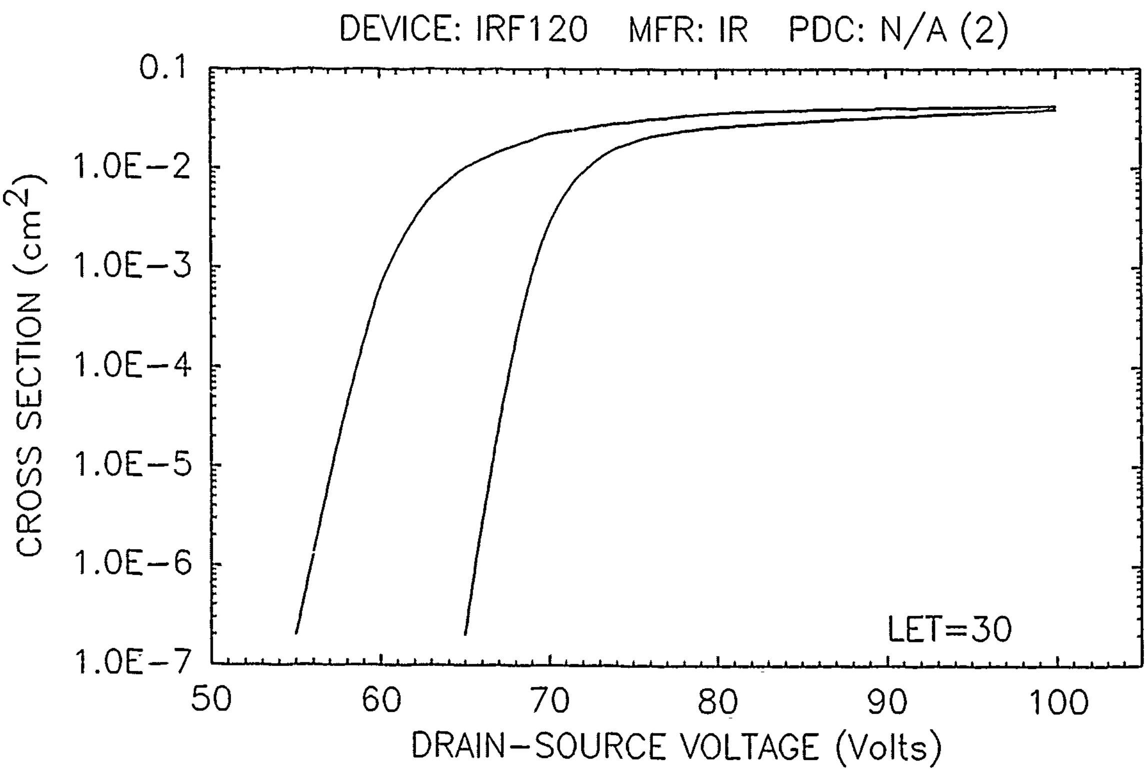

Figure 9. IRF120 SEB cross section versus V_{DS}.

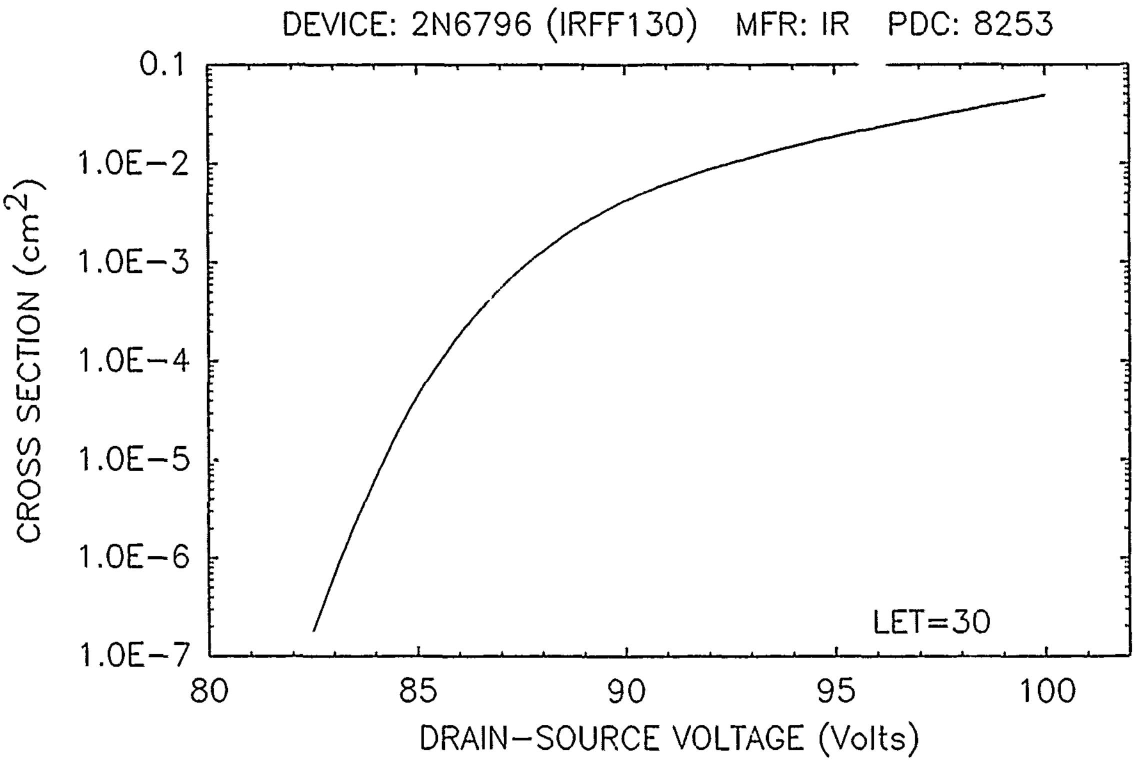

(a)

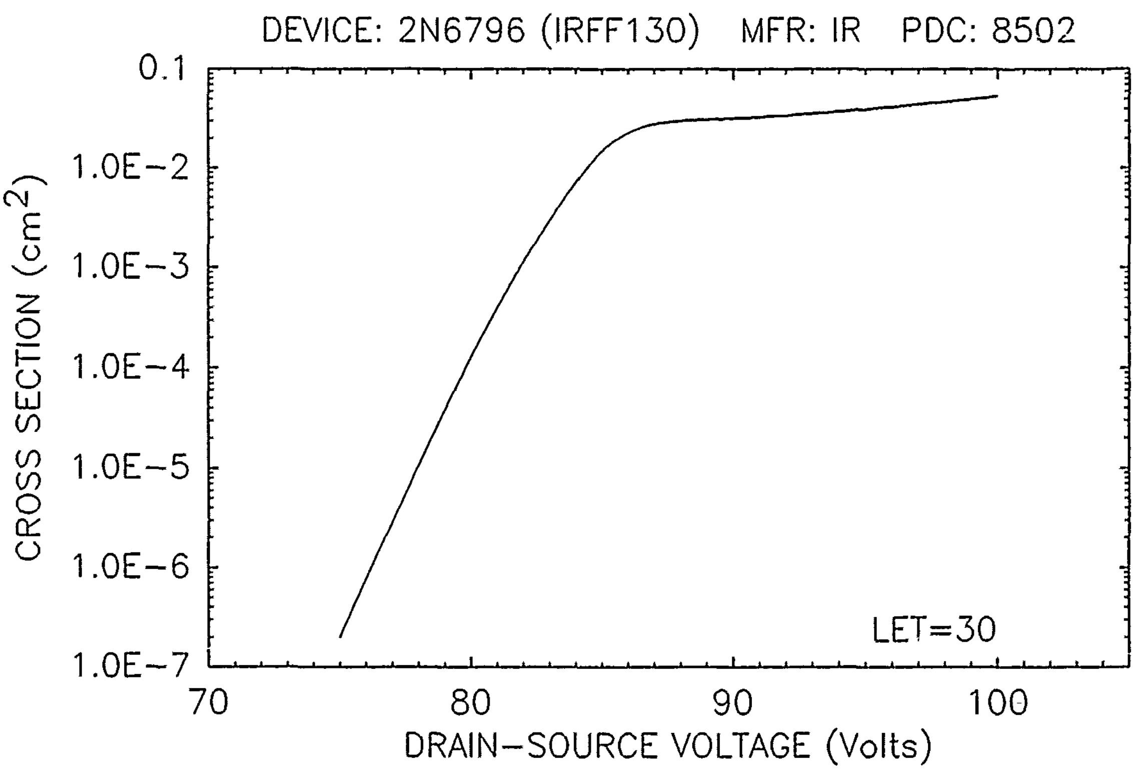

(b)

Figure 10. 2N6796 SEB cross section versus V_{DS}.

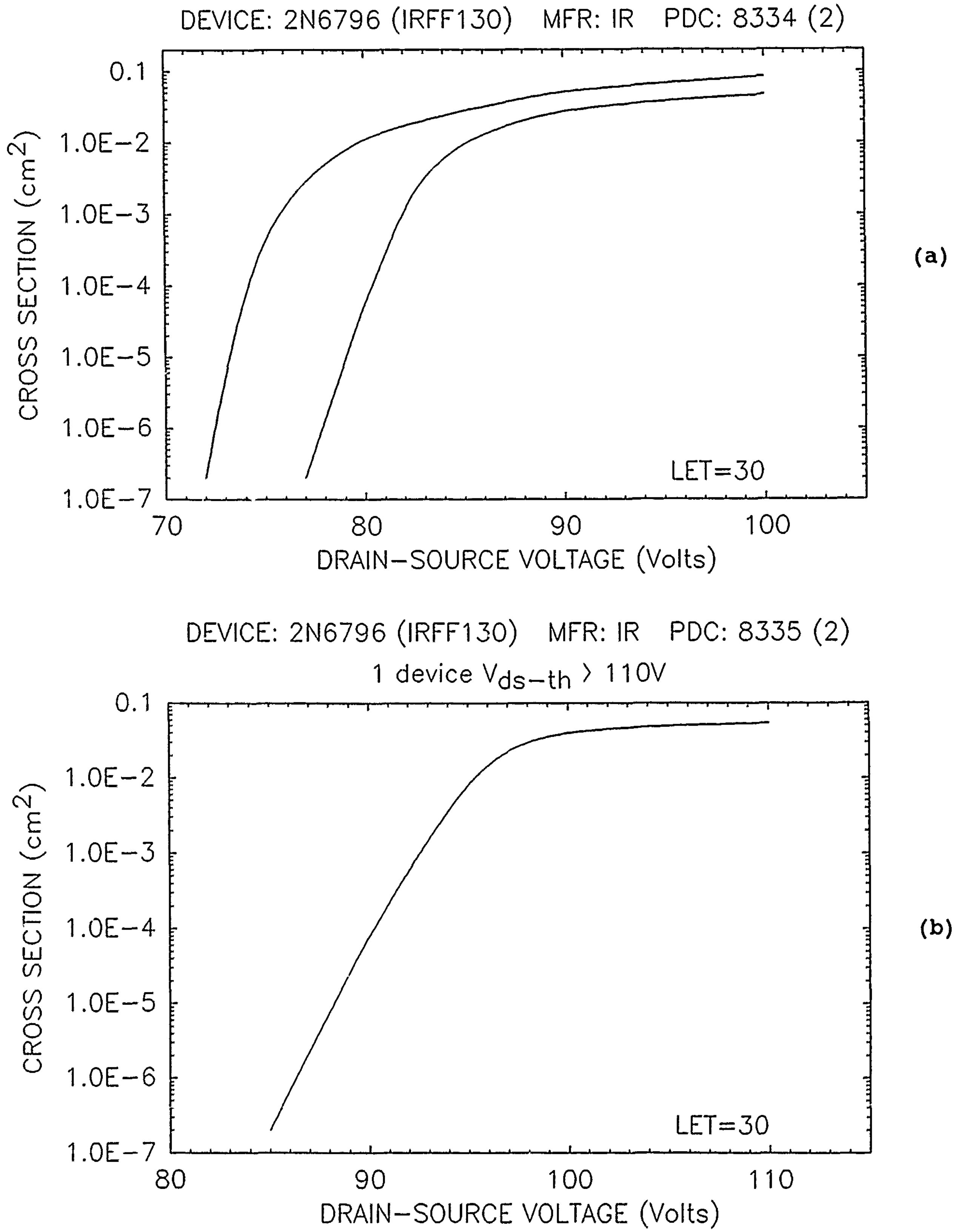

Figure 11. 2N6796 SEB cross section versus V_{DS}.

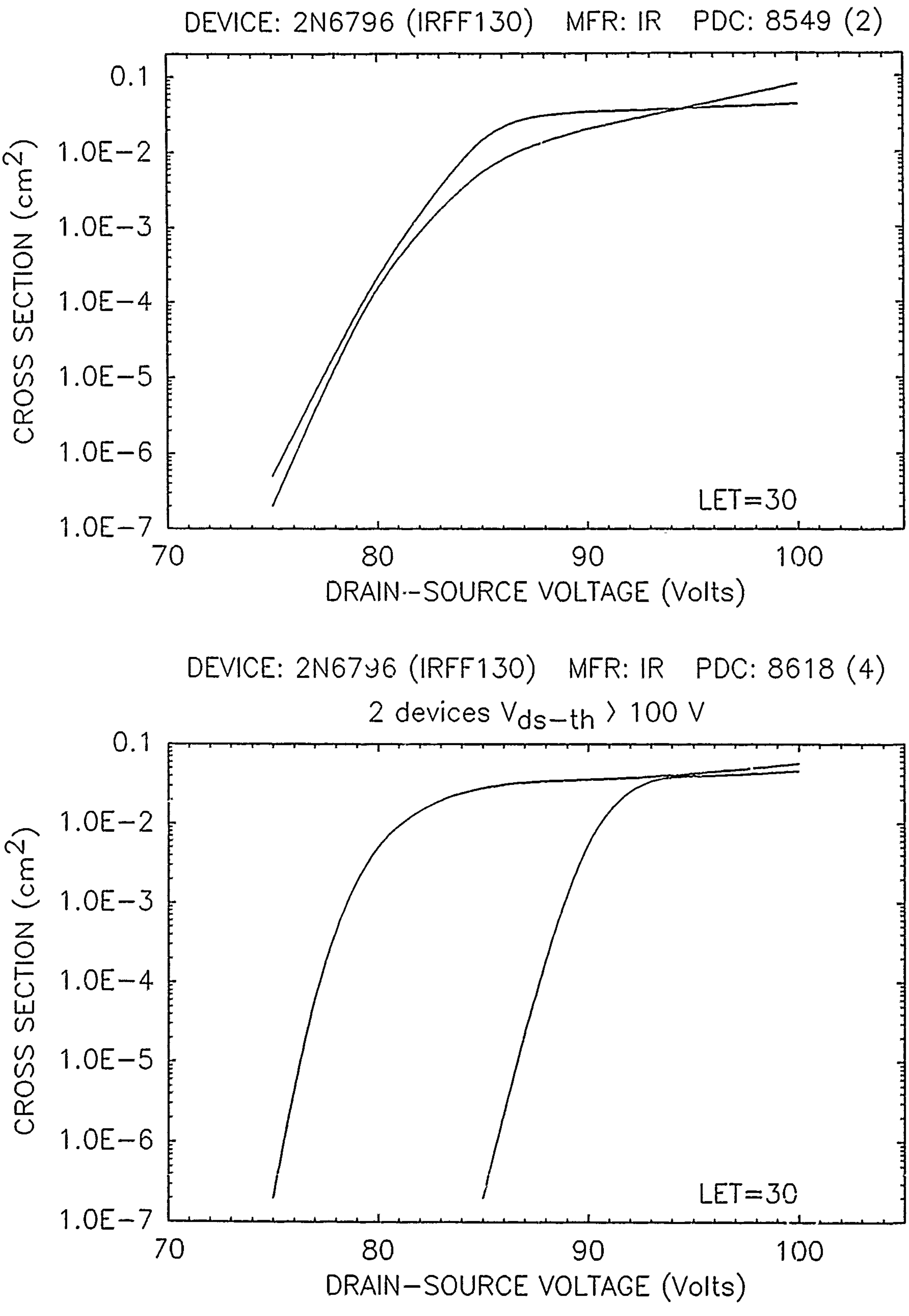

(a)

(b)

Figure 12. 2N6796 SEB cross section versus V_{DS}.

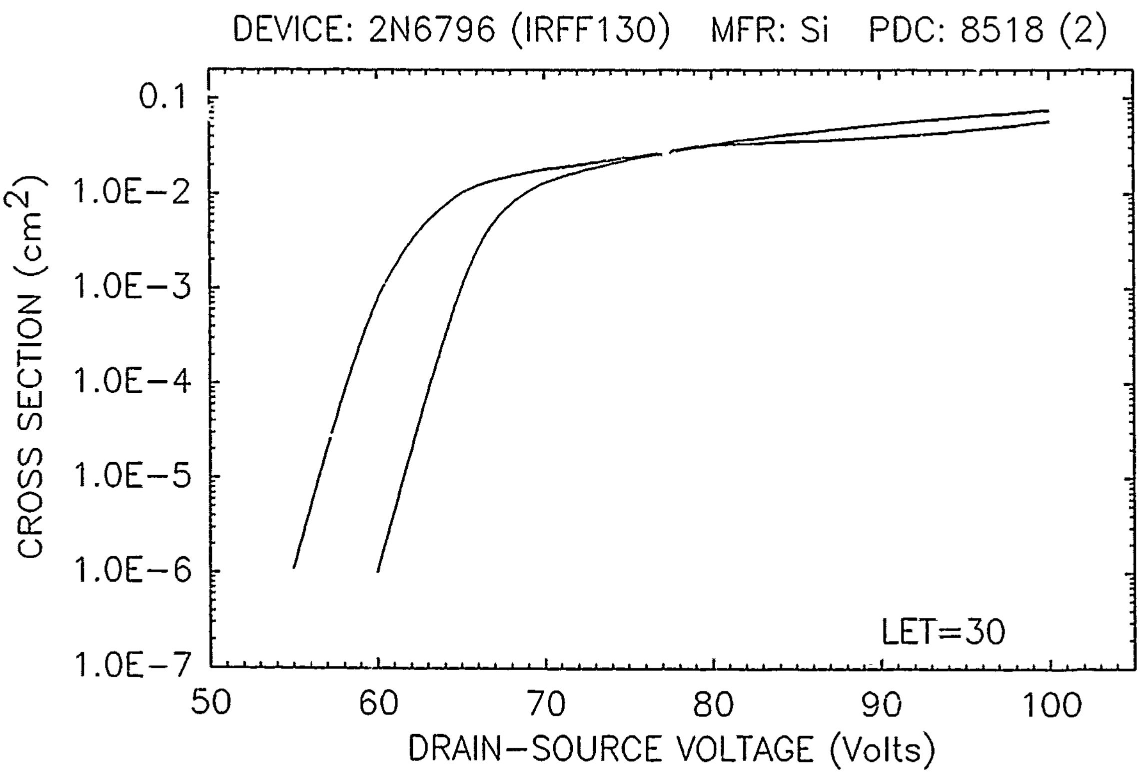

Figure 13. 2N6796 SEB cross section versus V_{DS}.

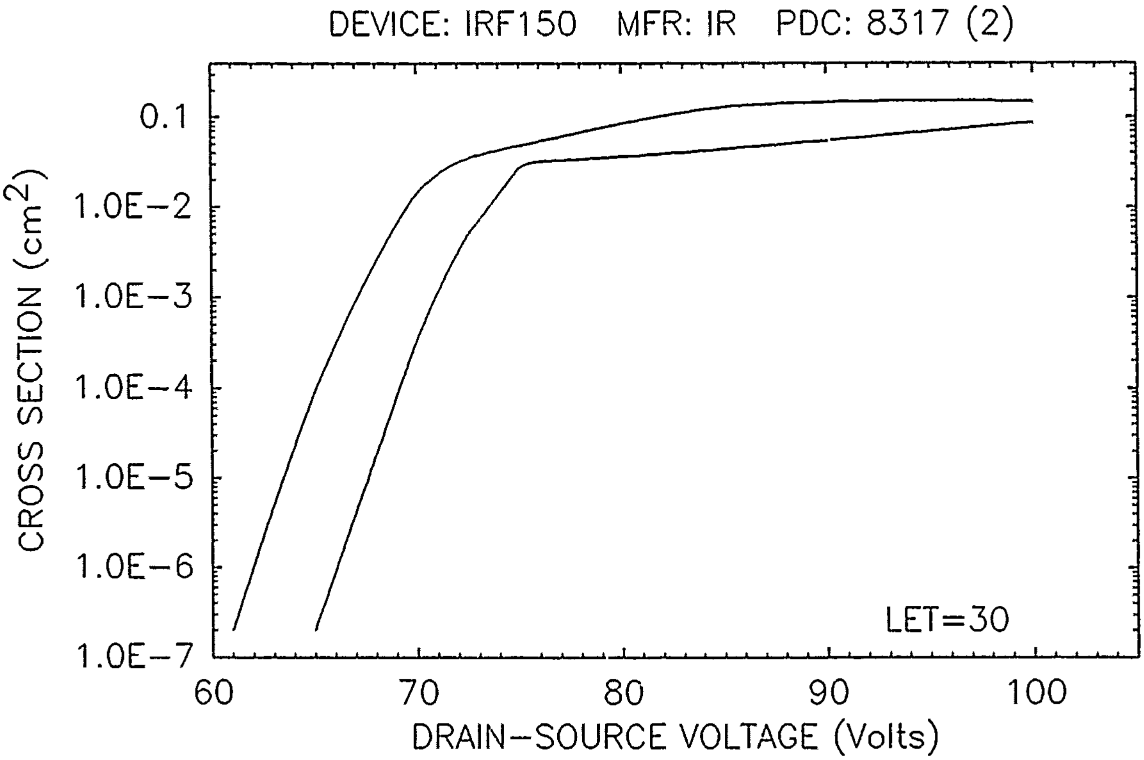

(a)

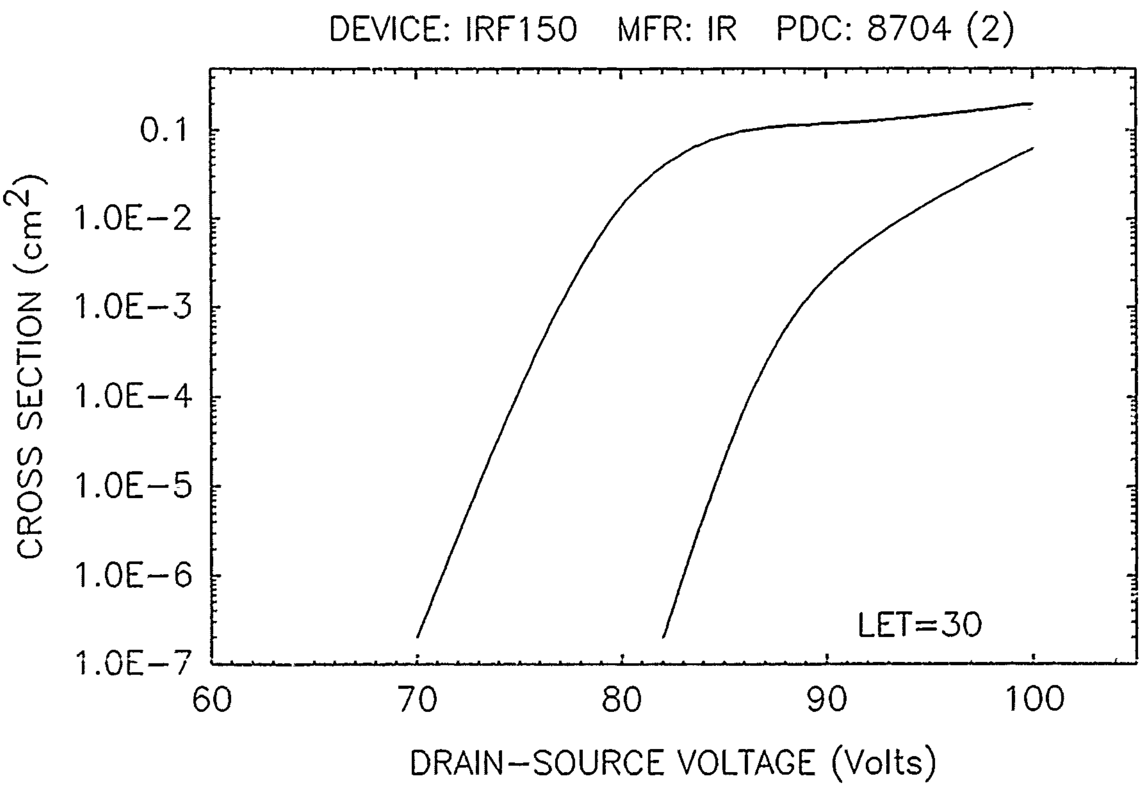

(b)

Figure 14. IRF150 SEB cross section versus V_{DS}.

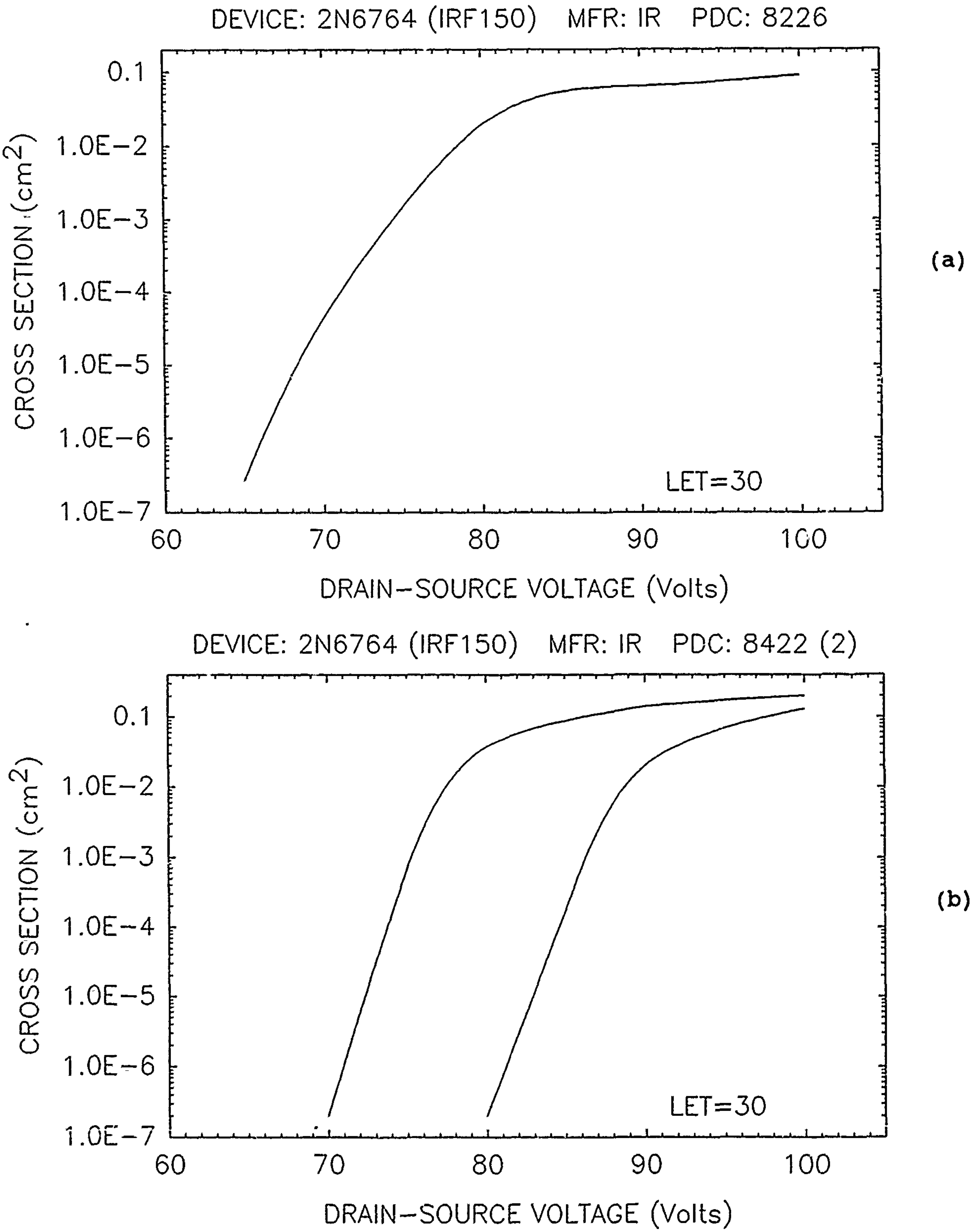

Figure 15. 2N6764 SEB cross section versus V_{DS}.

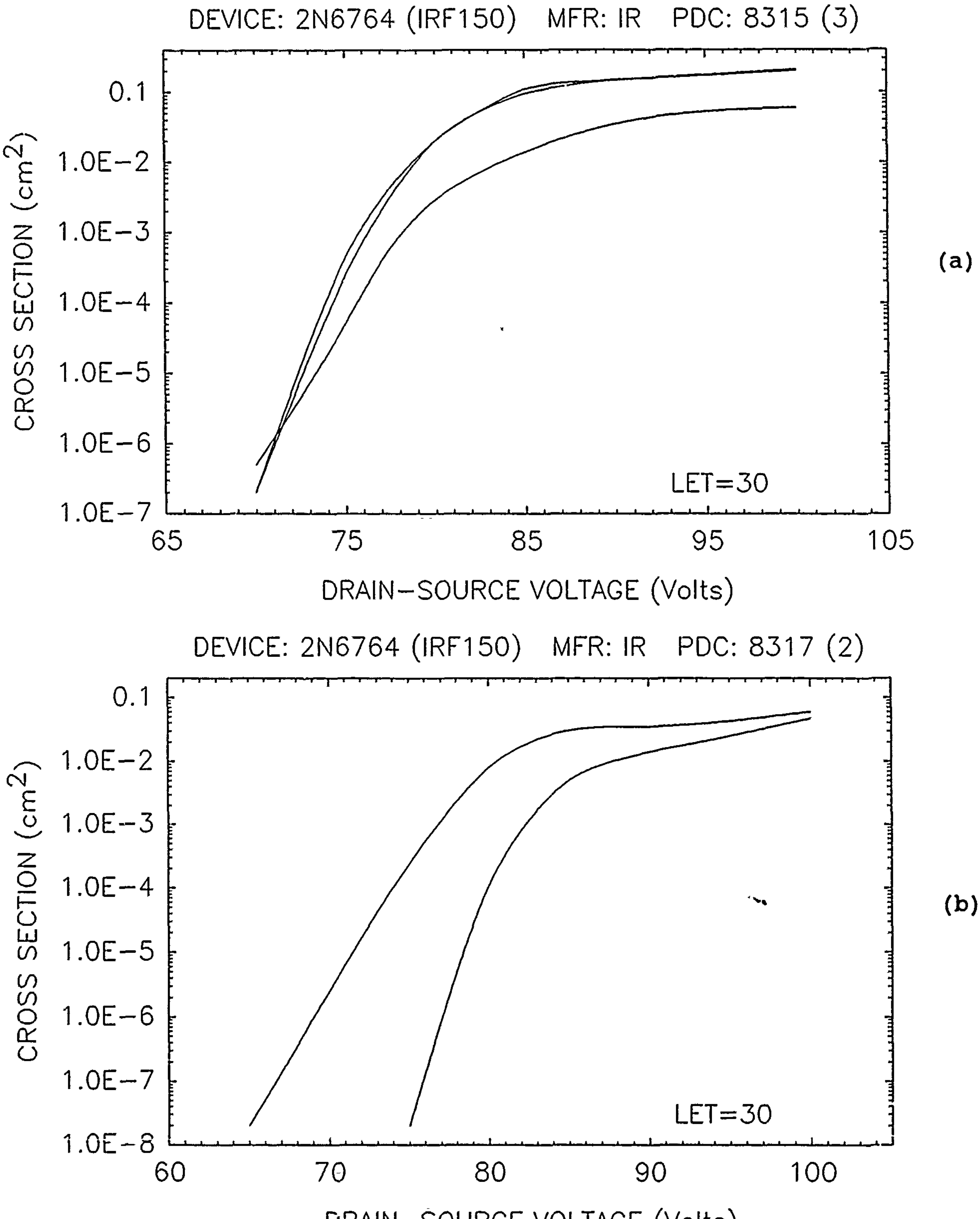

Figure 16. 2N6764 SEB cross section versus V_{DS}.

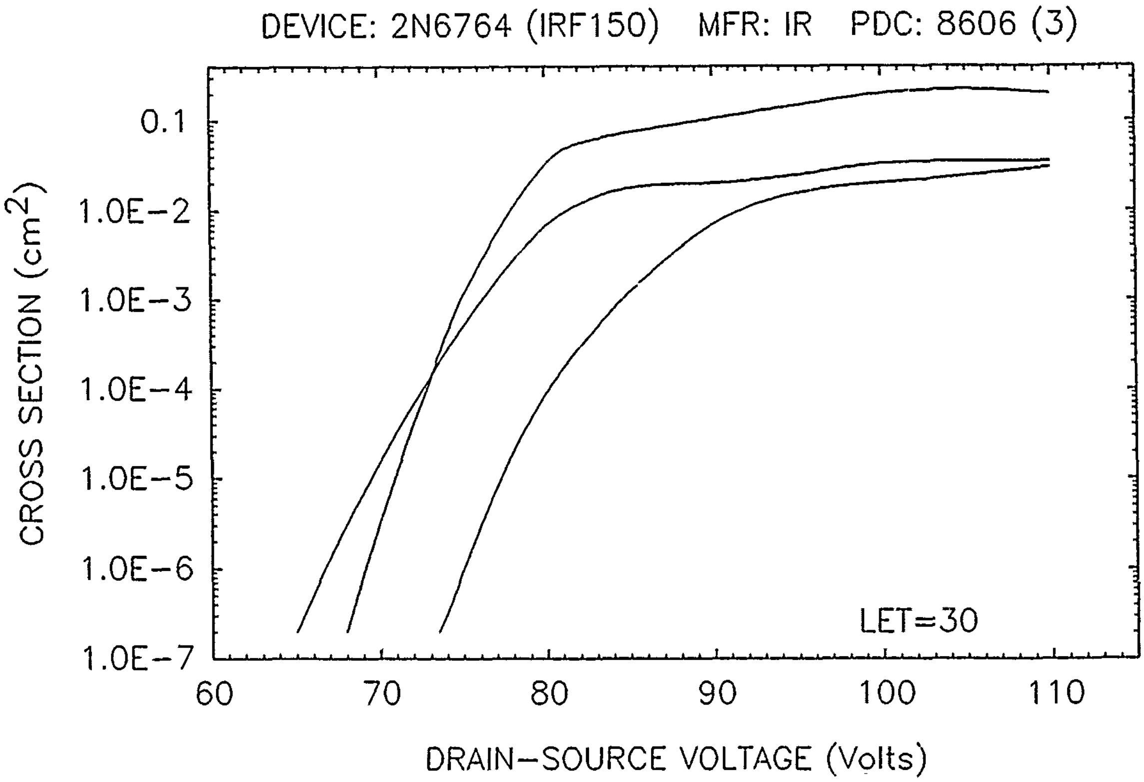

(a)

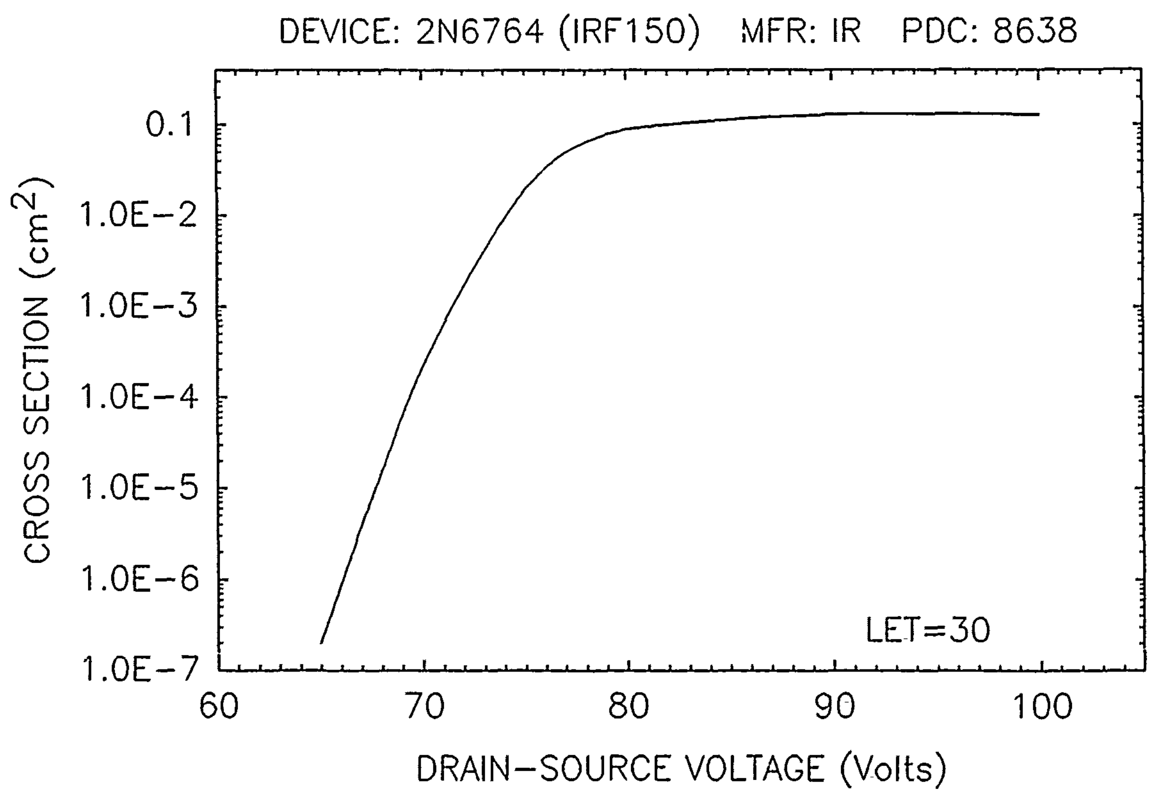

(b)

Figure 17. 2N6764 SEB cross section versus V_{DS}.

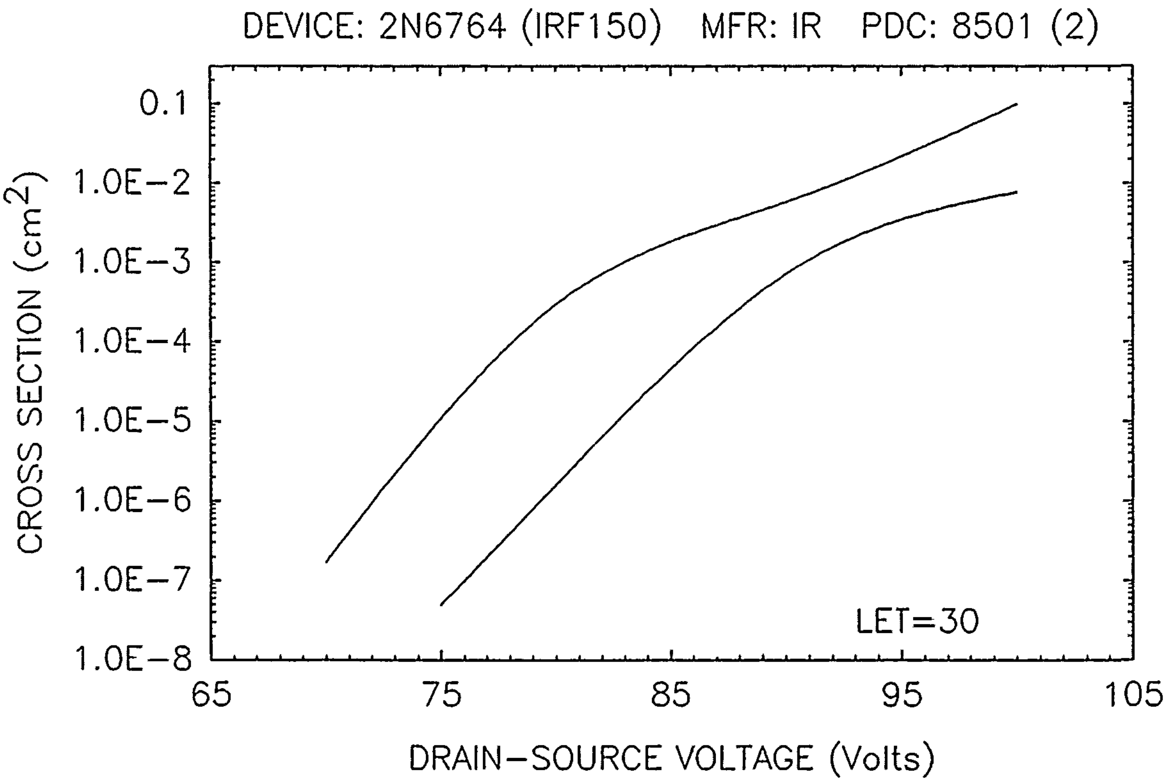

Figure 18. 2N6764 SEB cross section versus V_{DS}.

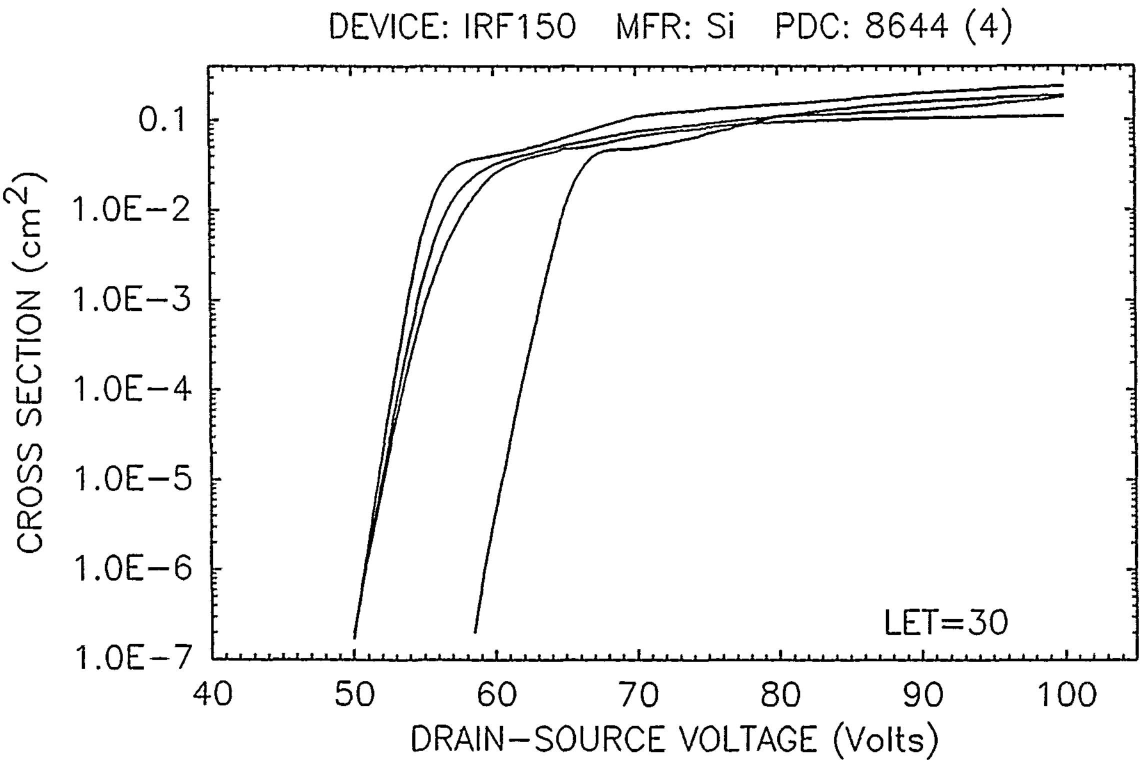

Figure 19. IRF150 SEB cross section versus V_{DS}.

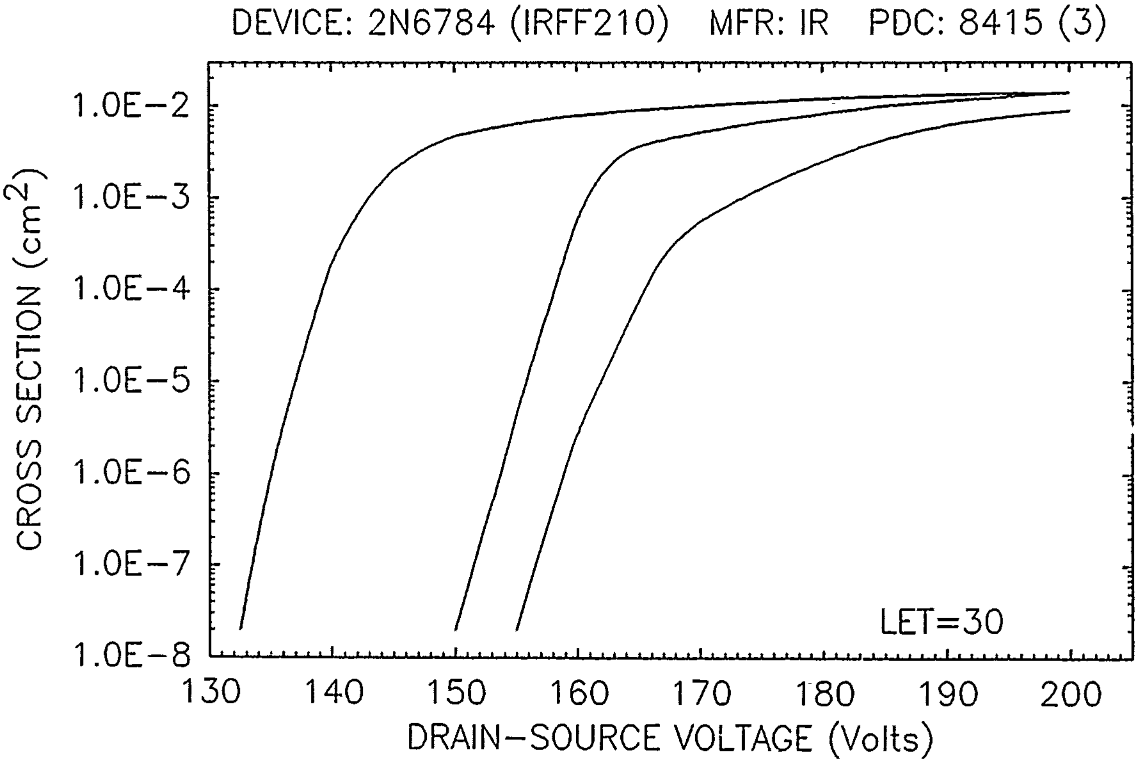

Figure 20. 2N6784 SEB cross section versus V_{DS}.

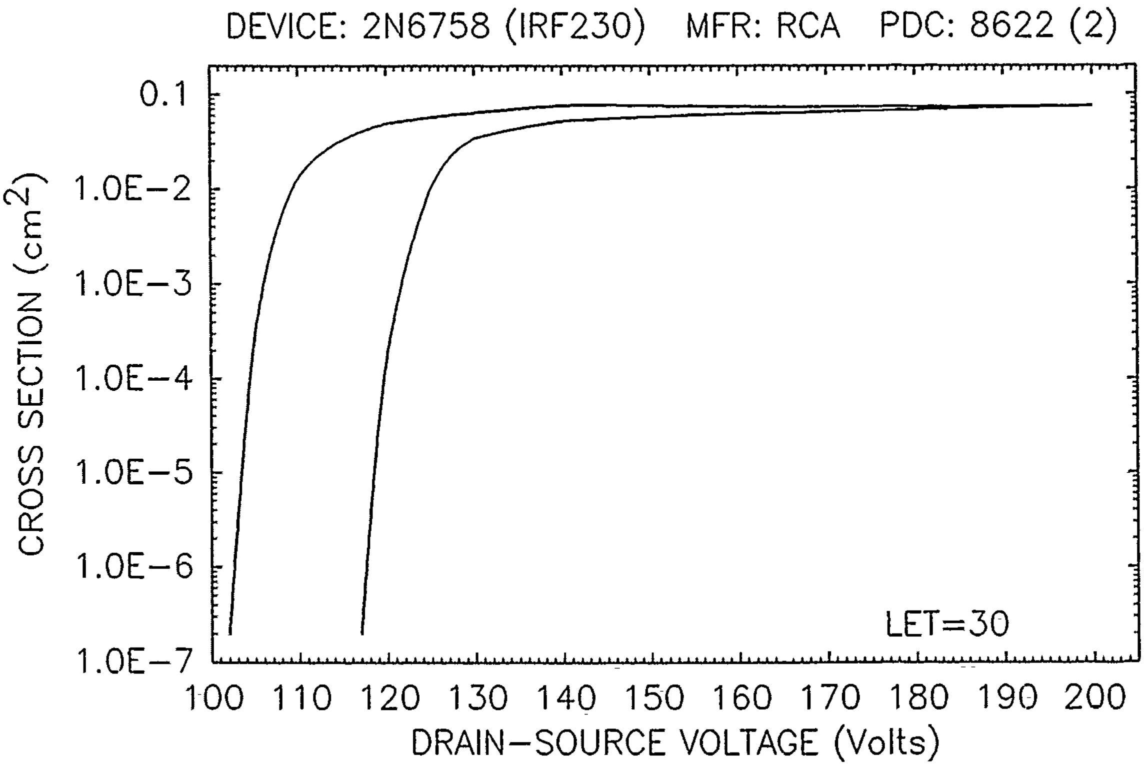

Figure 21. 2N6758 SEB cross section versus V_{DS}.

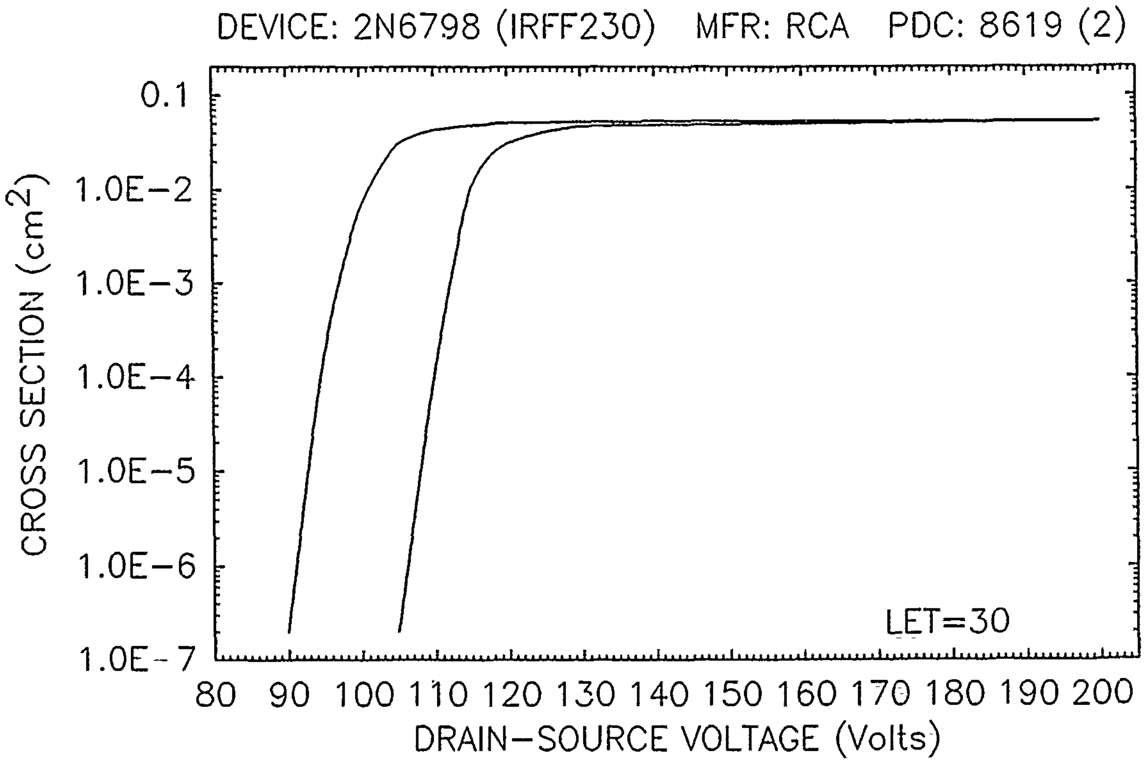

Figure 22. 2N6798 SEB cross section versus V_{DS}.

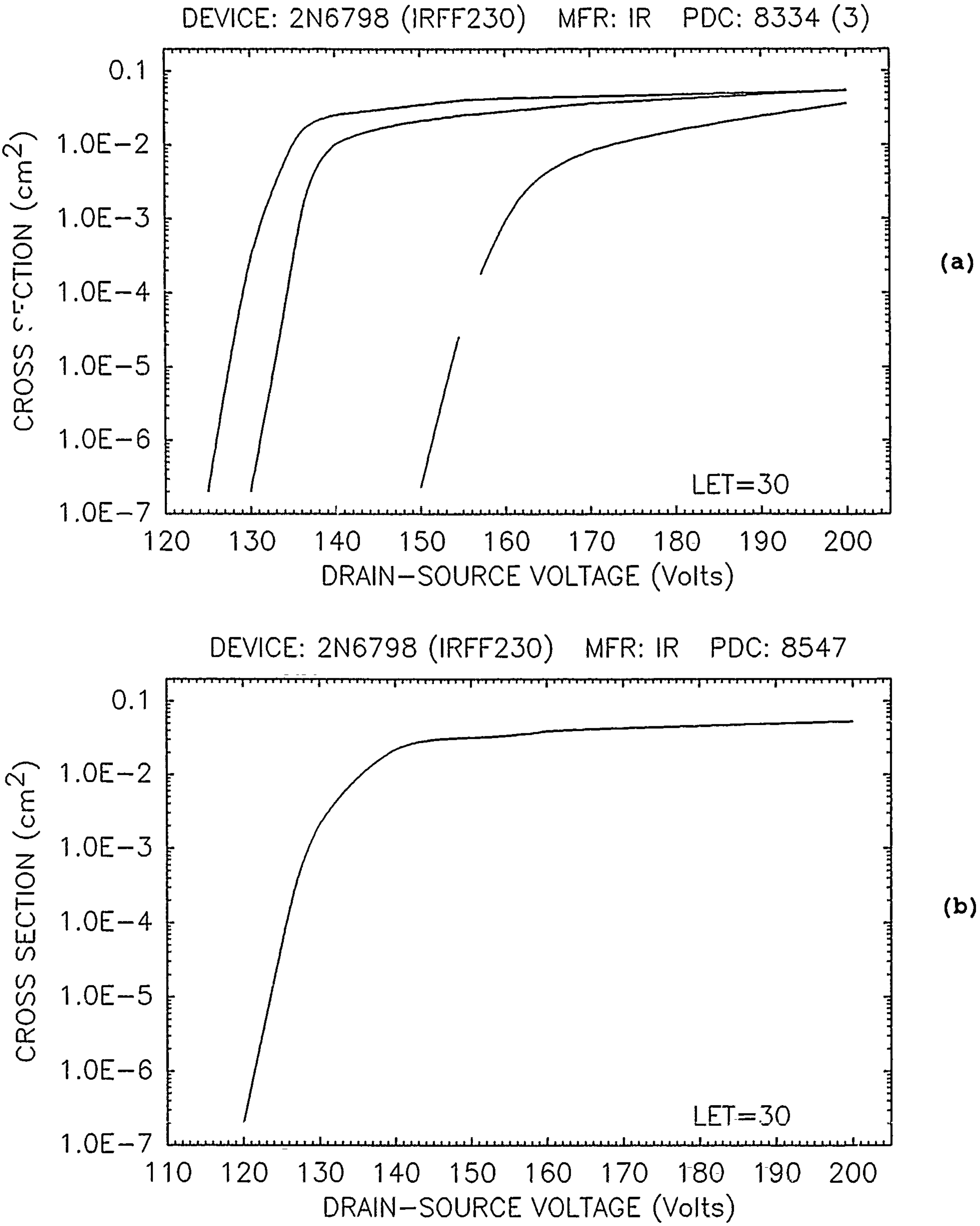

Figure 23. 2N6798 SEB cross section versus V_{DS}.

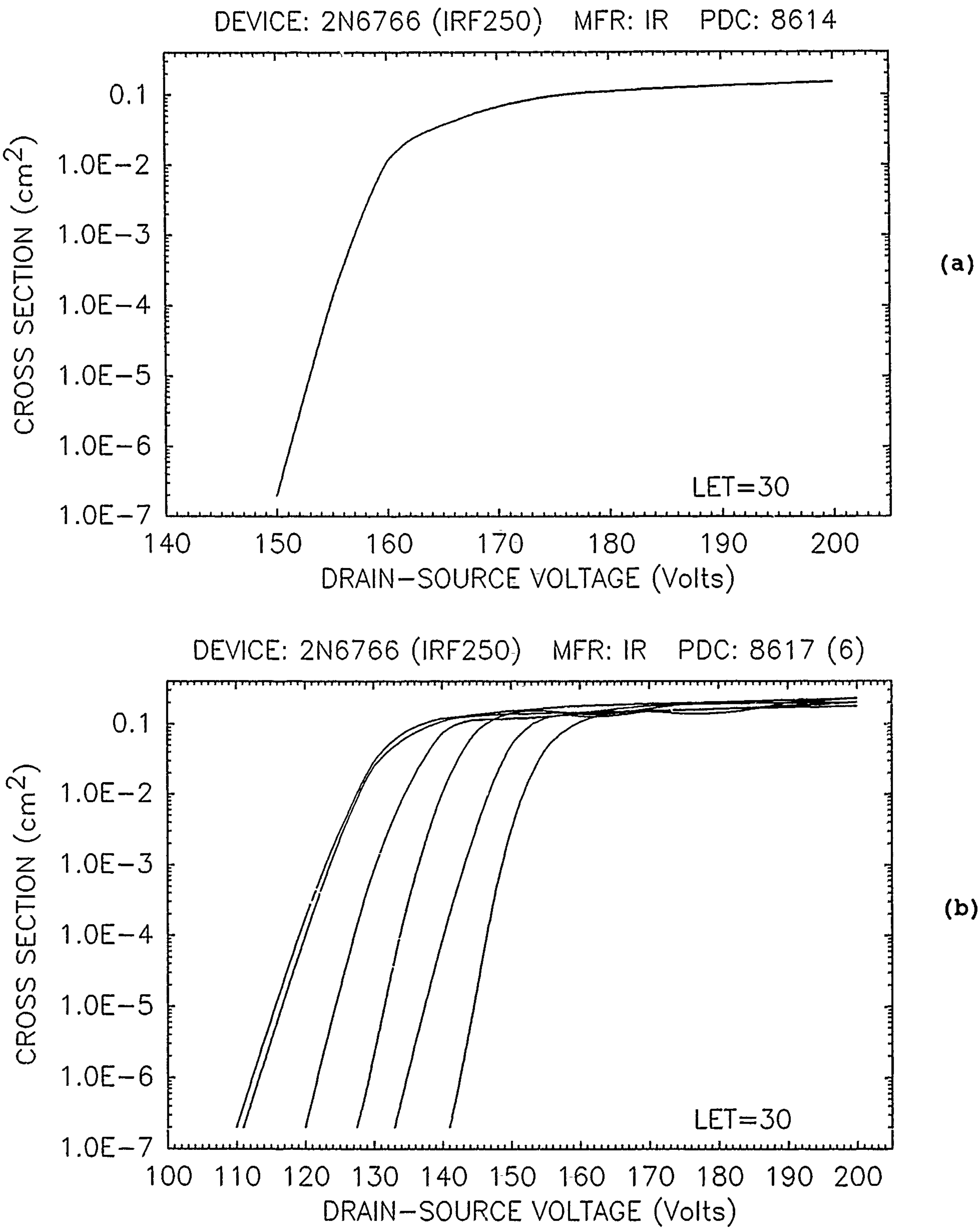

Figure 24. 2N6766 SEB cross section versus V_{DS}.

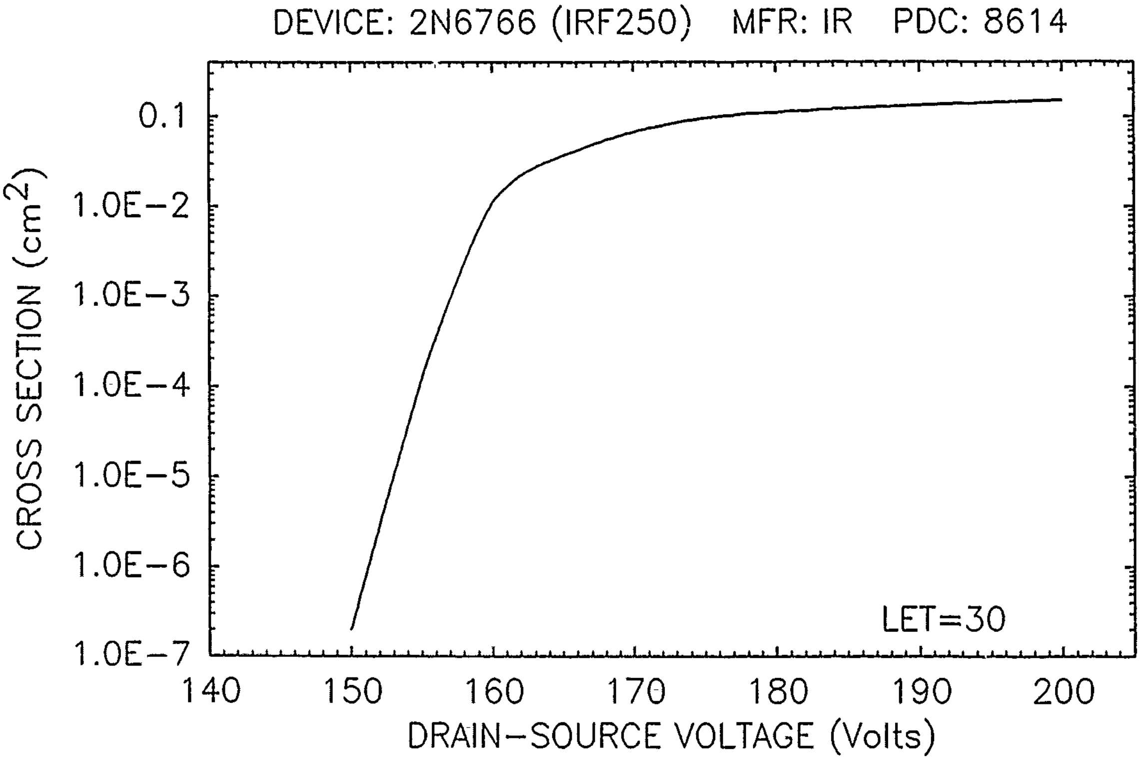

(a)

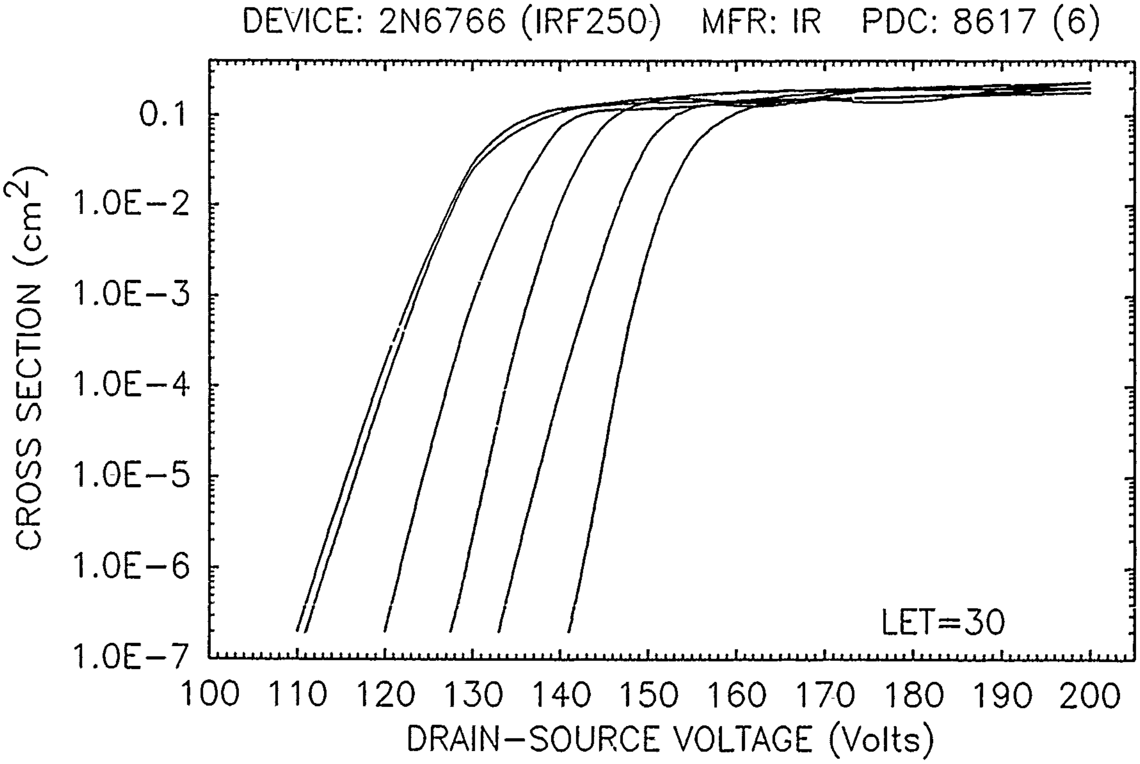

(b)

Figure 24. 2N6766 SEB cross section versus V_{DS}.

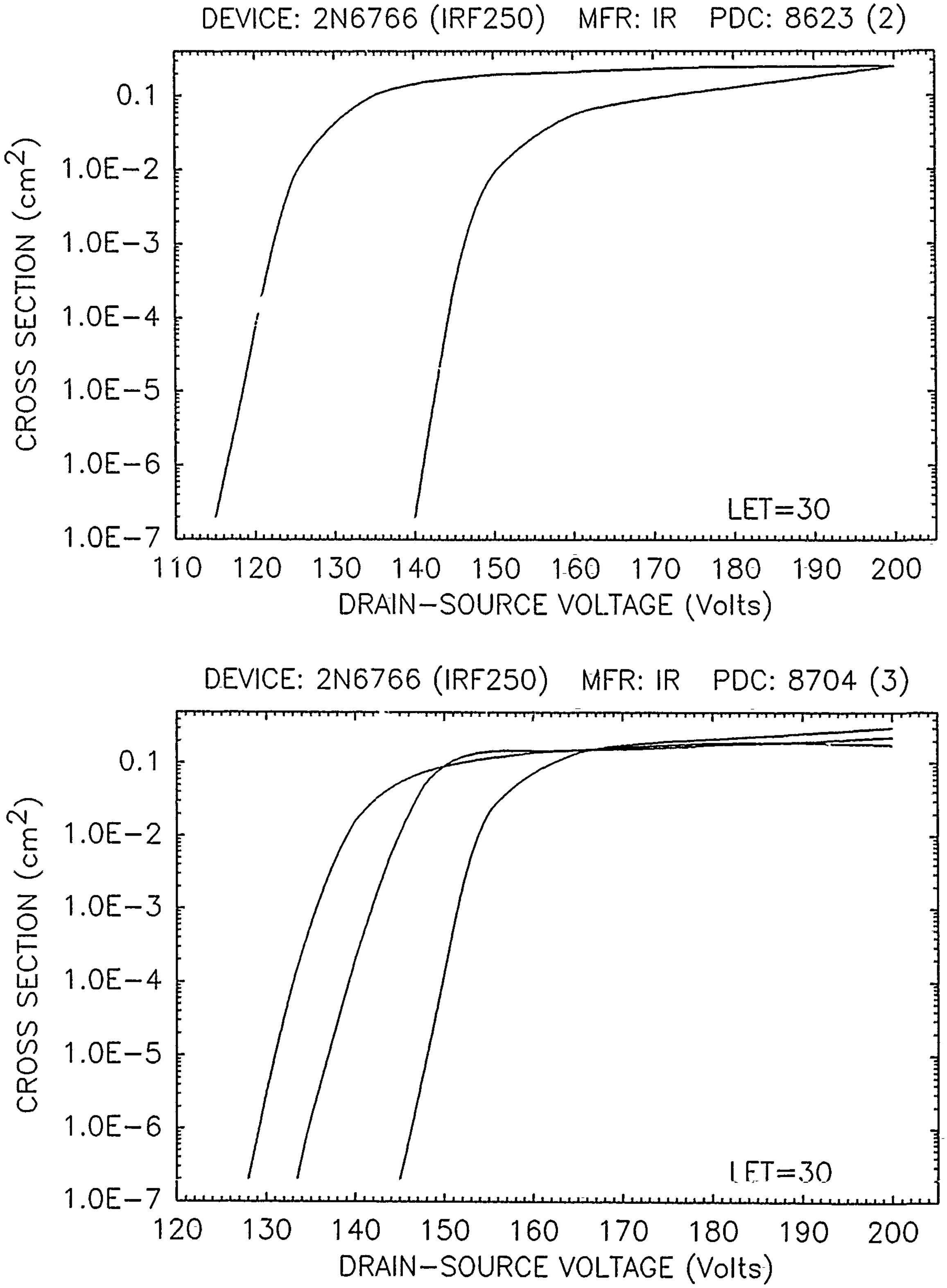

(a)

(b)

Figure 25. 2N6766 SEB cross section versus V_{DS}.

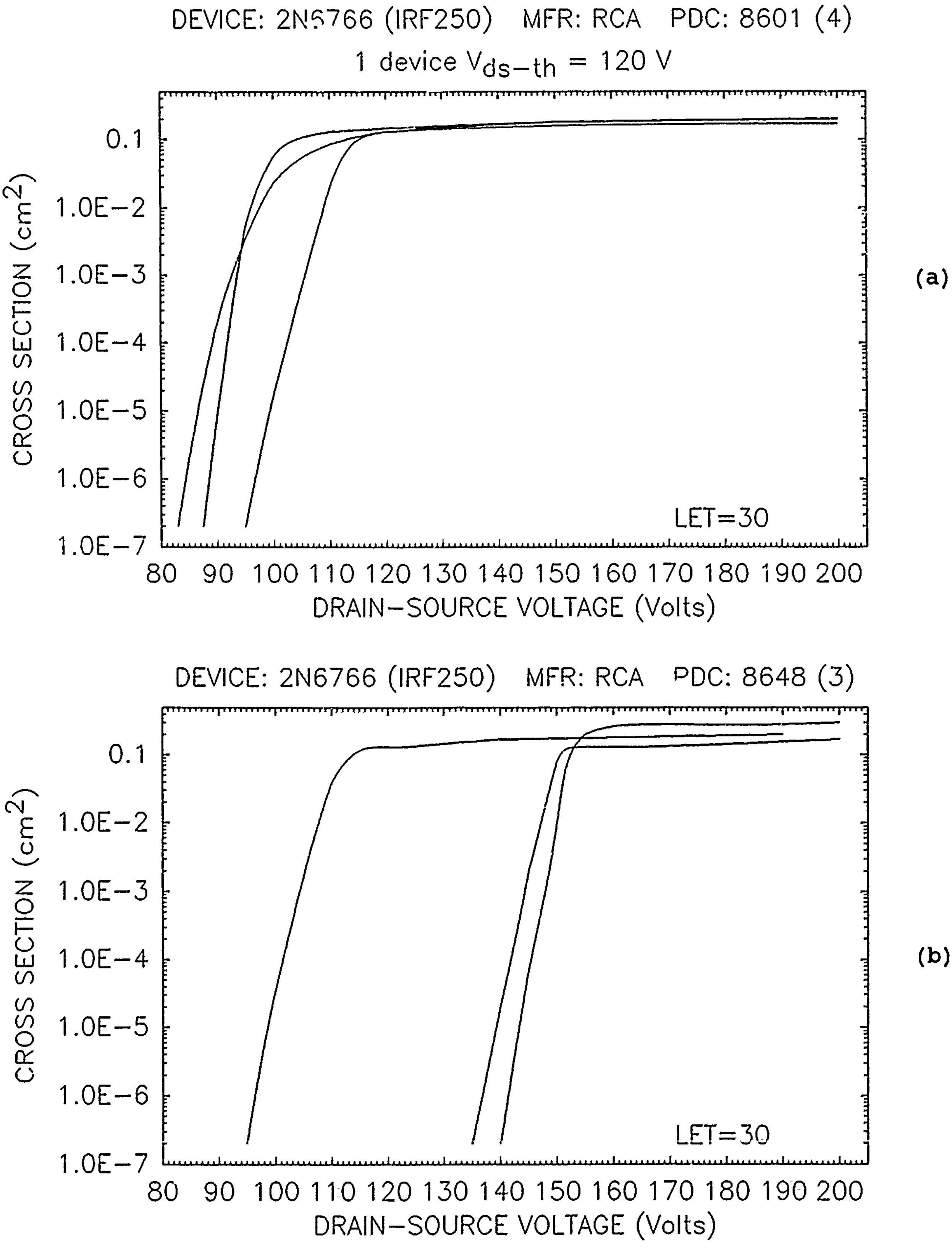

Figure 26. 2N6766 SEB cross section versus V_{DS}.

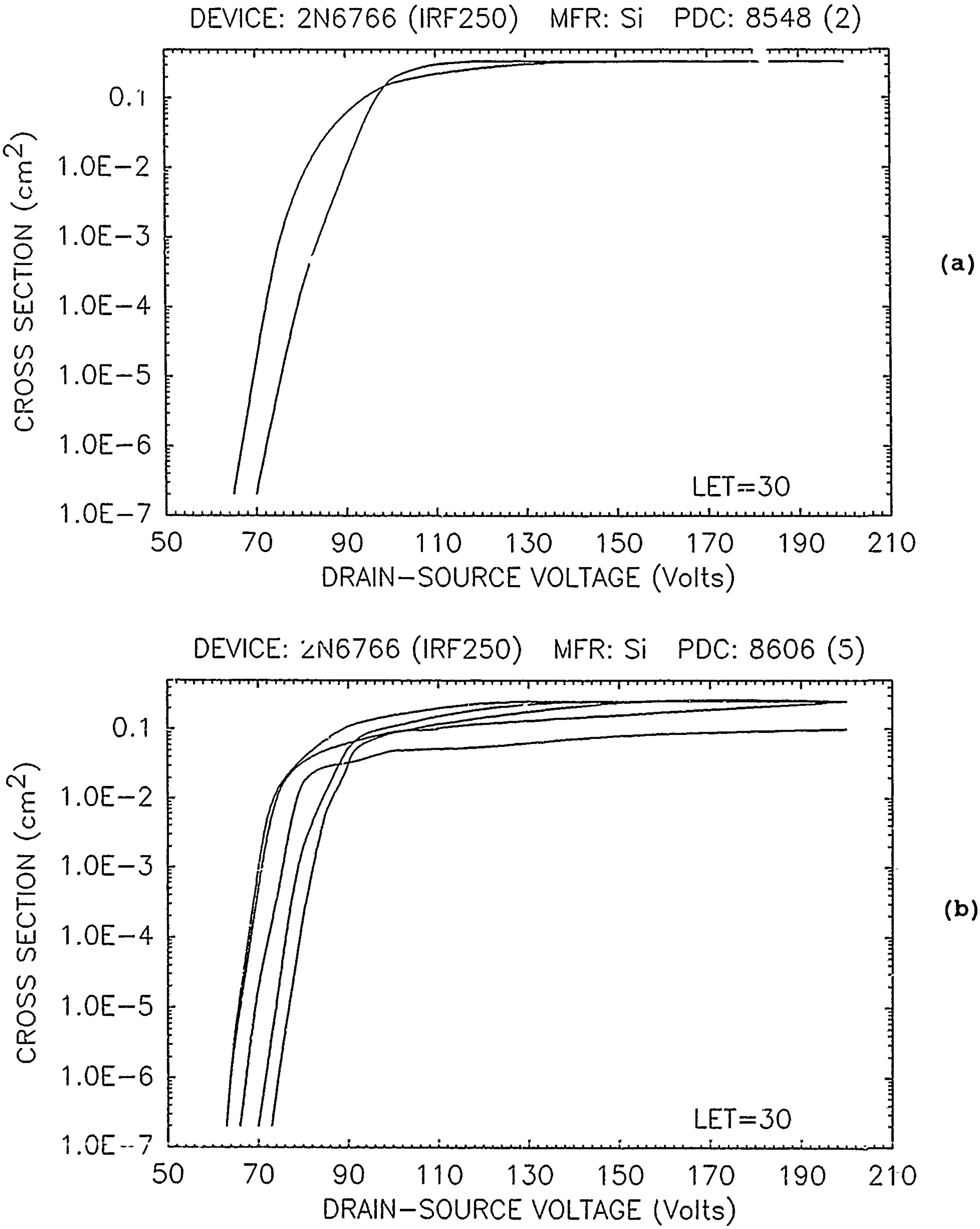

Figure 27. 2N6766 SEB cross section versus V_{DS}.

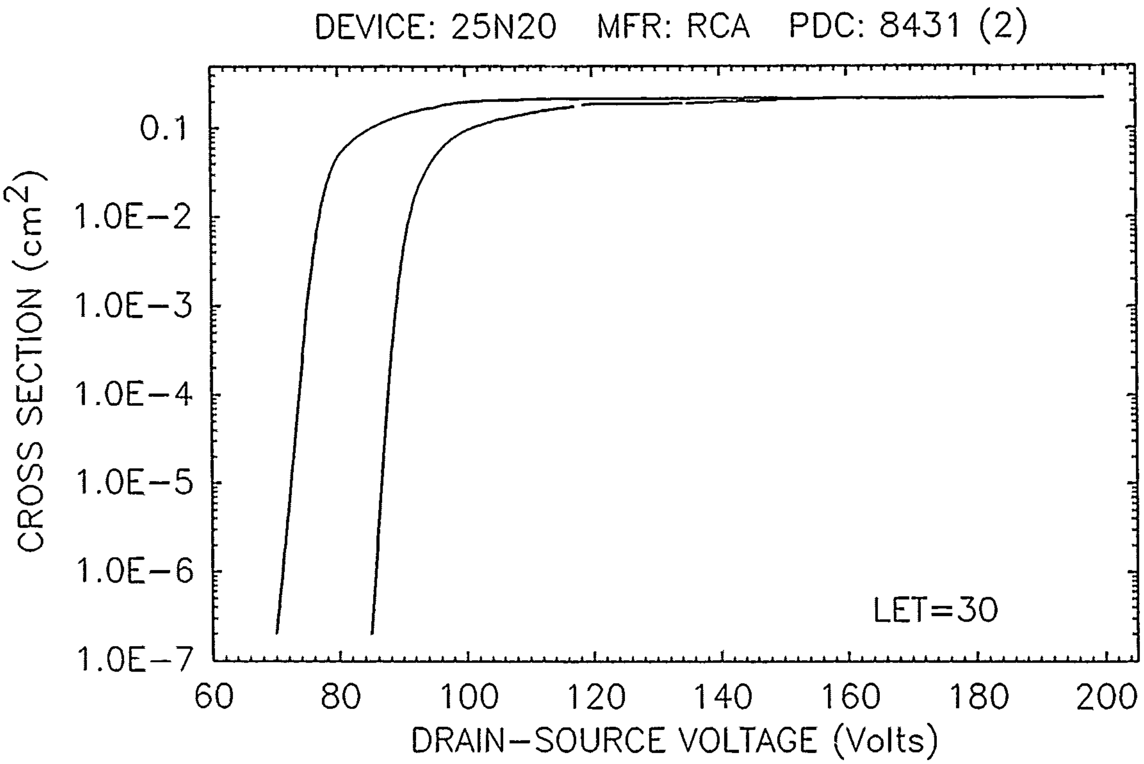

(a)

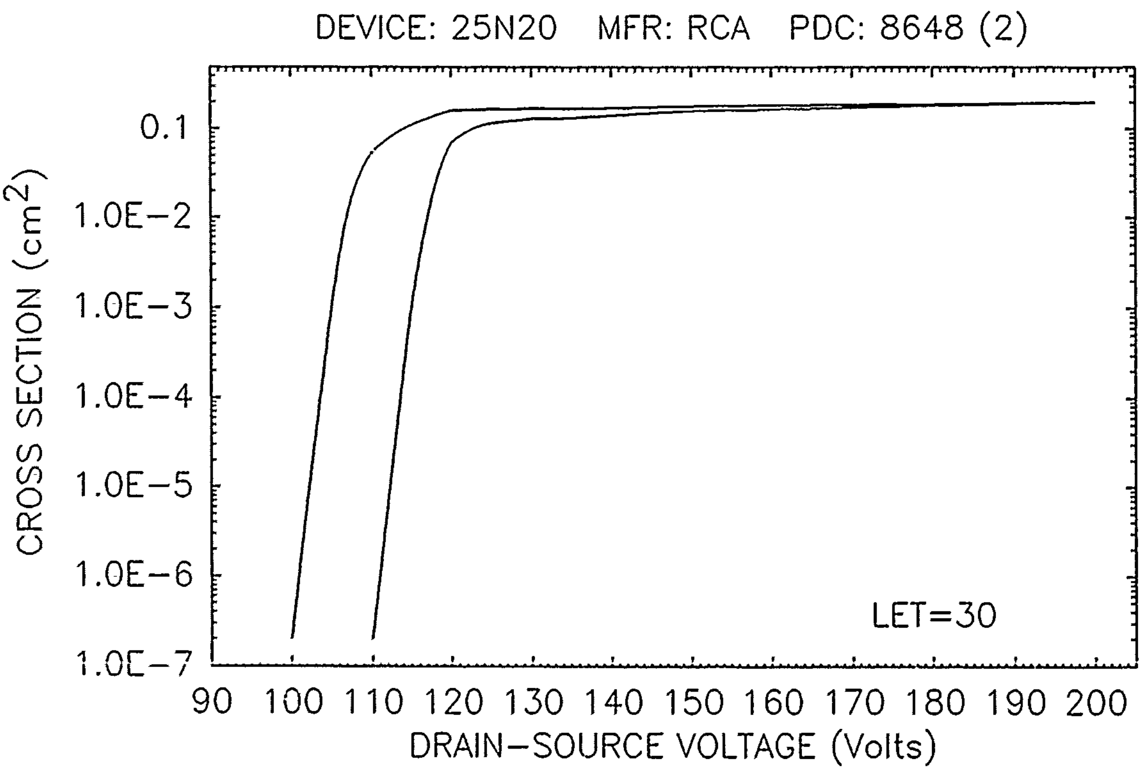

(b)

Figure 28. 25N20 SEB cross section versus V_{DS}.

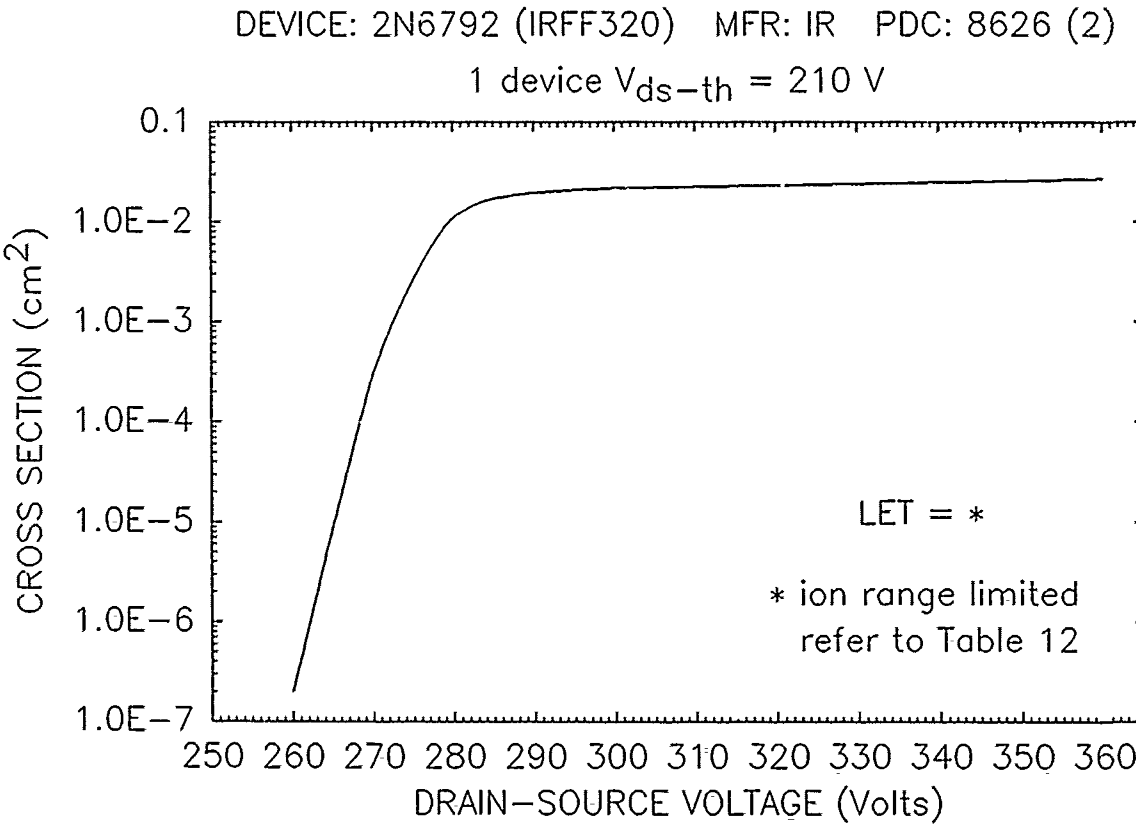

Figure 29. 2N6792 SEB cross section versus V_{DS}.

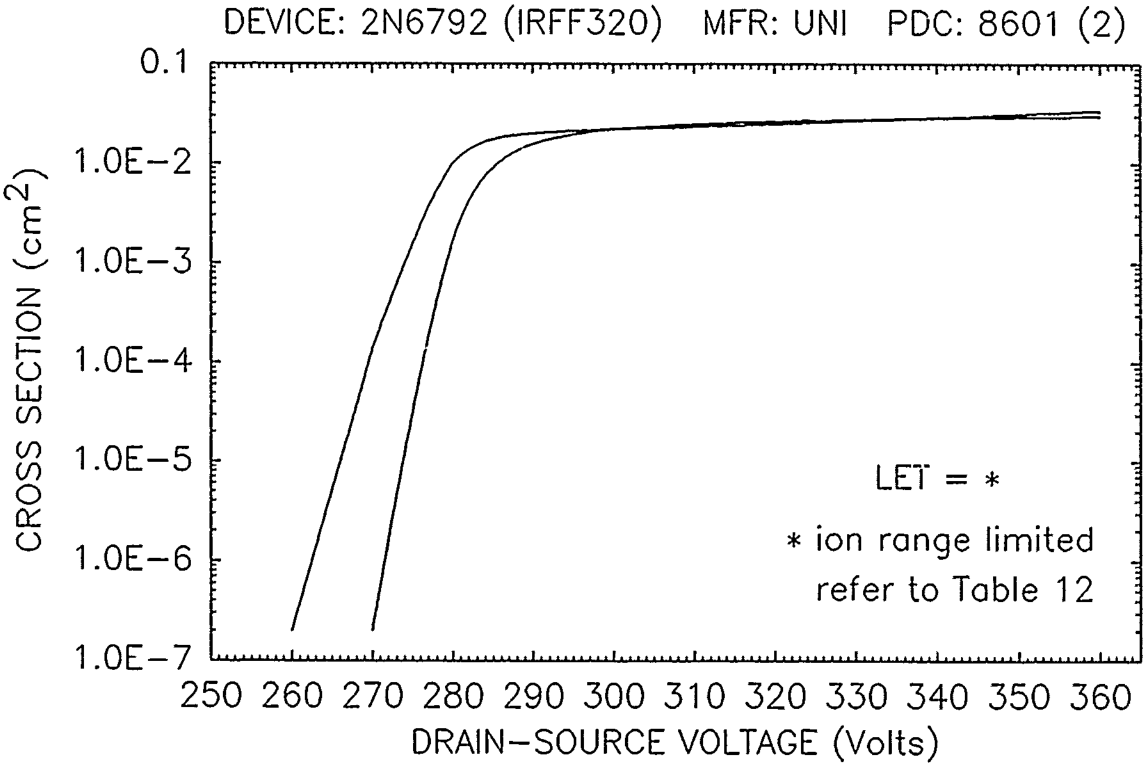

Figure 30. 2N6792 SEB cross section versus V_{DS}.

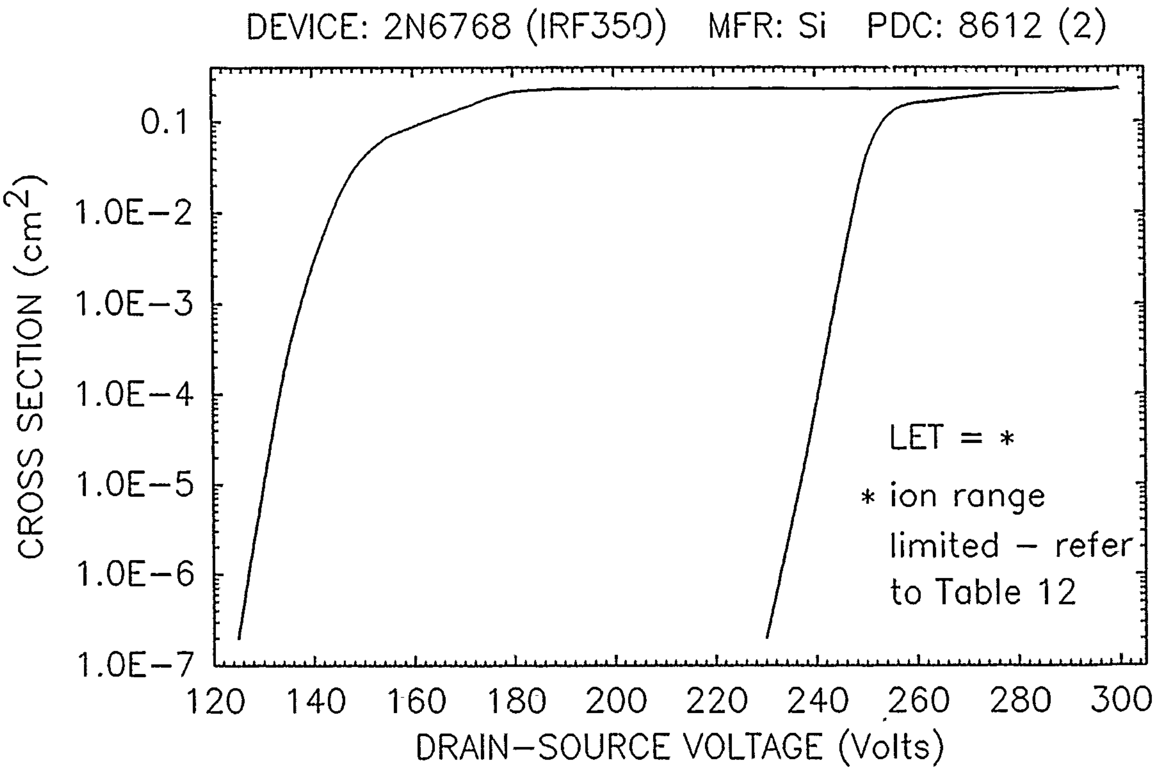

Figure 31. 2N6768 SEB cross section versus V_{DS}.

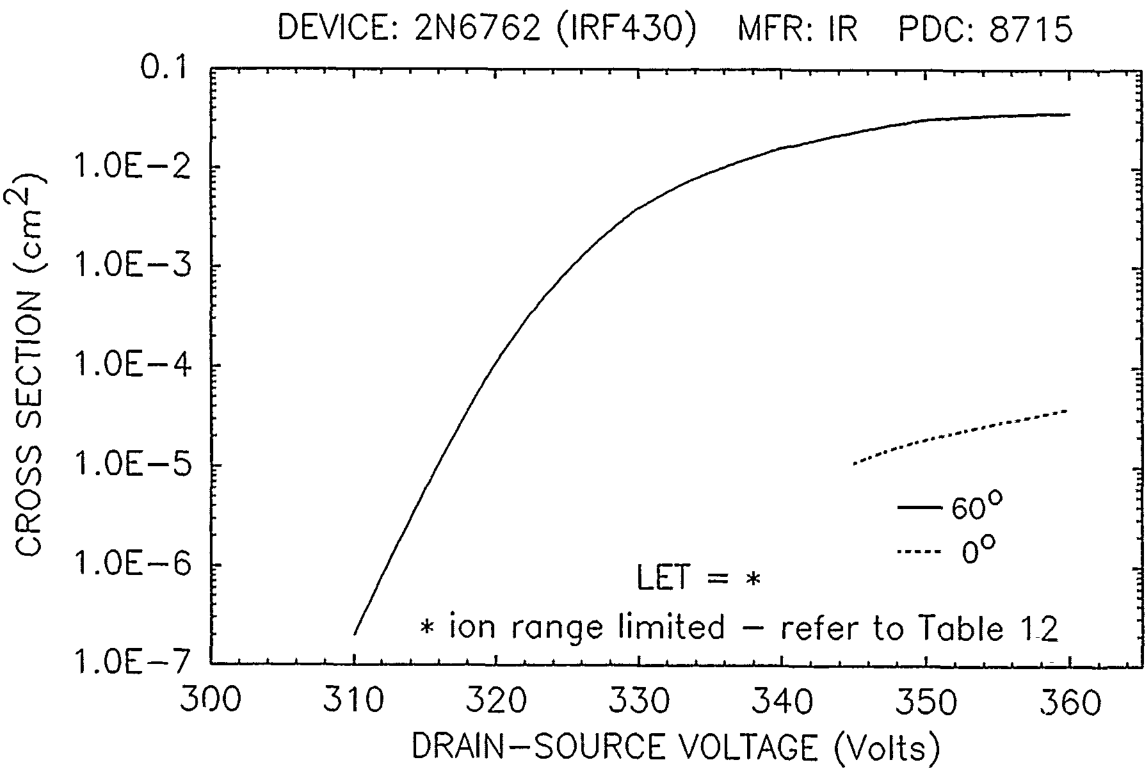

Figure 32. 2N6762 SEB cross section versus V_{DS}.

4.3 SINGLE EVENT BURNOUT TEST RESULT TRENDS.

As with the destructive tests, data for all device types indicated increasing drain-source burnout thresholds (V_{DSTH}) with decreasing ion LET.

As expected, there were no significant differences in the physical appearance of the chips and the burnout characteristics of a JEDEC and the equivalent non-JEDEC version of a device. Figure 33 illustrates the SEB characteristic of the 2N6764 and IRF150, the non-JEDEC equivalent of the 2N6764.

The n-channel devices tested exhibited a wide range of burnout susceptibility. Large variations in V_{DSTH} were observed within a package date code and between package date codes for some device types, while for other device types the opposite was observed -- little variation in V_{DSTH} -- in some cases across seven years of package date codes. For example, SEB threshold voltages of the RCA 2N6766 (BV_{DSS}=200v), all packaged in 1986, ranged between 90 and 145 volts -- a variation of 28% of BV_{DSS} (Figure 34(b)). In contrast, threshold voltages of the IR 2N6764 (BV_{DSS} = 100v), packaged from 1982 to 1986, all ranged between 60 and 75 volts -- a variation of only 15% of BV_{DSS} (Figure 34(a)).

For one device type, a discernible difference in structure appeared to be responsible for the observed variation in SEB sensitivity. Figure 35 illustrates the measured SEB

characteristics of the Siliconix 2N6660 MOSFETs with 8133, 8307, and 8624 package date codes. Note the large variation in SEB threshold voltage with date code. The 2N6660 is listed as "VMOS N ENH", 60-volt, 1.1-amp device with a fairly large $r_{DS}(on)$ of 3 ohms. Typical VMOS (vertical or V-shaped MOSFET) and HEXFET (hexagonal MOSFET) structures are shown in Figure 36. Note the absence of the p+ region in the center body region of the VMOS structure. It is the design of the p+ body-drain diode which manufacturers claim to be largely responsible for the device's ability to absorb energy in avalanche breakdown and significantly contributes to the essential requirement that the internal parasitic npn bipolar transistor not be allowed to approach the conducting state. The p+ body-drain diode in effect provides a shunt path for the avalanche current by avalanching first and subverting avalanching in the channel region, decreasing the probability of forward-biasing the parasitic bipolar transistor with attendant second breakdown and burnout.

The 1981- and 1983- dated devices were physically different from the 1986 devices. The earlier devices had an interdigitated gate-source structure without any evidence of closed HEXFET transistors and probably were VMOS enhancement mode devices. In contrast, the 1986-coded devices exhibited typical HEXFET transistor structures with a single gate pad. The devices appeared to be a scaled-down version of present DMOS HEXFETs. There were also differences in the measured breakdown voltages (BV_{DSSM}). The measured values averaged 64 volts, 108 volts, and 63 volts for the 8133-,

8307-,and 8624-dated devices, respectively. The differences in structure and breakdown voltages possibly explain the variation in observed SEB thresholds. The larger breakdown voltages, resulting in higher SEB thresholds for the 8307 versus the 8133 devices, and the improved structure, increasing the device avalanche capability, being responsible for the higher SEB thresholds of the 8624 devices as compared to the 8133- and 8307-dated MOSFETs.

The 2N6660 data presents the only example of a device fabricated with two different structures and indicates, for this device type, the marked increase of burnout susceptibility of VMOS as compared to a HEXFET structure. All the other devices tested during this effort appeared to be only fabricated with HEXFET structures.

An attempt was made to correlate measured breakdown voltages (BV_{DSSM}) and burnout thresholds (V_{DSTH}). The effort proved to be unsuccessful. Figure 37 illustrates a case where only two devices were tested and V_{DSTH} appeared to track with BV_{DSSM} and a case, typical of most of the data, where correlation could not be made -- the device with the highest BV_{DSSM} had the lowest V_{DSTH}.

One common trend, which was observed, was that the burnout cross section at threshold was several orders of magnitude less than the asymptotic value of the cross section (σ_{sat}), and the initial slope of the SEB characteristics often varied between device types. An example of the variation is shown in Figure 34. In addition, the value of σ_{sat} was observed to be directly related to

the size of the chip die, regardless of the voltage rating of the device, as illustrated by Figures 38 and 39. The IRFF120 and the IRFF320 had measured σ_{sat} values of 0.05 and 0.04 cm^2. The two device types are processed on the same size die[4] and have breakdown voltage ratings of 100 and 400 volts, respectively. Figure 39 illustrates SEB characteristics of three device types from one manufacturer (Siliconix). Measured saturated cross-section values of the IRF150, IRF250, and IRF350, 100V, 200V, and 400V BV_{DSS} devices were 0.24, 0.23, and 0.23 cm^2, respectively -- all are processed on the same size die. Additional examples and the ratio of measured σ_{sat} to chip size are presented in Table 7.

The chip active area (AA) in the table was estimated as 80% of the die size, and the ratio of σ_{sat}/AA was calculated using the average measured value of σ_{sat} for all manufacturers combined. The table suggests a method for estimating the saturation burnout cross section from a chip's physical size and an example is presented for the 2N6660, for which there were no listed dimensions. Possibly more important, the table indicates, with sufficiently large bias, ≈ 50% of the active area of the chip contributes to the burnout susceptibility of the device. Considering that the active area included the source contact and gate structure, σ_{sat} appears to reflect the total transistor area of the MOSFET. The results implied, that with applied V_{DS} >> V_{DSTH}, all the device transistors were equally sensitive to heavy-ion-induced burnout.

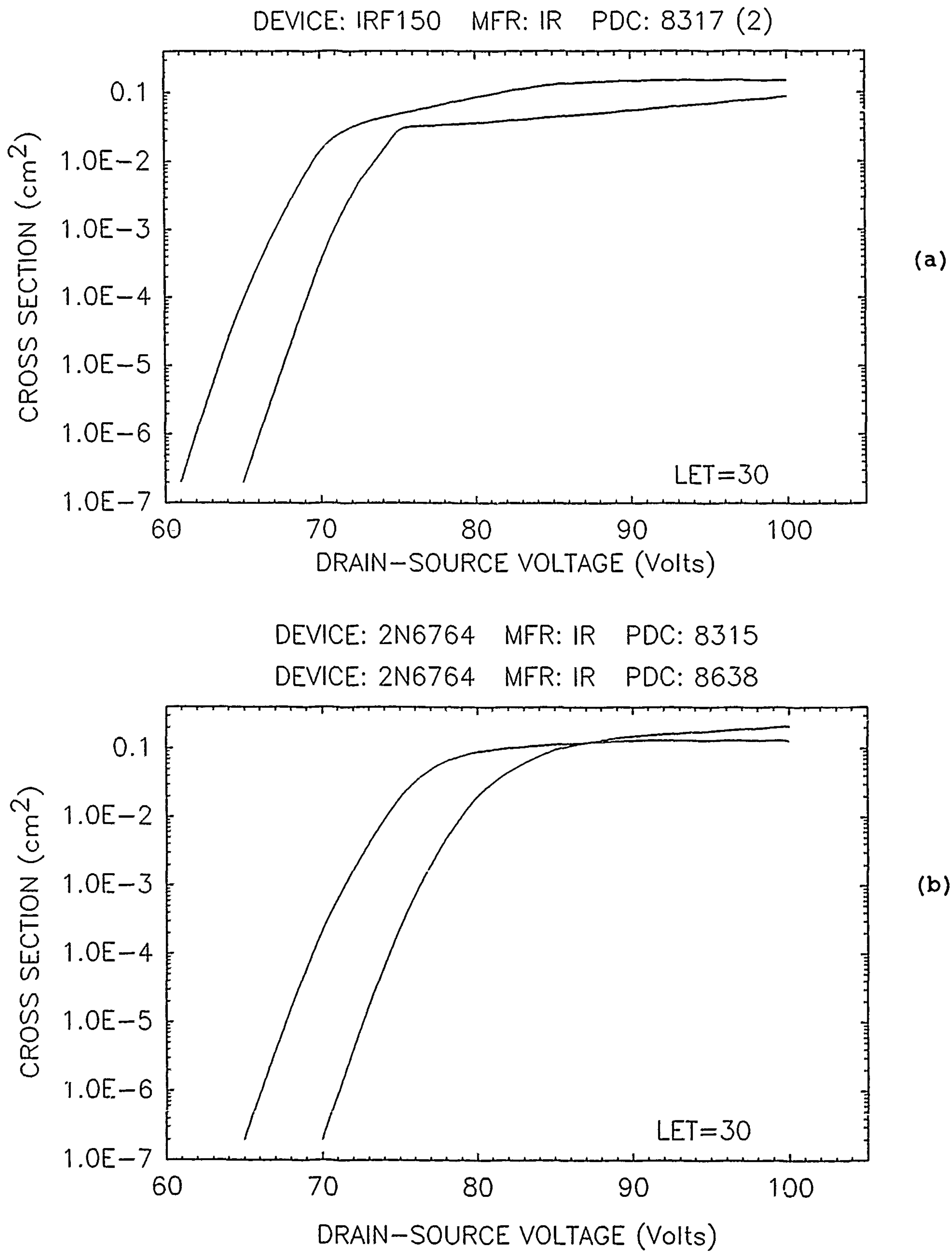

Figure 33. Non-JEDEC (a) versus JEDEC (b) equivalence.

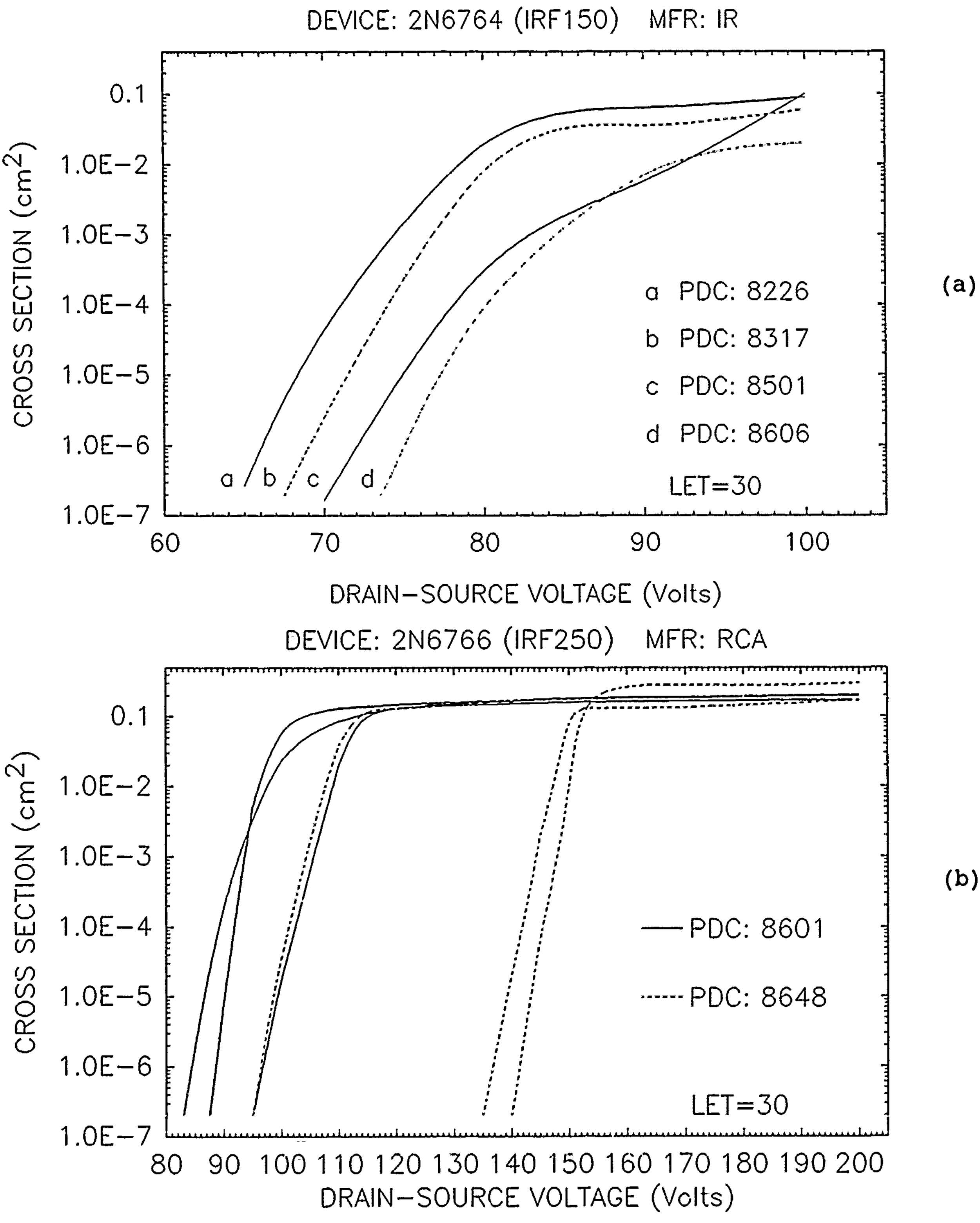

Figure 34. (a) 1982-1986 IR 2N6764 SEB characteristics
(b) 1986 RCA 2N6766 SEB characteristics.

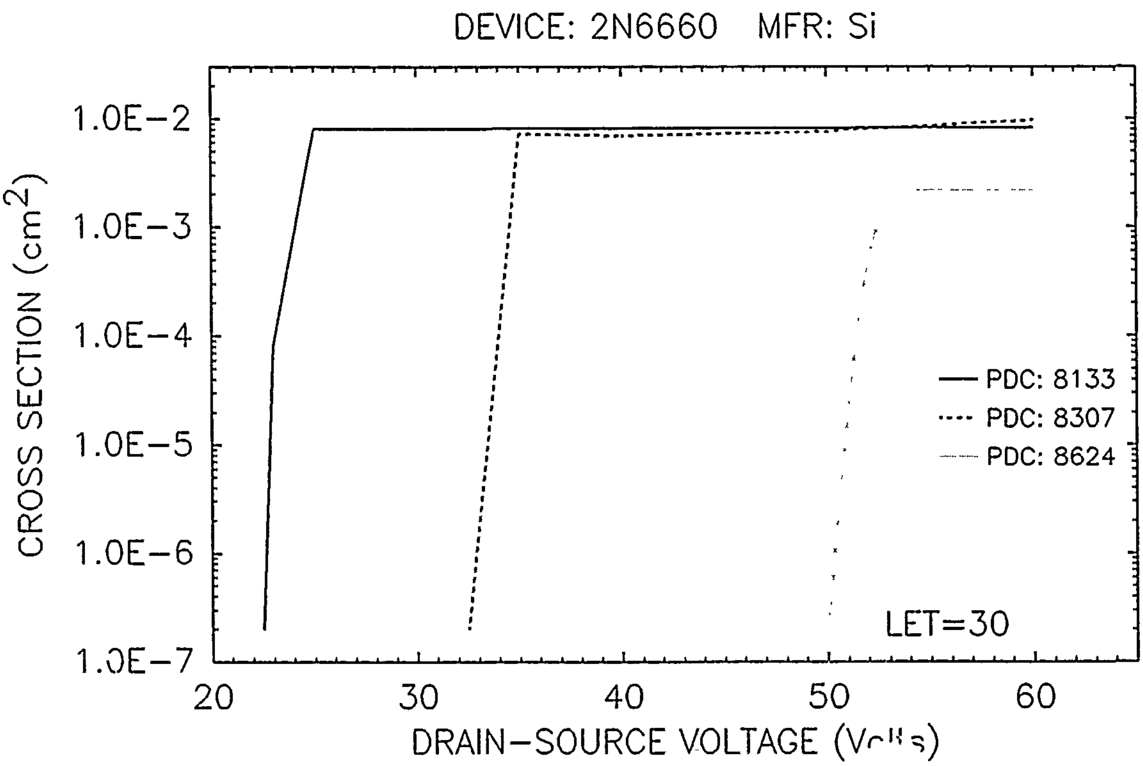

Figure 35. 2N6660 SEB cross section versus date code.

POWER MOS STRUCTURE

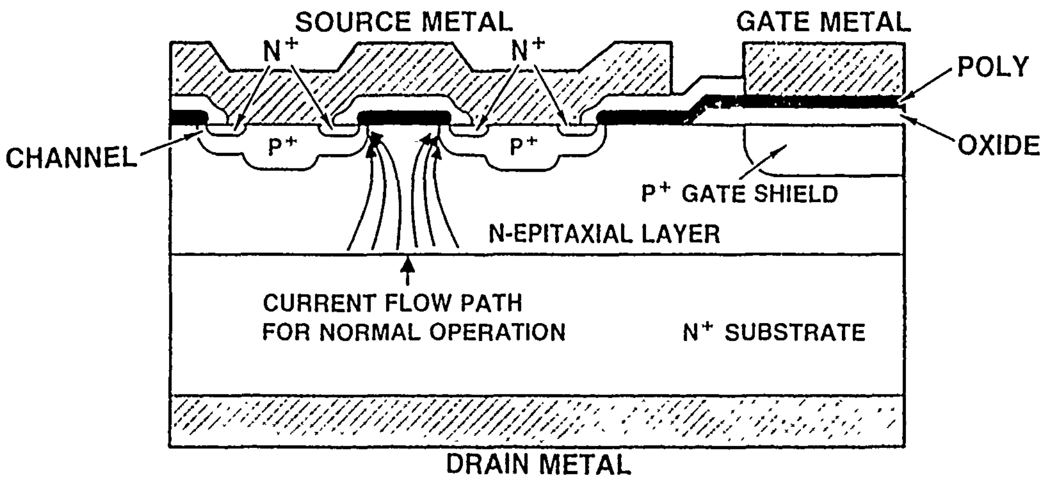

POWER MOSFET TOPOLOGY

SILOX	0.5 microns
SOURCE METAL	5.0 microns
OXIDE	0.8 microns
POLY	0.8 microns
P+ BODY	5.0 microns
N- DRAIN	5.0 - 35.0 microns (BV_{DSS} DEPENDENT)

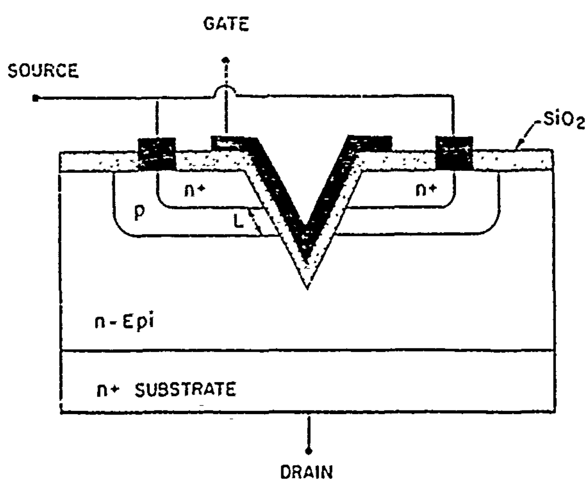

Figure 36. HEXFET and VMOS structure cross sections.

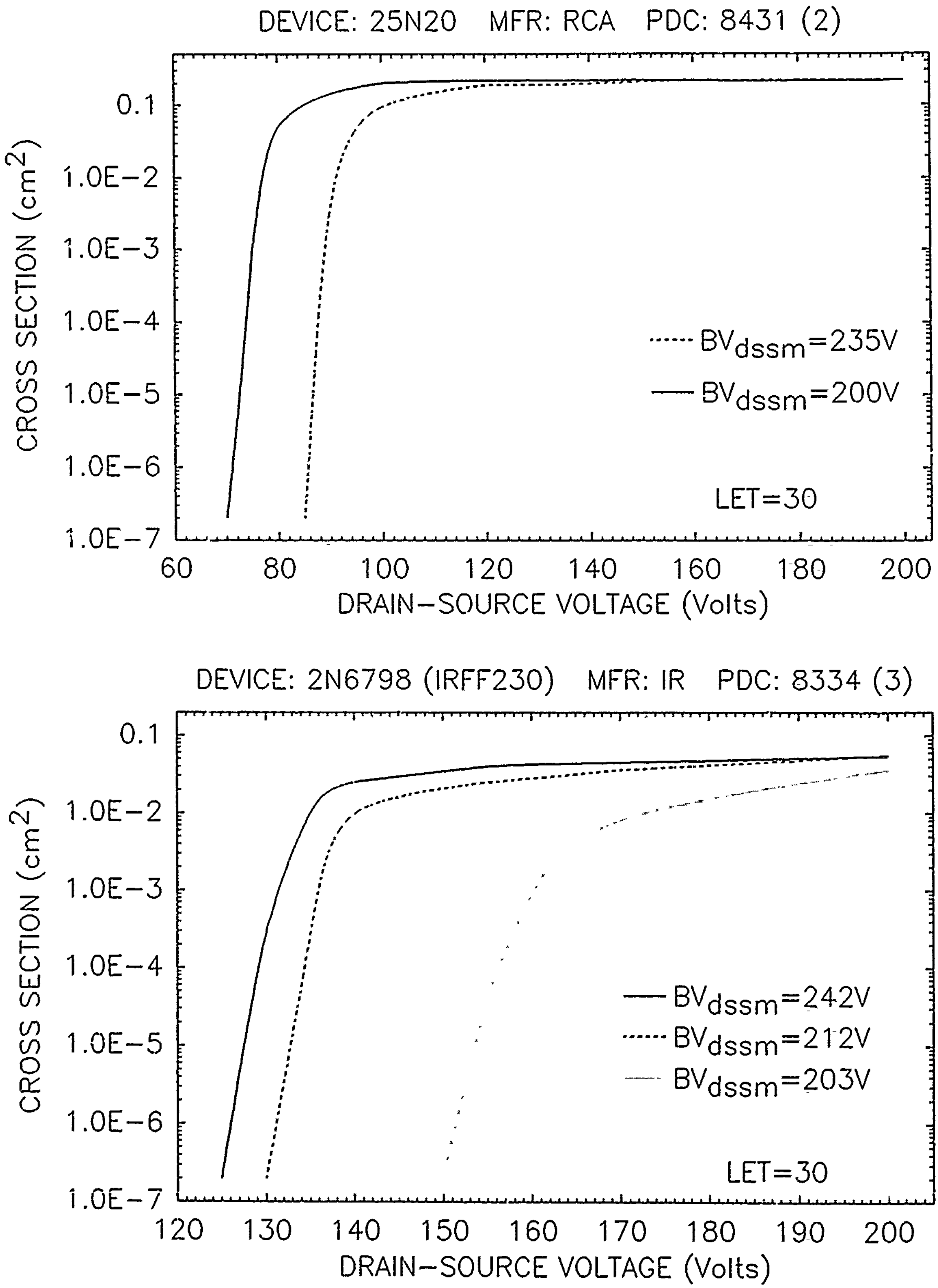

Figure 37. Correlation of V_{DSTH} with BV_{DSSM}.

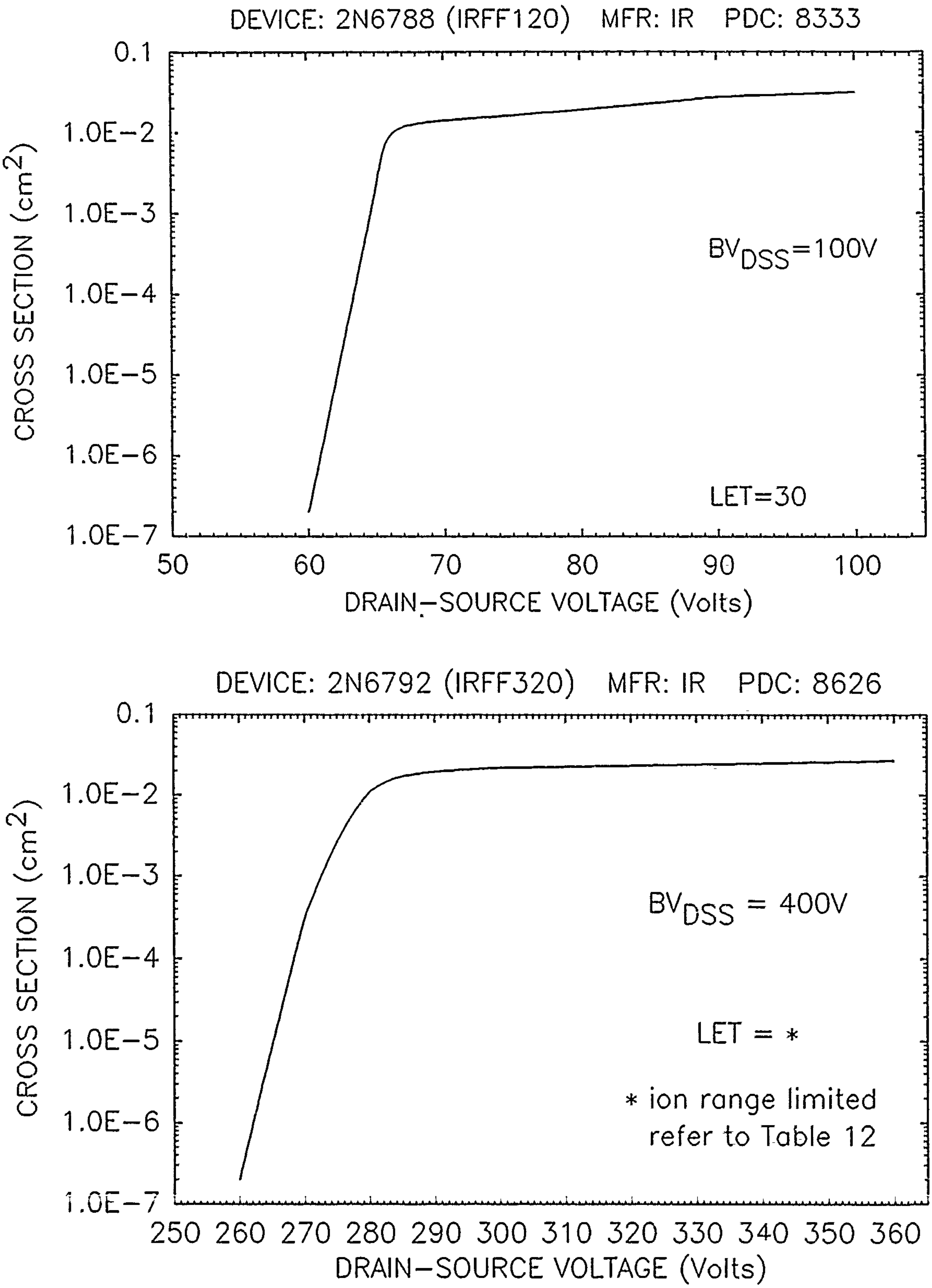

Figure 38. Saturated cross section versus BV_{DSS}.

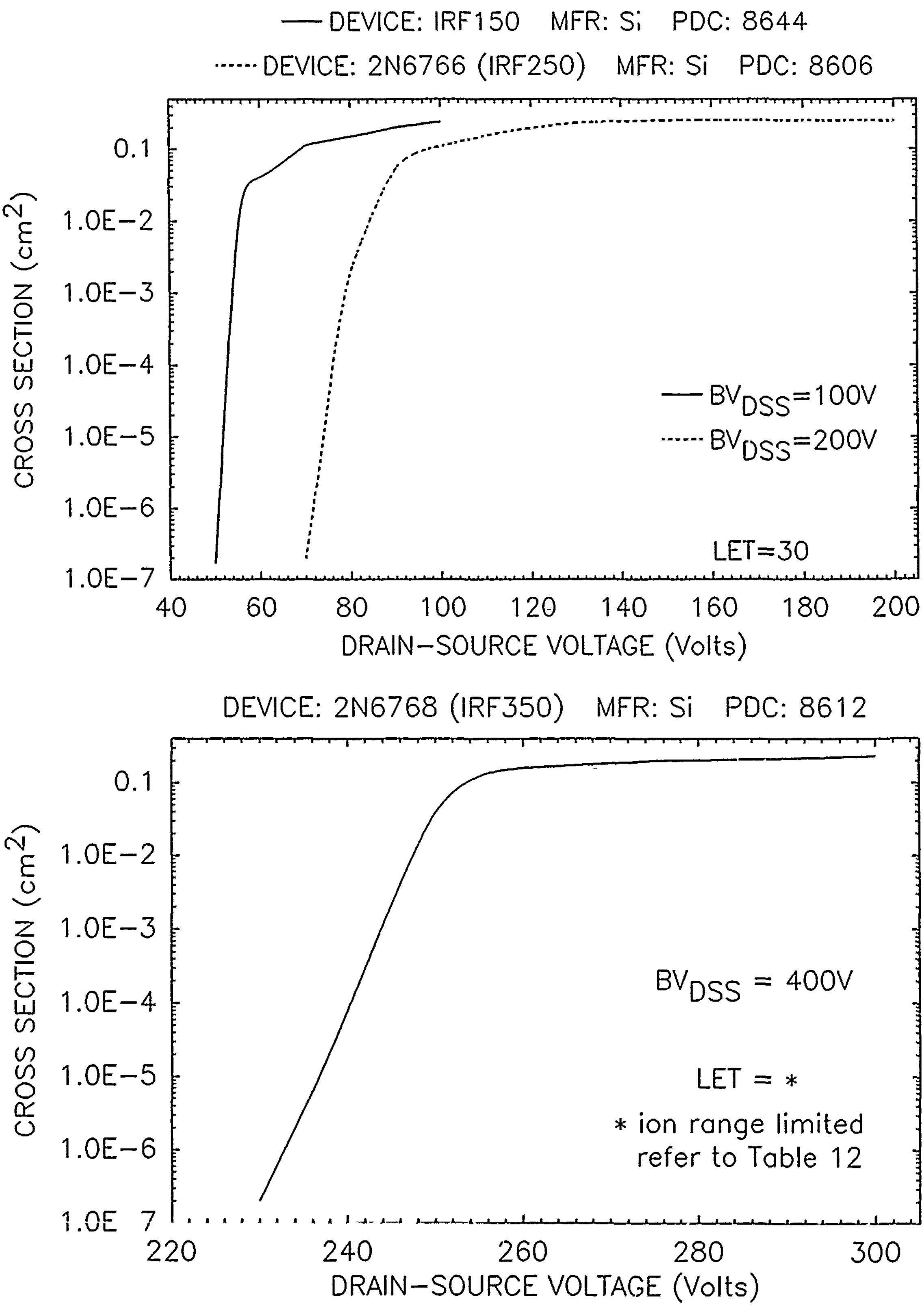

Figure 39. Saturated cross section versus BV_{DSS}.

Table 7. SEB saturated cross sections versus chip size.

HEXFET DIE	CHIP LENGTH (cm)	CHIP WIDTH (cm)	CHIP AREA (A) (cm2)	ESTIMATED ACTIVE AREA (.8A) (cm2)	DEVICE TYPE	MEASURED CROSS SECTION (cm2)	RATIO CROSS SECTION - 0.8A
HEX 1	.241	.175	4.2E-02	3.36E-02	IRFF110	NO SAT.	----
					IRFF210	1.3E-02	0.39
HEX 2	.348	.221	7.7E-02	6.15E-02	IRFF120	3.1E-02	0.50
					IRFF320	2.4E-02	0.39
HEX 3	.445	.292	1.3E-01	1.04E-01	IRFF130	5.7E-02	0.54
					IRF230	4.1E-02	0.39
					IRF430	NO SAT.	----
HEX 5	.653	.653	4.3E-01	3.40E-01	IRF150	1.4E-01	0.41
					IRF250	1.7E-01	0.50
					IRF350	1.4E-01	0.41
2N6660	.076*	.076*	5.8E-03	4.60E-03	2N6660	2.0E-03	0.43

* measured values

SECTION 5

HARDENED DEVICE TEST RESULTS

Fourteen International Rectifier (IR) "hardened" devices were tested with 247-MeV copper ions (11 devices) and 306-MeV krypton ions (3 devices). Two of the devices were also tested with 175-MeV argon ions. The 14 devices included 7 IRH150s (BV_{DSS}= 100V) and 7 IRH 254s (BV_{DSS} = 250V). In addition, eight RCA "hardened" developmental devices were tested with copper ions. The RCA devices included two 150-volt, 500-angstrom; four 300-volt, 500-angstrom and two 300-volt, 700-angstrom thick oxide devices. Tables 8 and 9 list the test results.

For all test biases, including V_{DS} = BV_{DSS}, there were no burnout failures of the seven IR IRH150s tested with copper or krypton ions. However, with V_{DS} = BV_{DSS}, gate damage was observed for both the devices exposed to krypton ions. The gate damage was manifested by an increase in gate leakage after a fluence of $\approx 1\text{x}10^6$ particles/cm^2.

There were also no failures of the five IRH254s exposed to copper ions for all test biases, including V_{DS} = BV_{DSS}. However, there was a burnout pulse detected with krypton ions and applied V_{DS} = BV_{DSS} (250v). "Over-limit" tests (drain-source biases > BV_{DSS} rated, but < BV_{DSS} measured) were performed on the two IRH254s with 8704-date codes. The devices were exposed to copper and argon ions incident at 0° and 60°. Burnout threshold voltages

measured 280, 300, and 265 volts for the 60° and 0° argon ion and 60° copper ion exposures, respectively. Gate leakage was observed during the 295-volt bias, 0° copper ion exposure -- refer to Table 8 for additional details.

Eight RCA hardened developmental devices with date code 8718 were tested with zero degree incident copper ions. All devices had thinner gate insulating oxides than standard MOSFETs -- the RCA Power MOSFET Data Book lists 1000 angstroms as the industry standard thickness of this oxide. The oxide had been thinned in an attempt to improve total dose hardness. Tested were 150-volt and 300-volt rated devices with 500- and 700-angstrom gate insulating oxide thicknesses. For all test bias conditions (including $V_{DS} = BV_{DSS}$ and, in one case, with $V_{DS} > BV_{DSS}$) no indications of burnout were observed. Gate structure degradation, manifested by an increase in gate leakage current, was detected for all devices. The minimum test bias at which gate leakage was detected was 150 volts for the 500-angstrom and 280 volts for the 700-angstrom devices. In some cases, leakage current annealing was observed.

Table 8. IR IRH150 and IRH254 test results.

PART TYPE	PDC	BVdss measured (Volts)	Vds (Volts)	ION	ANGLE (deg.)	BURNOUT CR.SECT. (cm2)
IRH150 (BVdss =100V)	8732-R	122	100	Cu	0	0
		123	100	Cu	0	0
		123	100	Cu	0	0
		124	100	Cu	0	0
	8704	120	100	Cu	0	0
			100	Cu	45	0
			100	Cu	60	0
	8723-R	125	100	Kr	0	0 (1)
	8723-R	124	90	Kr	0	0
			100	Kr	0	0 (2)
IRH254 (BVdss =250V)	8729-R	293	250	Cu	0	0
		295	250	Cu	0	0
		297	250	Cu	0	0
		293	250	Cu	0	0
	8704	309	250	Cu	0	0
			300	Ar	0	1.4E-5
			280	Ar	60	4.4E-5
	8704	305	250	Cu	0	0
			295	Cu	0	0 (3)
			265	Cu	60	5.0E-4
			300	Ar	0	4.4E-5
			280	Ar	60	1.4E-3
	8729-R	294	225	Kr	0	0
			250	Kr	0	7.8E-7 (4)

(1) Gate leakage
(2) Gate leakage after 7E5 p/cm2
(3) Gate leakage after 1E5 p/cm2
(4) Gate leakage after 1.2E6 p/cm2

Table 9. RCA hardened developmental devices test results.

DEVICE	BVdss measured (Volts)	Vds (Volts)	ION	ANGLE (deg.)	BURNOUT CR.SECT. (cm2)
150 Volt 500 Angstrom	242	150	Cu	0	0
	241	100	Cu	0	0 (1)
		200	Cu	0	0
300 Volt 500 Angstrom	345	300	Cu	0	0
	375	250	Cu	0	0 (2)
		300	Cu	0	0
	343	175	Cu	0	0 (3)
		300	Cu	0	0
	355	200	Cu	0	0 (4)
		300	Cu	0	0
300 Volt 700 Angstrom	305	280*	Cu	0	0 (5)
	303	280*	Cu	0	0 (6)

* Test stopped when gate leakage was detected

(1) Gate leakage after 1E4 p/cm2
(2) Gate leakage after 6E4 p/cm2
(3) Gate leakage after 6E4 p/cm2
(4) Gate leakage after 2E4 p/cm2
(5) Gate leakage after 1E5 p/cm2
(6) Gate leakage after 2.2E5 p/cm2

SECTION 6

ELEVATED TEMPERATURE TEST RESULTS

A limited amount of data was obtained on the sensitivity of power MOSFET SEB susceptibility with increased temperature. Burnout cross sections of four devices, representing three device types, were measured at temperatures of 25°C, 50°C, and 100°C. The results are illustrated in Figures 40 and 41. At the highest temperature, an increase of approximately 10% in the 25°C burnout threshold was observed. Sze[5] indicates that at higher temperatures, the breakdown voltage of a Si junction increases and offers the explanation that the increase is the result of the hot carriers passing through the depletion layer losing part of their energy to optical phonons. The value of the electron-phonon mean free path decreases with increasing temperature; therefore, the carriers lose more energy to the crystal lattice along a given distance traveled at constant field. Hence, the carriers must pass through a greater potential difference before they can generate an electron-hole pair, effectively decreasing the electron-hole pair impact generation rate. The reference shows predicted values for the change in breakdown voltage as a function of temperature, parametric with impurity concentration. For an increase of 100°C and an impurity concentration of 10^{15} cm^{-3}, an increase of ≈ 10% in breakdown voltage is predicted. Conversely, the common-emitter current gain should increase and the emitter-base bias to support avalanche decrease, making it easier to turn

on the parasitic bipolar transistor when the device is hot. The results indicate that the decrease in impact ionization generation rate appears to dominate the increased transistor gain and reduced avalanche emitter-base voltage, resulting in a decrease in SEB susceptibility with increased temperature.

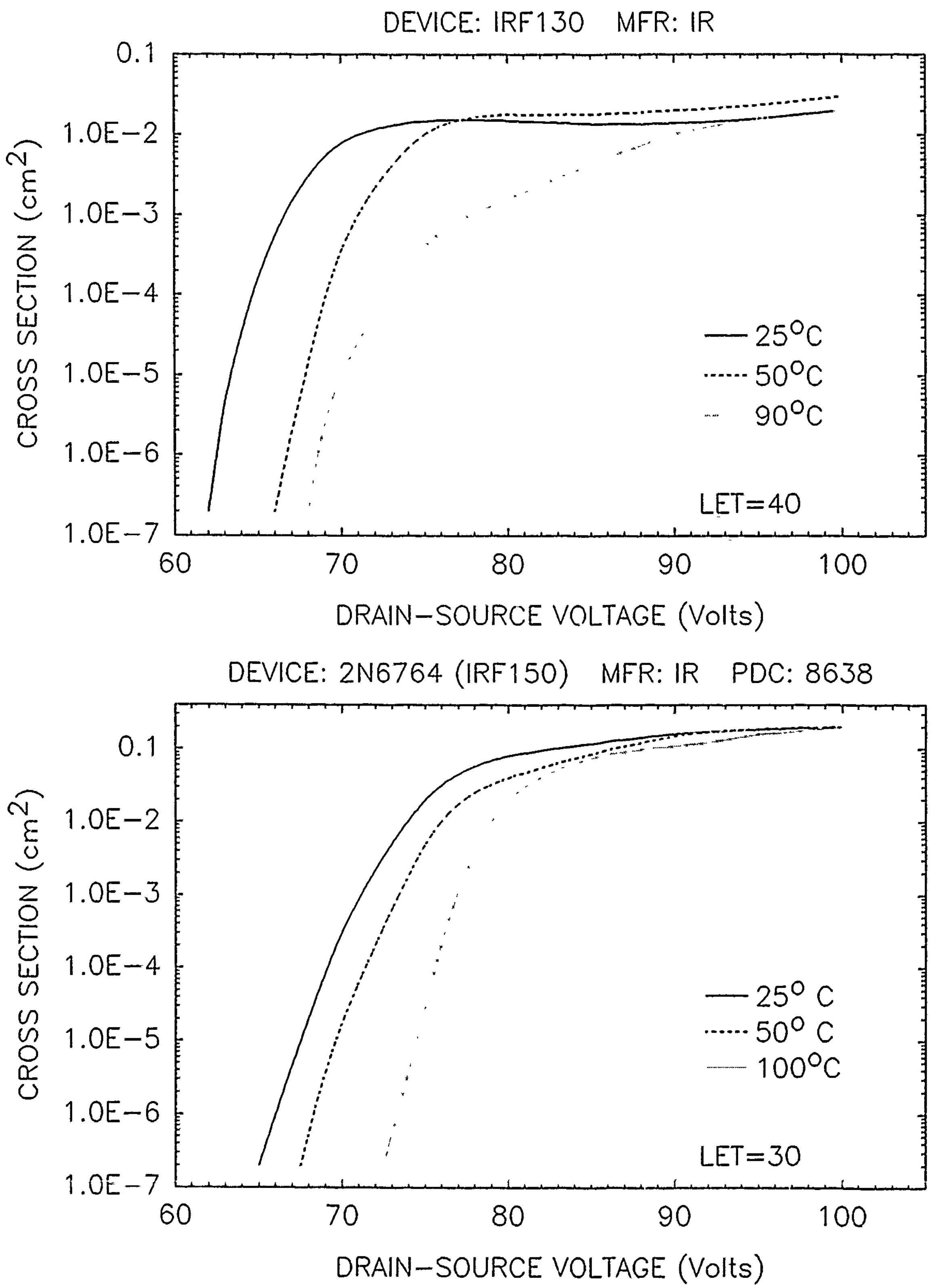

Figure 40. SEB cross section versus temperature.

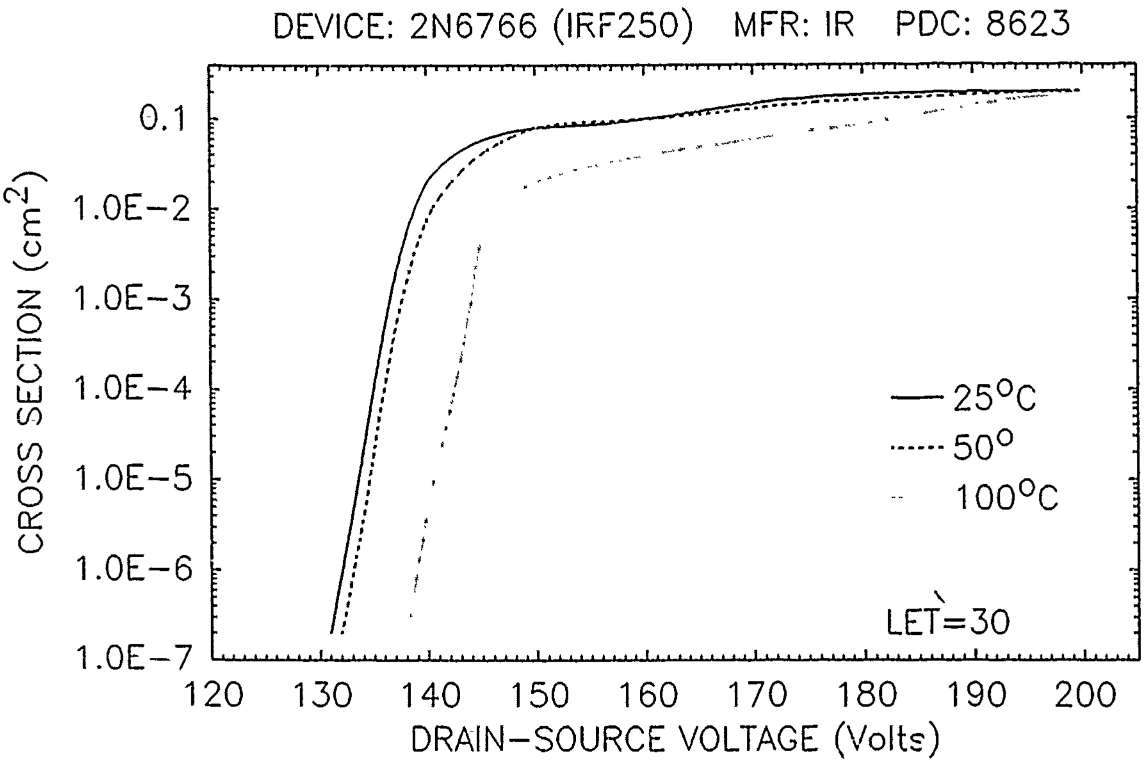

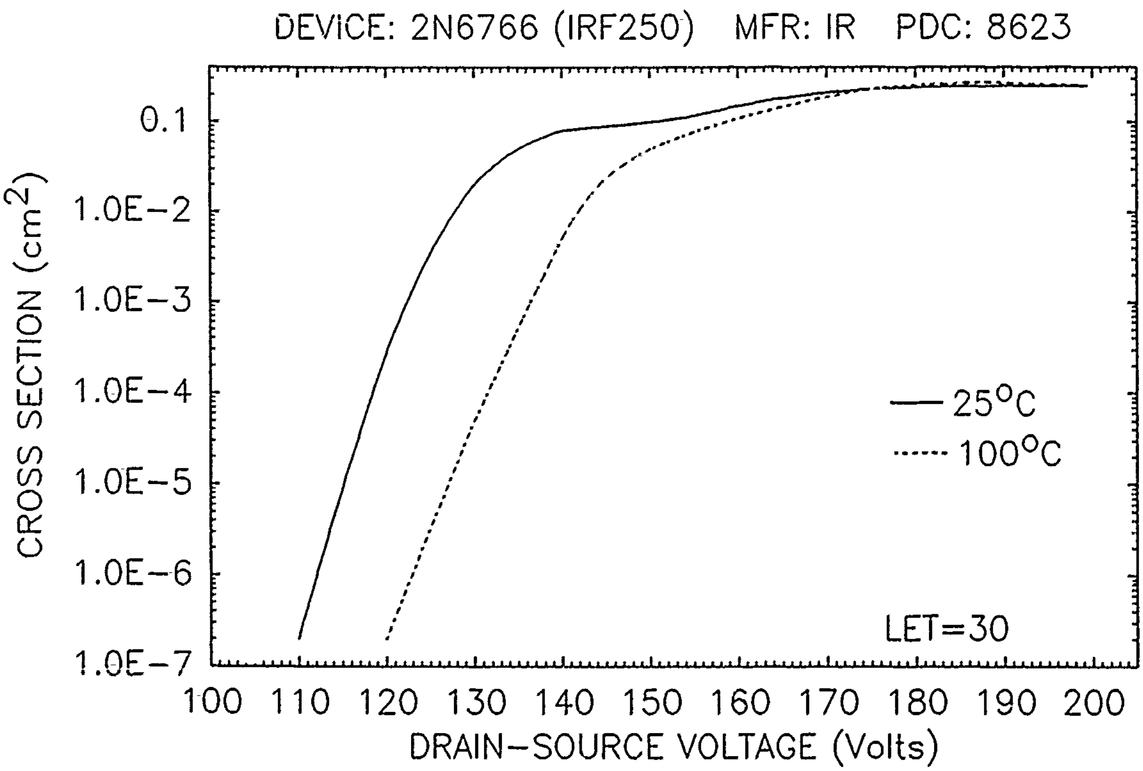

Figure 41. SEB cross section versus temperature.

SECTION 7

TOTAL DOSE AND GATE BIAS EFFECT ON SEB

A modest effort was expended to determine any gross effects of ionizing radiation on the SEB characteristics of power MOSFETs. The burnout cross sections of four 2N6764 (BV_{DSS} = 100v) devices, two with 5 Krad(Si) and two with 20 Krad(Si) total ionizing dose, were compared to cross sections of similar devices with no ionizing radiation exposure. The results are illustrated in Figure 42. No obvious differences were observed in the post-irradiation SEB characteristics of the devices exposed to ionizing radiation.

In addition, a number of devices were tested to determine the effect of gate-source (V_{GS}) bias on SEB. Almost all the SEB characteristics of Section 3 were measured with V_{GS} = -10 volts -- the n-channel MOSFET "hard" off. Figure 43 illustrates typical results for two devices - each device characterized with gate-source biases of -10, 0 and +2 volts. As illustrated by the figure, no discernable difference in SEB cross sections as a function of gate bias was observed.

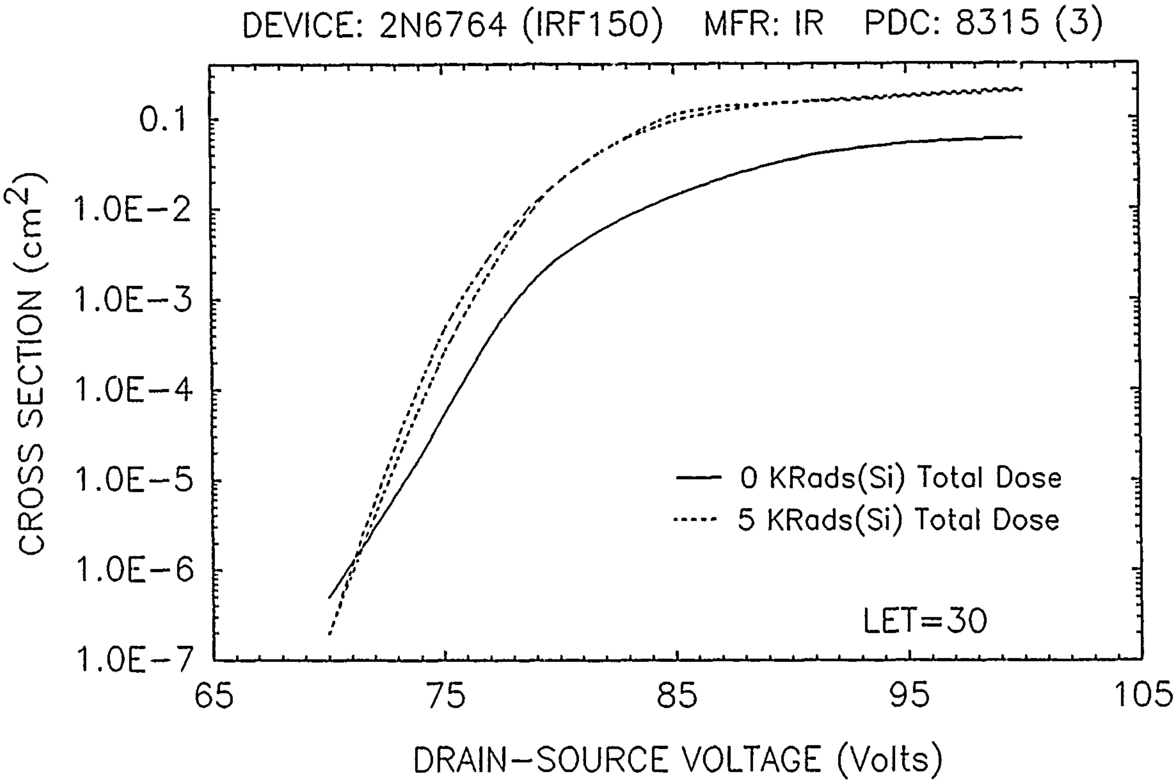

(a)

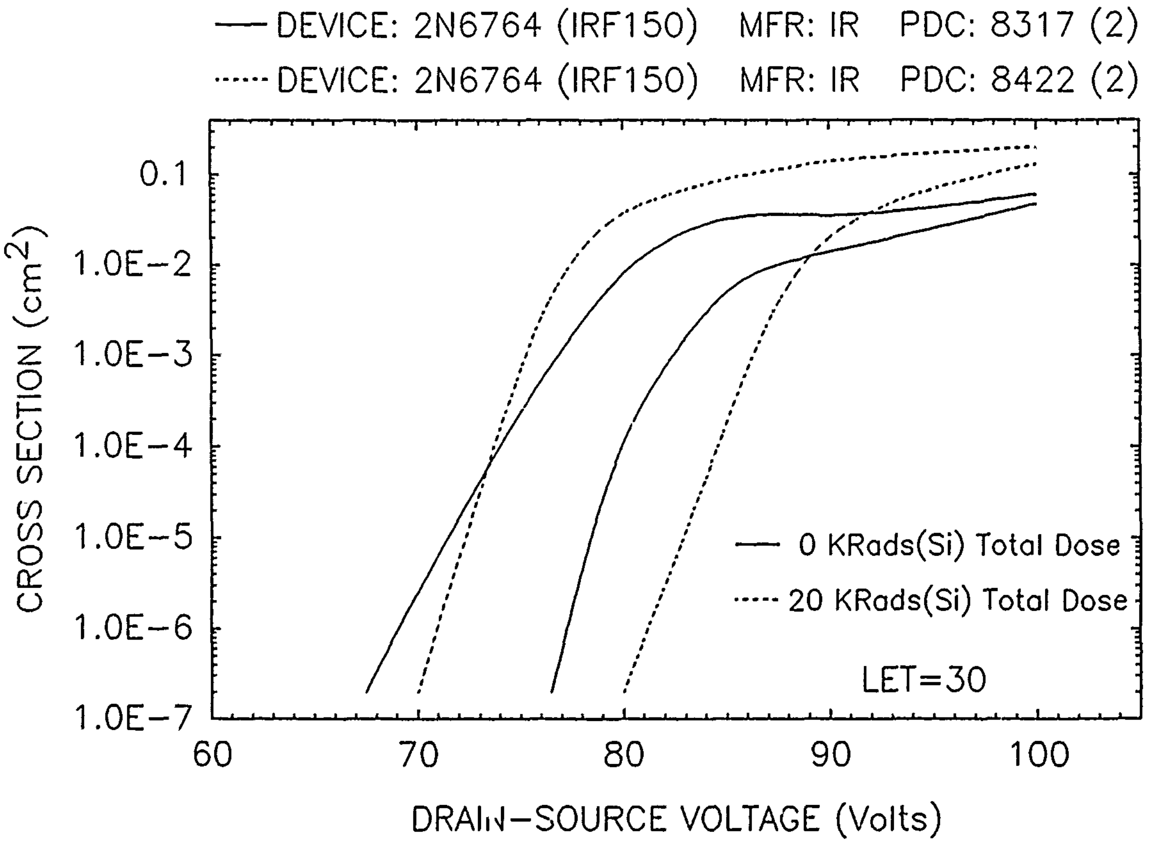

(b)

Figure 42. Post total dose SEB characteristics (a) 5 krad (Si) (b) 20 krad (Si).

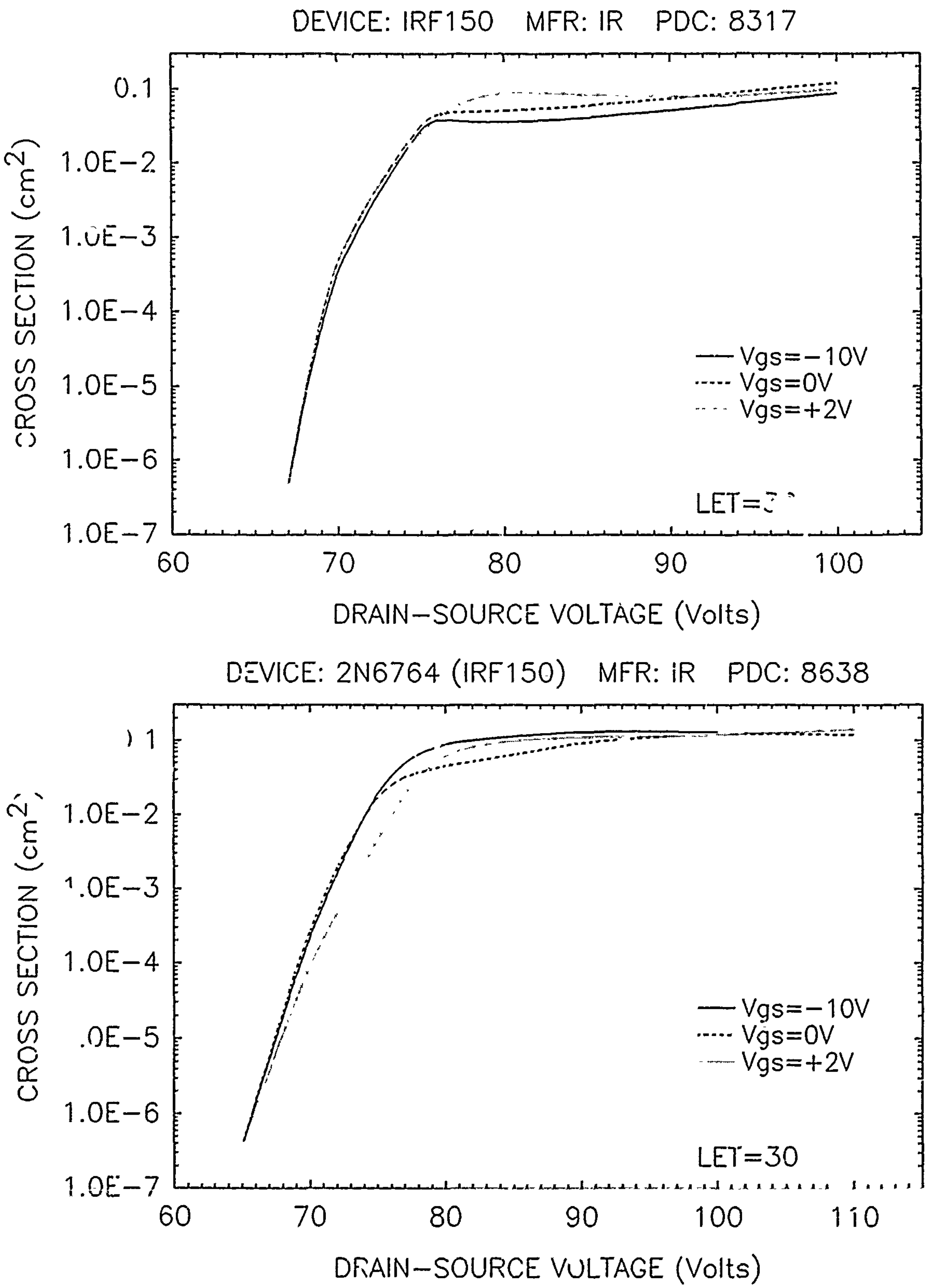

Figure 43. SEB characteristics versus gate bias.

SECTION 8

INDUCTIVE CURRENT LIMITING TEST RESULTS

In many applications, inductive loads are present between the source of power and the drain of a switched MOSFET. The test effort included a limited qualitative inquiry into the effect of a series inductor on SEB susceptibility -- anticipating an effect somewhat analagous to that of the current-limiting resistor of the nondestructive test circuit.

Tests were performed by measuring the device SEB threshold voltage with resistive current limiting, substituting an inductor for the resistor and exposing the device with V_{DS} incremented between exposures until failure was observed. Two tests were performed with a 20 mH toroid in series with the drain and all other tests with inductors ranging in value between 15 and 120 μH. The results are listed in Table 10. In all cases, with one exception, the failure voltage with an inductor was greater than the resistively measured V_{DSTH} for burnout. The results suggest the possibility that burnout could be prevented if the inductive load is large enough -- $\approx$ 60 μH for the 100-volt and $\approx$ 120 μH for the 200-volt BV_{DSS} devices tested. The effect of the inductor was to limit the avalanche current and reduce the drain-source voltage, by L di/dt, to a voltage below the value needed to sustain avalanche and second breakdown.

The intent of the test was to determine if an inductive load had any effect on SEB. The limited amount of test results clearly showed SEB improvement, depending on inductance value. In cases where MOSFET SEB data indicates a questionable amount of margin between design bias values and burnout threshold voltages without inductive current limiting, further testing should be performed to quantify burnout susceptibility improvement, reflecting specific application inductance values.

Table 10. Power MOSFET inductor tests (LET=30 MeV/mg/cm2).

DEVICE TYPE	MFR	PDC	W/O IND. Vds-th (Volts)	WITH INDUCTOR VALUE (uH)	Vds PASS	FAIL
2N6660	Si	8209	27.5	30	60	---
2N6660	Si	8209	27.5	15	60	---
2N6660	Si	8133	22.5	30	50	60
2N6660	Si	8209	32.5	60	60	---
2N6660	Si	8209	32.5	15	50	60
2N6660	Si	8133	22.5	60	50	60
IRFF130	IR	8334	85	15	100	---
IRFF130	IR	8334	75	30	100	---
IRFF130	IR	8549	80	15	100	---
IRFF130	IR	8549	80	30	---	100
IRFF130	IR	8253	85	35	100	---
IRF130	Si	8502	75	47	100	---
IRF130	Si	8518	55	20000	100	---
2N6764	IR	8317	65	30	100	110
2N6764	IR	8317	70	15	80	100
2N6764	IR	8638	70	30	90	100
2N6764	IR	8606	70	15	90	100
2N6766	IR	8617	140	20000	160	---
2N6766	IR	8623	160	60	170	180
2N6766	IR	8623	175	15	---	175
2N6766	IR	8623	145	120	200	---
2N6766	IR	8623	157	30	---	170
2N6766	IR	8617	130	60	135	150
2N6766	IR	8617	125	60	140	150
2N6766	IR	8617	120	30	125	140
2N6766	IR	8614	140	30	150	160
2N6766	RCA	8601	90	20	175	200
2N6766	RCA	8648	100	20	150	175
2N6766	RCA	8601	100	120	200	---
2N6766	RCA	8601	90	60	150	160
2N6766	RCA	8601	125	30	135	150

SECTION 9

PROTON TEST RESULTS

Twenty-six devices representing eight device types were tested with 50-MeV and 150-MeV protons from the Harvard Cyclotron. Table 11 lists the devices tested and summarizes the results. Figure 44 illustrates the proton cross section data for the 2N6660 and [illegible] MOSFETs.

[illegible] indicated in the table, exposure to protons induced failure in some of the n-channel devices tested. Failures were observed in three of the eight device types tested. However, the failure cross sections were small (< 10^{-8} cm^2) and, perhaps more significantly, most of the V_{DS} burnout biases were at or near the rated device breakdown voltage. Almost all of the tests were performed with 150-MeV protons, but data taken with 50-MeV and 150-MeV protons indicated no differences. Despite the small amount of test data on these devices with heavy ions other than copper, there appeared to be a correlation between the proton and heavy ion test results. In all cases, with one exception, devices which failed with protons also failed exposure to 67-MeV nitrogen ions (LET ≈ 3). The small burnout cross section and nitrogen ion data correlation support a proton-nucleus reaction in silicon as the cause of the proton-induced ionization leading to failure.

Table 11. Power MOSFET proton test results.

PART TYPE	NON-JEDEC P/N	BVdss (Volts)	MFR	PDC	NO. OF DEV.	NO.OF DEV. FAILED	% OF RATED BVdss AT FAILURE	AVERAGE FAILURE FLUENCE
2N6660	----	60	Si	(1)8133	3	3	67, <83,<91	4.8E+08
				(1)8307	3	2	<100, 100	4.5E+10
				(2)8624	1	0	* ----	---
2N6756	IRF130	100	IR	8126	1	0	* ----	---
2N6796	IRFF130	100	IR	8549	1	0	* ----	---
			Si	8518	2	0	* ----	---
2N6764	IRF150	100	IR	8315	1	0	* ----	---
				8606	2	0	* ----	---
IRH150	----	100	IR	8644	1	0	* ----	---
2N6766	IRF250	200	GE	8608	2	2	90, 95	1.3E+10
2N6756			IR	8610	1	1	100	5.3E+10
			RCA	8550	2	2	90, 100	7.0E+09
			Si	8548	2	2	90, 90	1.8E+09
				8606	2	2	88, 90	1.2E+10
25N20	----	200	RCA	8431	2	2	88, <100	9.0E+09
IRH254	----	250	IR	8644	1	0	** ----	---

* Tested at maximum bias (Vds=BVdss)
** Tested at maximum bias of 200V
(1) VMOS structure
(2) HEXFET structure

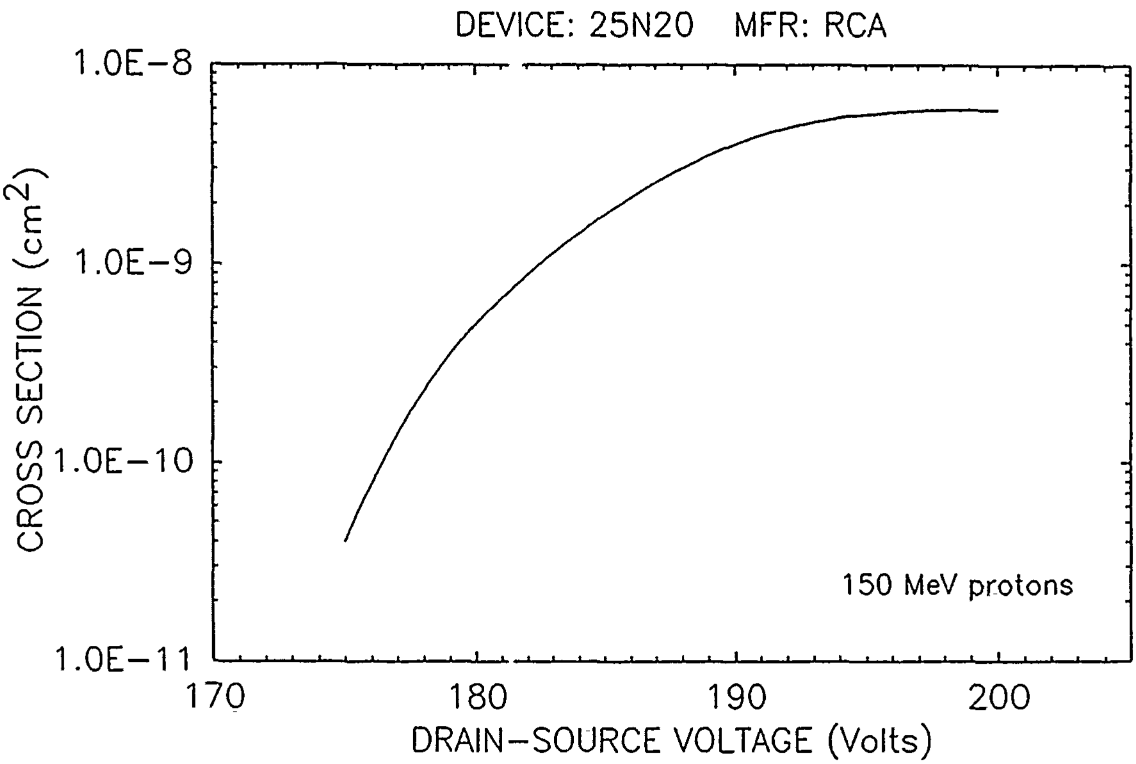

(a)

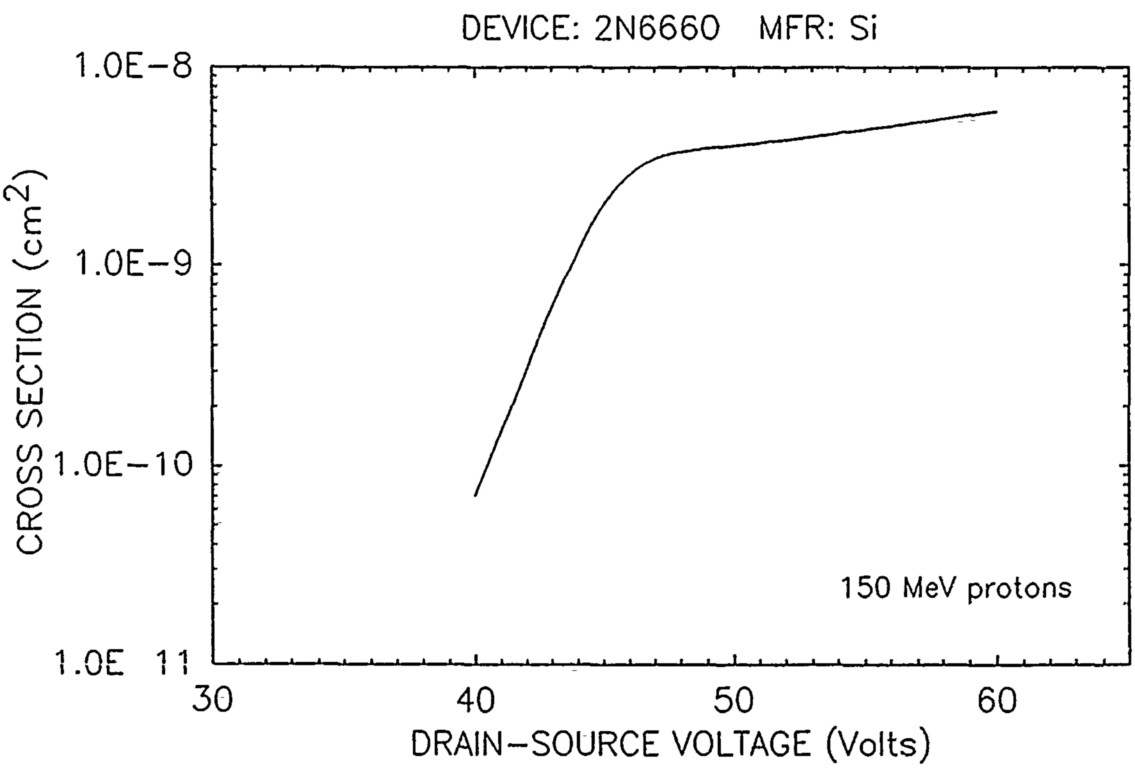

(b)

Figure 44. (a) 25N20 (b) 2N6660 proton SEB characteristics.

SECTION 10

SEB CHARACTERIZATION WITH ION ANGLE OF INCIDENCE

Some burnout cross-section measurements were performed as a function of ion angle of incidence. Examples of the observed opposing trends in MOSFET response as a function of ion angle of incidence and device breakdown voltage are indicated in Figures 45 and 46. Burnout threshold voltages (V_{DSTH}) slightly decreased with increasing exposure angle for the lowest (60V) and highest (500V -- not shown) rated devices, whereas V_{DSTH} increased with increasing exposure angle for the 100-, 200-, and 400-volt devices. The apparent contradiction in trends can possibly be explained by particle range limitations with angles of incidence.

Table 12 lists the LET values of 247-MeV copper ions incident at 0° and 60° as a function of penetrated depth in silicon[8]. The distances were chosen to coincide with the body-drain junction depletion depths of the various voltage rated devices. The depletion depth was calculated using Sze's avalanche voltage versus impurity concentration for one-sided abrupt junctions in Si and the relationship for the depletion width (W_D) given by:

$$W_D = \left[\frac{2 \epsilon \epsilon_o V}{q N_D} \right]^{1/2}$$

The results of the calculations indicated that after 0°-incident ions penetrate to the depletion depth of a 300-volt device and

60°-incident ions penetrate to the depletion depth of a 60-volt device, the LET of the ions begin to degrade. In addition, the 60°-incident ions are stopped within the depletion layer of devices with breakdown voltages greater than 200 volts. The calculations suggest that possibly the 0° data for the 400-, and 500-volt devices, and the 60° data for the 100-, 200-, 300-, 400-, and 500-volt devices was affected by ion range limitations. The calculations further suggest that the trend in the data with angle of incidence for the 60-volt devices, devices with the shallowest active depth, was not affected by particle range limitations. The unaffected 60-volt HEXFET data in Fig. 46 indicates a slight decrease (less than 1%) in V_{DSTH} with 60°- versus 0°-incident ions. This slight decrease could possibly be caused by the slightly higher value of LET of the 60°-incident ions within the 60-volt device depletion region (refer to Table 12). Considering the magnitude of the change in V_{DSTH} and increase in LET, it is believed the 60-volt device data supports the inference that, in the absence of ion range limitations, there is little or no change in V_{DSTH} with ion angle of incidence.

Table 12. LET of 0- and 60-degree incident Cu vs. vertical distance (Si).

POWER MOSFET FEATURE	VERTICAL DIST. (D) (um)	0 DEGREE 247 MeV COPPER ION PATH LENGTH (um)	0 DEGREE 247 MeV COPPER AFTER DEPTH (D) ENERGY (MeV)	0 DEGREE 247 MeV COPPER AFTER DEPTH (D) LET (MeV/mg/cm2)	60 DEGREE 247 MeV COPPER ION PATH LENGTH (um)	60 DEGREE 247 MeV COPPER AFTER DEPTH (D) ENERGY (MeV)	60 DEGREE 247 MeV COPPER AFTER DEPTH (D) LET (MeV/mg/cm2)
MOSFET Surface	0	0	247	30.1	0	247	30.1
Metal/Oxide-Si Interface	7	7	197	31.6	14	144	33.3
Body-Drain Metallurgical Junc.	10	10	175	32.3	20	97	33.7
BVdss=60V Depletion Depth	13	13	152	33.1	26	51	31.3
BVdss=100V Depletion Depth	16	16	129	33.6	32	14	20.7
BVdss=200V Depletion Depth	20	20	97	33.7	40 (1)	--	--
BVdss=300V Depletion Depth	28	28	37	28.8	40 (2)	--	--
BVdss=400V Depletion Depth	33	33	10	17.9	40 (2)	--	--

(1) Stopped at depletion width
(2) Stopped within depletion region

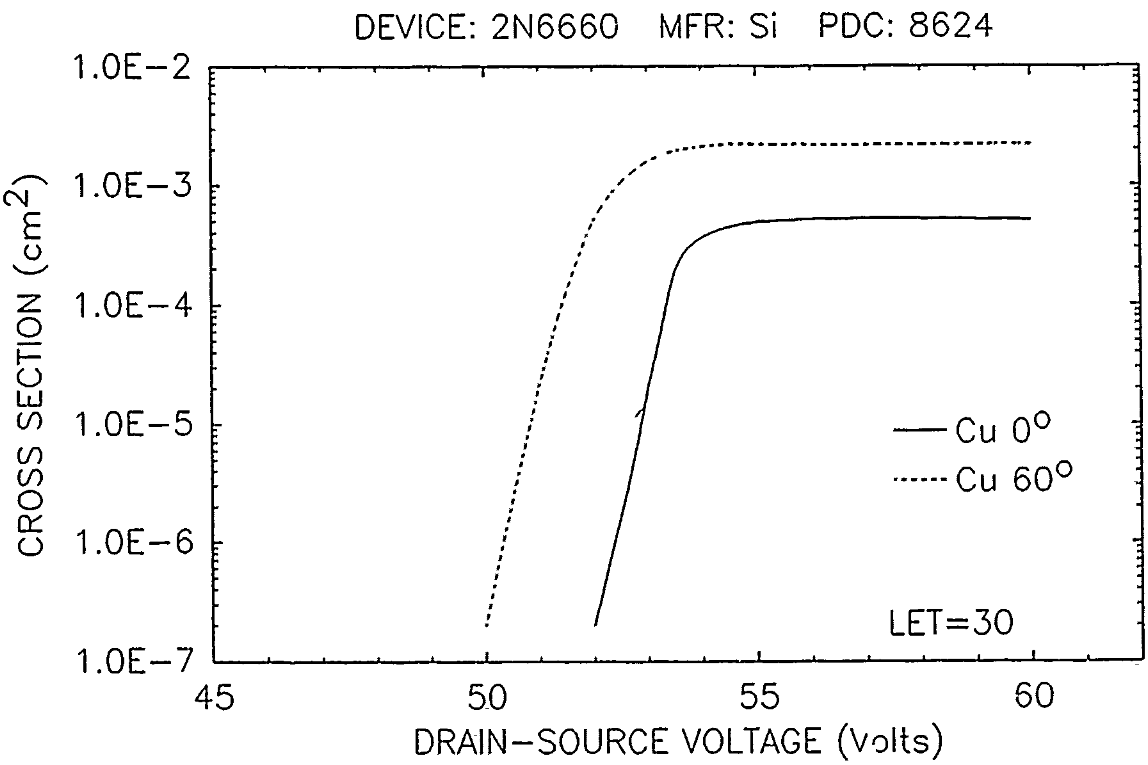

(a)

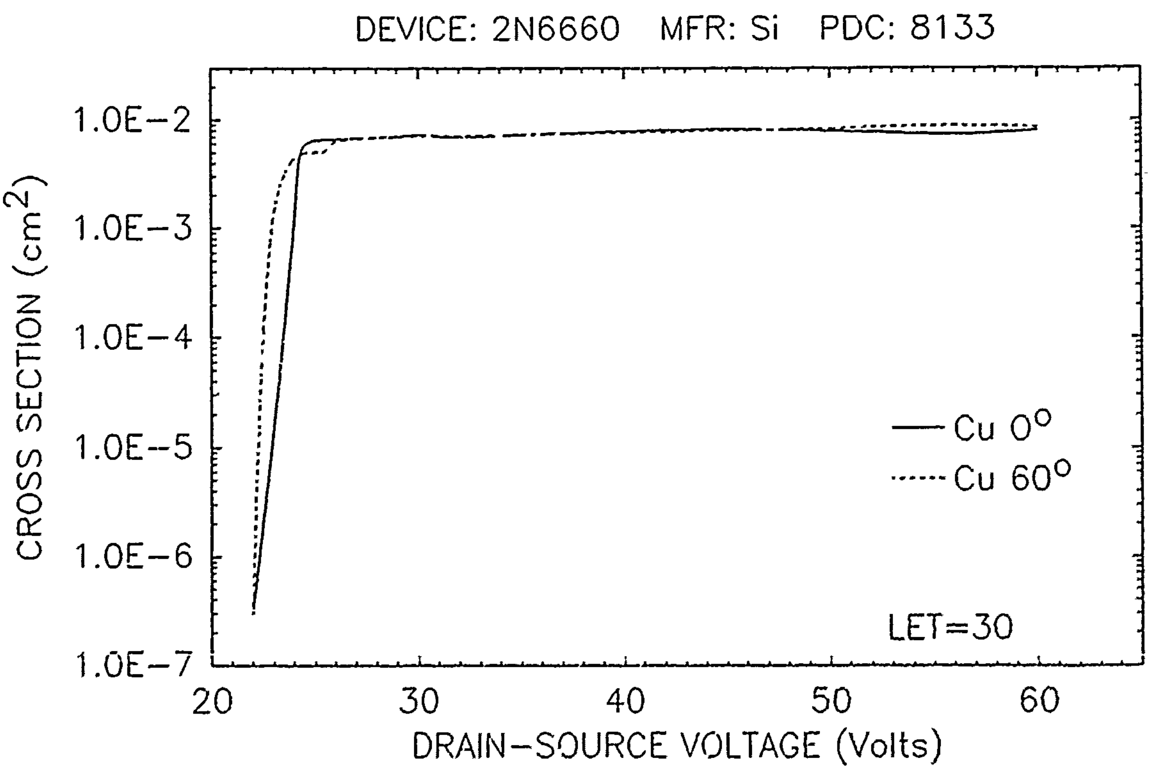

(b)

Figure 45. (a) HEXFET and (b) VMOS SEB cross section versus angle of incidence.

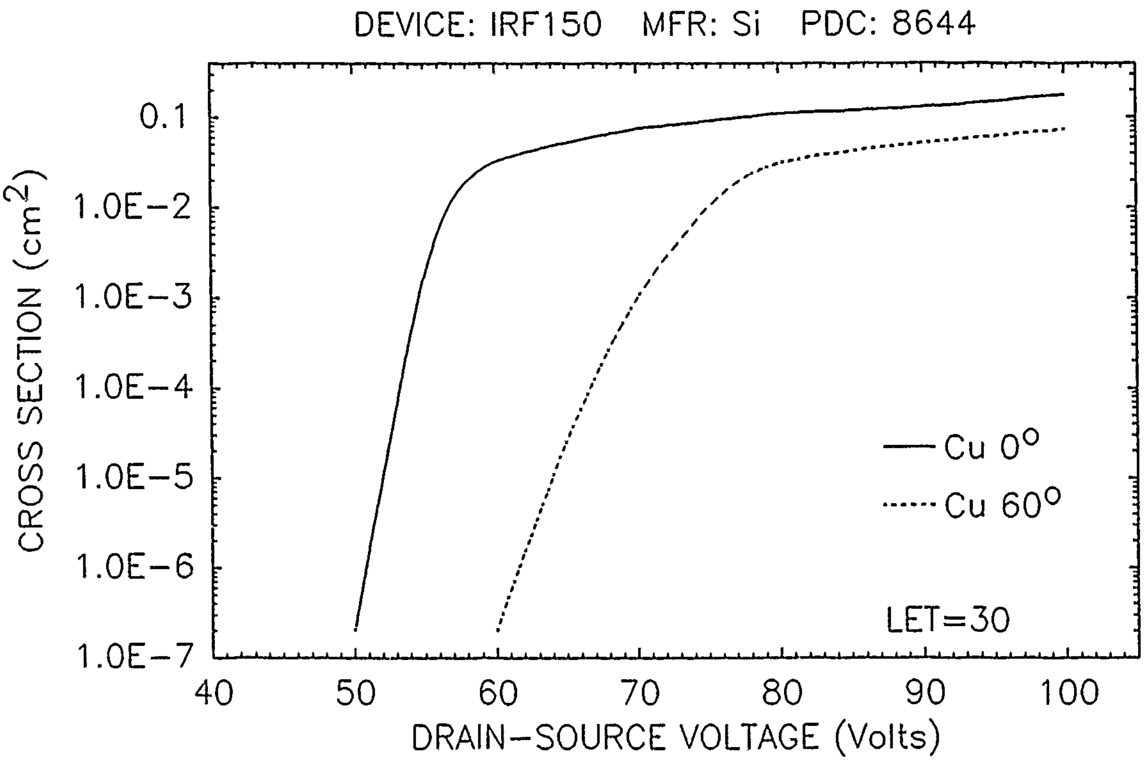

(a)

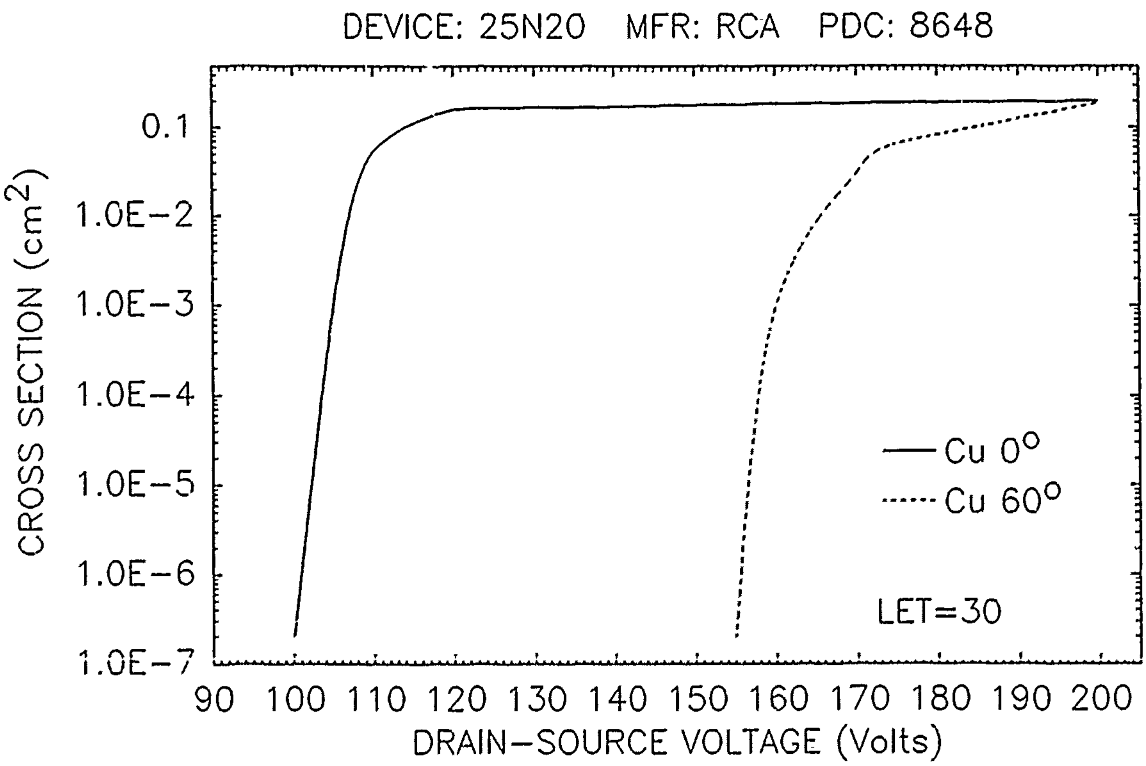

(b)

Figure 46. (a) IRF150 and (b) 25N20 SEB cross section versus angle of incidence.

SECTION 11

POSSIBLE FAILURE MECHANISMS

At least two types of failures have been observed during the power MOSFET testing effort, failures associated with the silicon junctions of the field effect transistor and failures of the gate oxide-polysilicon structure. Silicon junction failures were catastrophic, manifest in drain-source short circuits. Gate structure failures resulted in an increase in gate leakage or catastrophic rupture of the gate oxide. Both types of failures have been observed in other power MOSFET tests[6]. During this test effort, only n-channel MOSFET failures were observed, and only a small percentage of the n-channel failures were gate failures. P-channel devices tested were found to be insensitive to heavy ion induced burnout. Because of the relative immunity of the p-channel devices, only a few types were tested, decreasing the probability of observing any p-channel gate failures.

Gate structure failures were mainly observed in the hardened devices. Some of the hardened developmental devices had thinned insulating gate oxides to improve total dose hardness and appeared to be more vulnerable to ion-induced gate structure damage. With the exception of the devices with thinned gate oxides, the results do not necessarily indicate that hardened devices are more susceptible to induced gate failure, but reflect the fact that these devices were tested with higher applied drain-source biases without silicon burnout. A possible failure mechanism is that the

electrically neutral high-concentration core region of the heavy ion particle track effectively caused the localized collapse of the drain depletion region, for an instant, resulting in a large potential difference across the ion track in the gate oxide. If the resultant electric field in the oxide is large enough, the gate oxide will breakdown and possibly rupture. The observed failures appeared to require both large bias and high LET particle and, in the case of the thinned-oxide devices, appeared to be gate bias dependent.

Figure 47 illustrates a typical DMOS transistor cross section and includes the body-drain diode and parasitic bipolar transistor, formed by the source and body diffusions and the drain region. The body-drain diode and parasitic transistor are effectively in parallel with the field effect transistor of the device and together determine the MOSFET rated breakdown voltage, BV_{DSS}. The resistance R_B is internal to the structure and has a value determined by the resistivity and dimensions of the p-body beneath the source. The power MOSFET's ability to sustain blocking voltages requires that the internal parasitic bipolar transistor never approach the conducting state. The effect of forward biasing the parasitic is shown in Figure 48. The figure illustrates bipolar transistor breakdown characteristics for various base-emitter bias conditions. The resistor R in the figure is effectively R_B for a power MOSFET. Avalanching and "dv/dt turn-on" are two principal mechanisms which can cause

lateral current flow in the p-body region with the resultant voltage drop across R_B tending to forward bias the base-emitter junction of the parasitic bipolar transistor. The purpose of the p+ body-drain diode, designed with a lower breakdown voltage, is to initiate avalanche and reduce the voltage across the channel body-drain junction, thereby circumventing avalanching and lateral current flow in the p-body region. In addition, the diode provides a vertical low-impedance shunt path for the avalanche current through the p+ portion of the body to the source metallization (ground).

A third mechanism which can cause lateral current flow in the p-body region is exposure to energetic heavy ions. Lateral current through R_B can result from the charge collected from the ionization track of a particle traversing the high-field drain depletion region of the FET. If the ion-induced lateral current through R_B is sufficient to forward bias the base-emitter junction of the parasitic bipolar transistor, the transistor will begin to conduct, and the breakdown characteristics of the structure will be determined by the collector-emitter breakdown voltage under forward bias conditions -- the BV_{CER} characteristic of Figure 48. If the applied drain-source voltage is greater than BV_{CEO}, the avalanche current can become regenerative and the excessive local power dissipation caused by current-induced avalanche (CIA)[7] leads to device burnout.

The mechanism described requires the following conditions for second breakdown and burnout:

1) The charge collected from the particle ionization track must generate sufficient voltage to forward bias the base-emitter junction of the parasitic transistor. The condition implies that the ion track location cause lateral current to flow across the FET body. An ionization track through the p+ portion of the body would not satisfy this condition. But an ionization track through the FET channel region, depositing sufficient charge in the drain depletion layer, could initiate the condition leading to parasitic transistor turn-on and second breakdown.

2) The applied drain-source voltage must be greater than the collector-emitter breakdown voltage of the forward-biased parasitic transistor (BV_{CEO}).

Hohl and Galloway[3] have presented an analytic model of a power MOSFET -- quantitatively explaining the mechanisms leading to burnout in power MOSFETs exposed to heavy ions. The model appears to agree with the suggested burnout mechanism of this section.

Section 2 presents data indicating p-channel MOSFETs to be insensitive to induced burnout with applied $V_{DS} = BV_{DSS}$. The results support the suggested burnout failure mechanism of this section. The electron-hole pair generation rate G from impact ionization

is given by Sze[5] as

$$G = \alpha_n \, n \, v_n + \alpha_p \, p \, v_p$$

where α_n and α_p are the respective electron and hole generation rates, defined as the number of electron-hole pairs generated by an electron or hole per unit distance traveled. Sze indicates, in the presence of a high electric field, α_n to be an order of magnitude greater than α_p. This would mean that, for a p-type drain, less charge would be collected by the body region -- the base of the parasitic -- than for an analogous n-type device. In addition, due to differences in resistivity for equal body impurity concentrations, the resistance of the n-body of the annel device would be less than for a corresponding n-channel i. The combination of lower impact ionization rate and lower resistanc. would make it more difficult to turn on the parasitic transistor, resulting in the p-channel MOSFET being less sensitive to heavy-ion-induced burnout.

The suggested failure mechanism does not require the ion to completely penetrate the device depletion region, but only deposit sufficient charge to cause the activation of the parasitic transistor -- a condition supported by Californium-252 test results. Fission particles of Cf-252 have a maximum range between 12 and 15 μm in silicon and decrease in LET with penetration depth. According to the calculations in ' ole 12, the ions of

Cf-252 would be stopped within the drain depletion regions of devices with BV_{DSS} > 100 volts. The saturated cross section for a 2N6766, BV_{DSS} = 200v, measured at V_{DS} = 200v with Cf-252 -- ions stopped in the depletion region -- was 0.20 cm^2. The saturated cross section of the same device type measured at V_{DS} = 200v with 247 MeV copper ions (range ≈ 40 μm) -- ions penetrating through the depletion region -- was 0.21 cm^2.

An observed trend in the data was for the burnout cross section at threshold, $V_{DS} = V_{DSTH}$, to be several orders of magnitude less than the cross-section asymptotic value with $V_{DS} \gg V_{DSTH}$. In addition, the initial slope of the SEB characteristics varied for different device types. The cross-section data for the HEXFET 2N6660 (BV_{DSS} = 60v) indicated saturation with an applied bias of V_{DSTH} + 5v. Some of the 2N6766s (BV_{DSS} = 200v) required V_{DS} = V_{DSTH} + 25v for saturation. The 2N6660, the device with the smallest chip die and the least number of transistors, had the simplest gate structure. The 2N6766 had a more complex structure with a gate pad and several gate stripes and transistors adjacent to gate stripes terminating the gate shield. The greater slope of the SEB characteristics of the more complex devices suggests regions of different burnout sensitivity with $V_{DS} \approx V_{DSTH}$, perhaps influenced by the variation in the field across the complex structure. However, as illustrated in Section 4.3, with $V_{DS} \gg V_{DSTH}$ variations in the field across the device topography become less critical, and all transistors contribute to the heavy-ion-induced burnout of the device.

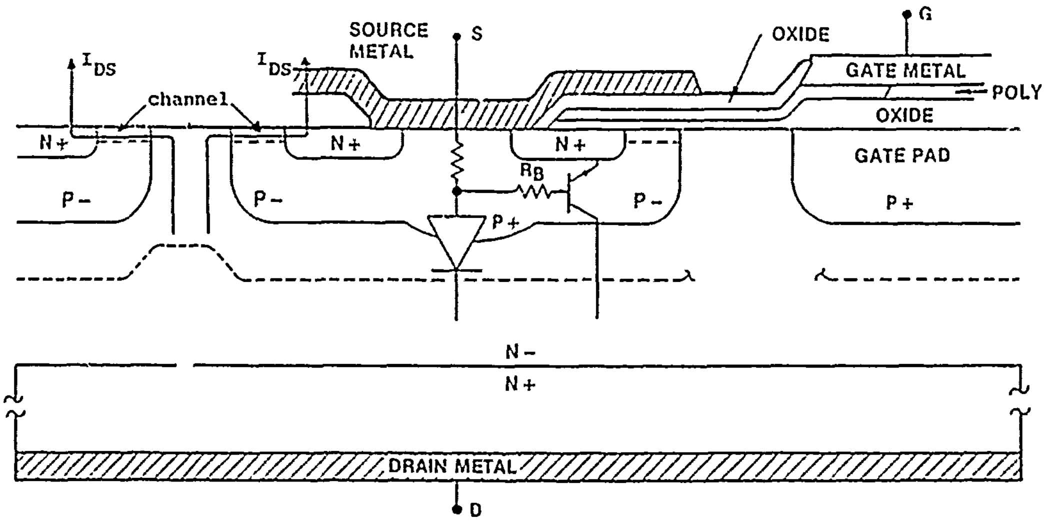

SILOX, S-METAL, OXIDE	6.3	MICRONS	
POLY	.8	MICRONS	
OXIDE	.8	MICRONS	
P BODY	5.0	MICRONS	
N-EPI LAYER	5-35	MICRONS	(BV_{DSS} DEPENDENT)

Figure 47. HEXFET structure cross section.

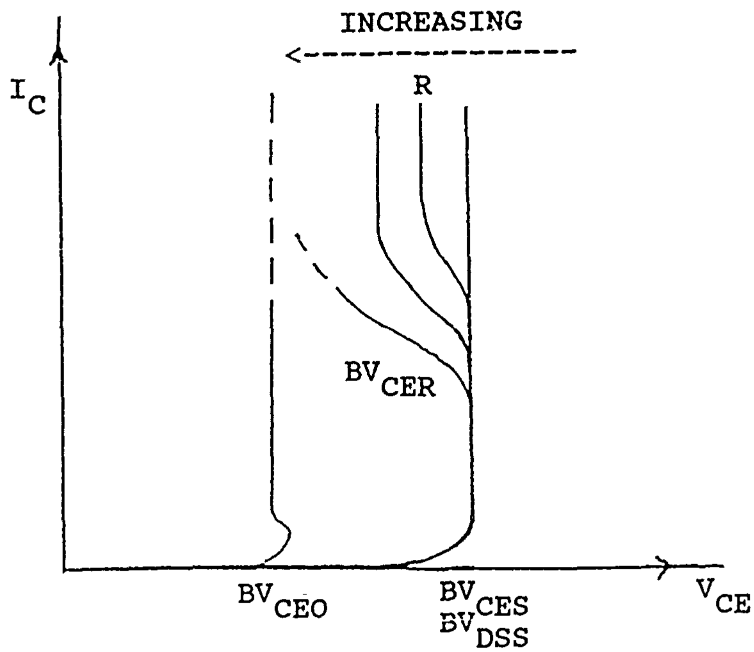

Figure 48. Bipolar transistor breakdown characteristics.

SECTION 12

LIST OF REFERENCES

1) A. E. Waskiewicz, J. W. Groninger, V. H. Strahan, and D. M. Long, "Burnout of Power MOS Transistors with Heavy Ions of Californium-252," IEEE Trans. Nuc. Sci., NS-33, pp. 1710-1713, 1986.

2) D. L. Oberg and J. L. Wert, "First Nondestructive Measurements of Power Mosfet Single Event Burnout Cross Sections," IEEE Trans. Nuc. Sci., NS-34, p. 1736, 1987.

3) J. H. Hohl and K. F. Galloway, "Analytical Model for Single Event Burnout of Power Mosfets," IEEE Trans. Nuc. Sci., NS-34, pp. 1275-1280, 1987.

4) International Rectifier "HEXFET Power MOSFET Designer's Manual," 4th Edition, 1987.

5) S. M. Sze, "Physics of Semiconductor Devices," 2nd. ed., John Wiley & Sons, New York, 1981.

6) T. A. Fischer, "Heavy-Ion-Induced, Gate-Rupture Burnout in Power MOSFETs," IEEE Trans. Nuc. Sci., NS-34, pp. 1786-1791, 1987.

7) T. F. Wrobel, F. N. Coppage and A. J. Smith, "Current Induced Avalanche in Epitaxial Structures," IEEE Trans. Nuc. Sci., NS-32, pp. 3991-3995, 1985.

8) J. F. Ziegler, J. P. Biersack, and U. Littmark, "The Stopping and Range of Ions in Solids," Vol. 1, Pergamon Press, New York, 1985.

DISTRIBUTION LIST

DNA-TR-UNNUMBERED

DEPARTMENT OF DEFENSE

ASSISTANT TO THE SECRETARY OF DEFENSE
ATOMIC ENERGY
ATTN: EXECUTIVE ASSISTANT

DEFENSE ELECTRONIC SUPPLY CENTER
ATTN: DEFC-EAA

DEFENSE INTELLIGENCE AGENCY
ATTN: DT-1B
ATTN: RTS-2B

DEFENSE LOGISTICS AGENCY
ATTN: DLA-QEL W T HUDDLESON

DEFENSE NUCLEAR AGENCY
ATTN: RAEE (TREE)
4 CYS ATTN: TITL

DEFENSE NUCLEAR AGENCY
ATTN: TDTT W SUMMA

DEFENSE TECHNICAL INFORMATION CENTER
2 CYS ATTN: DTIC/FDAB

DNA PACOM LIAISON OFFICE
ATTN: DNALO

FIELD COMMAND DEFENSE NUCLEAR AGENCY
ATTN: FCPF R ROBINSON

JOINT DATA SYSTEM SUPPORT CTR
ATTN: C-312 R MASON
ATTN: C-330

JOINT STRAT TGT PLANNING STAFF
ATTN: JK (ATTN: DNA REP)
ATTN: JKCS, STUKMILLER
ATTN: JPEM

NATIONAL COMMUNICATIONS SYSTEM
ATTN: NCS-TS

STRATEGIC AND THEATER NUCLEAR FORCES
ATTN: DR E SEVIN

DEPARTMENT OF THE ARMY

HARRY DIAMOND LABORATORIES
ATTN: SLCHD-NW-RP

NUCLEAR EFFECTS DIVISION
ATTN: R WILLIAMS

U S ARMY BALLISTIC RESEARCH LAB
ATTN: SLCBR-VL D RIGOTTI

U S ARMY ELECTRONIC TECH DEV LAB
ATTN: SLCET-SI R. ZETO

U S ARMY GARRISON
ATTN: LIBRARY BLDG 80112

U S ARMY MISSILE COMMAND
ATTN: AMCPM-HA-SE-MS

U S ARMY MISSILE COMMAND/AMSMI-RD-CS-R
ATTN: AMSMI-RD-CS-R

U S ARMY NUCLEAR & CHEMICAL AGENCY
ATTN: MONA-NU

U S ARMY RESEARCH OFFICE
ATTN: R GRIFFITH

U S ARMY STRATEGIC DEFENSE CMD
ATTN: CSSD-H-SAV
ATTN: CSSD-H-YA R K DUDNEY

U S ARMY TEST AND EVALUATION COMD
ATTN: AMSTE-TA-C R K SPARKS

DEPARTMENT OF THE NAVY

NAVAL AIR SYSTEMS COMMAND
ATTN: AIR 931A

NAVAL ELECTRONICS ENGRG ACTVY, PACIFIC
ATTN: CODE 250 D OBRYHIM

NAVAL POSTGRADUATE SCHOOL
ATTN: CODE 1424 LIBRARY

NAVAL RESEARCH LABORATORY
ATTN: CODE 5813 W JENKINS
ATTN: CODE 6816 H HUGHES

NAVAL SURFACE WARFARE CENTER
ATTN: CODE H21 F WARNOCK
ATTN: CODE H23 R SMITH

NAVAL SURFACE WARFARE CENTER
ATTN: CODE H-21

NAVAL TECHNICAL INTELLIGENCE CTR
ATTN: NISC LIBRARY

NAVAL UNDERWATER SYS CENTER
ATTN: 8092

NAVAL WEAPONS CENTER
ATTN: CODE 343

NAVAL WEAPONS EVALUATION FACILITY
ATTN: CLASSIFIED LIBRARY

NAVAL WEAPONS SUPPORT CENTER
ATTN: CODE 6054 D PLATTETER

OFC OF THE DEP ASST SEC OF THE NAVY
ATTN: L J ABELLA

OFC OF THE DEPUTY CHIEF OF NAVAL OPS
ATTN: NOP 985F

SPACE & NAVAL WARFARE SYSTEMS CMD
ATTN: CODE 50451
ATTN: NAVELEX 51024 C WATKINS
ATTN: PME 117-21

DEPARTMENT OF THE AIR FORCE

AERONAUTICAL SYSTEMS DIVISION
ATTN: ASD/ENSS

AIR FORCE CTR FOR STUDIES & ANALYSIS
2 CYS ATTN: AFCSA/SAMI R GRIFFIN

AIR UNIVERSITY LIBRARY
ATTN: AUL-LSE

OGDEN AIR LOGISTICS COMMAND
ATTN: OO-ALC/MMEDD
ATTN: OO-ALC/MMGR

ROME AIR DEVELOPMENT CENTER, AFSC
ATTN: RBR J BRAUER

ROME AIR DEVELOPMENT CENTER, AFSC
ATTN: ESR

SPACE DIVISION/YA
ATTN: YAS

SPACE DIVISION/YAR
ATTN: YAR CAPT STAPANIAN

SPACE DIVISION/YD
ATTN: YD

SPACE DIVISION/YE
ATTN: YE

STRATEGIC AIR COMMAND/XRFS
ATTN: XRFS

WEAPONS LABORATORY
ATTN: NTC M SCHNEIDER
ATTN: NTCAS J FERRY
ATTN: NTCOX W KEMP
ATTN: NTCT MAJ HUNT
ATTN: NTCTD
ATTN: NTCTR R MAIER
ATTN: SUL
ATTN: TAS MAJ SQUILLER

WRIGHT RESEARCH & DEVELOPMENT CENTER
ATTN: AFWAL/ELE
ATTN: AFWAL/MLTE

3416TH TECHNICAL TRAINING SQUADRON (ATC)
ATTN: TTV

DEPARTMENT OF ENERGY

DEPARTMENT OF ENERGY
ATTN: ESHD

LAWRENCE LIVERMORE NATIONAL LAB
ATTN: L-13 D MEEKER
ATTN: L-156 J YEE
ATTN: L-156 R KALIBJIAN
ATTN: L-84 H KRUGER
ATTN: W ORVIS

LOS ALAMOS NATIONAL LABORATORY
ATTN: E LEONARD

SANDIA NATIONAL LABORATORIES
ATTN: ORG 2100
ATTN: ORG 2126 J E GOVER
ATTN: ORG 2146 T A DELLIN
ATTN: T F WROBEL 2126

OTHER GOVERNMENT

CENTRAL INTELLIGENCE AGENCY
ATTN: OSWR/NED
ATTN: OSWR/STD/MTB

DEPARTMENT OF TRANSPORTATION
ATTN: ARD-350

NASA
ATTN: CODE 313 V DANCHENKO
ATTN: CODE 600 E STASSINOPOULOS
ATTN: CODE 660 J TRAINOR
ATTN: CODE 724.1 M JHABVALA

NATIONAL BUREAU OF STANDARDS
ATTN: C WILSON
ATTN: CODE A327 H SCHAFFT
ATTN: CODE A347 J MAYO-WELLS
ATTN: CODE A353 S CHAPPELL
ATTN: CODE C216 J HUMPHREYS
ATTN: P ROITMAN

DEPARTMENT OF DEFENSE CONTRACTORS

AEROJET ELECTRO-SYSTEMS CO
ATTN: D TOOMB

AEROSPACE CORP
ATTN: A AMRAM
ATTN: M HOPKINS
ATTN: N SRAMEK
ATTN: W KOLASINSKI

ALLIED-SIGNAL, INC
ATTN: DOCUMENT CONTROL

AMPEX CORP
ATTN: B RICKARD
ATTN: K WRIGHT

ANALYTIC SERVICES, INC (ANSER)
ATTN: A HERNDON
ATTN: A SHOSTAK

BDM INTERNATIONAL INC
ATTN: C M STICKLEY

BDM INTERNATIONAL INC
ATTN: D WUNSCH

BOEING CO
ATTN: A JOHNSTON
ATTN: D EGELKROUT
ATTN: I ARIMURA

BOOZ-ALLEN & HAMILTON, INC
ATTN: R MCCOSKEY

CALIFORNIA INSTITUTE OF TECHNOLOGY
ATTN: C BARNES

CALSPAN CORP
ATTN: R THOMPSON

CHARLES STARK DRAPER LAB, INC
ATTN: J BOYLE
ATTN: N TIBBETTS
ATTN: P GREIFF
ATTN: W D CALLENDER

CINCINNATI ELECTRONICS CORP
ATTN: L HAMMOND

CLEMSON UNIVERSITY
ATTN: P J MCNULTY

COMPUTER SCIENCES CORP
ATTN: A SCHIFF

DAVID SARNOFF RESEARCH CENTER, INC
ATTN: R SMELTZER

E-SYSTEMS, INC
ATTN: K REIS

E-SYSTEMS, INC
ATTN: DIVISION LIBRARY

EATON CORP
ATTN: R BRYANT

ELECTRONIC INDUSTRIES ASSOCIATION
ATTN: J KINN

FORD AEROSPACE CORPORATION
ATTN: TECHNICAL INFO SERVICES

GENERAL ELECTRIC CO
ATTN: DOCUMENTS LIBRARY
ATTN: TECHNICAL LIBRARY

GENERAL ELECTRIC CO
ATTN: B FLAHERTY
ATTN: G BENDER
ATTN: L HAUGE

GENERAL ELECTRIC CO
ATTN: G GATI

GENERAL ELECTRIC CO
ATTN: D NERAD

GENERAL ELECTRIC CO
ATTN: J MILLER
ATTN: P HEILAND

GENERAL ELECTRIC COMPANY
ATTN: D TOSCA

GENERAL RESEARCH CORP
ATTN: A HUNT

GEORGE WASHINGTON UNIVERSITY
ATTN: A FRIEDMAN

GRUMMAN AEROSPACE CORP
ATTN: J ROGERS

GTE GOVERNMENT SYSTEMS CORPORATION
ATTN: J A WALDRON

H. M. WEIL CONSULTANTS, INC
ATTN: H WEIL

HARRIS CORP
ATTN: J C LEE
ATTN: J W SWONGER

HARRIS CORPORATION
ATTN: E YOST
ATTN: W ABARE

HONEYWELL INC
ATTN: R JULKOWSKI

HONEYWELL, INC
ATTN: MS 725-5
ATTN: MS 830-4A

HONEYWELL, INC
ATTN: R BELT

HUGHES AIRCRAFT CO
ATTN: W SCHENET

HUGHES AIRCRAFT CO
ATTN: J HALL

HUGHES AIRCRAFT COMPANY
ATTN: E KUBO
ATTN: L DARDA

IBM CORP
ATTN: H MATHERS

IBM CORP
ATTN: J ZIEGLER

IBM CORP
ATTN: N HADDAD

IIT RESEARCH INSTITUTE
ATTN: I MINDEL

INSTITUTE FOR DEFENSE ANALYSES
ATTN: TECH INFO SERVICES

IRT CORP
ATTN: MDC

JAYCOR
ATTN: M TREADAWAY
ATTN: R STAHL
ATTN: T FLANAGAN

JAYCOR
ATTN: R SULLIVAN

JAYCOR
ATTN: C ROGERS

JOHNS HOPKINS UNIVERSITY
ATTN: R MAURER

JOHNS HOPKINS UNIVERSITY
ATTN: G MASSON

KAMAN SCIENCES CORP
ATTN: K LEE

KAMAN SCIENCES CORP
ATTN: DIR SCIENCE & TECH DIV
ATTN: J ERSKINE
ATTN: N BEAUCHAMP

KAMAN SCIENCES CORP
ATTN: E CONRAD

KAMAN SCIENCES CORPORATION
ATTN: D PIRIO

KAMAN SCIENCES CORPORATION
ATTN: DASIAC
ATTN: R RUTHERFORD

KAMAN SCIENCES CORPORATION
ATTN: DASIAC

KEARFOTT GUIDANCE AND NAVIGATION CORP
ATTN: J D BRINKMAN
ATTN: R SPIENGEL

LITTON SYSTEMS INC
ATTN: F MOTTER
ATTN: S MACKEY

LOCKHEED MISSILES & SPACE CO, INC
ATTN: F JUNGA
ATTN: REPORTS LIBRARY

LOCKHEED MISSILES & SPACE CO, INC
ATTN: B KIMURA
ATTN: E HESSEE
ATTN: J C LEE
ATTN: J CAYOT
ATTN: L ROSSI
ATTN: P BENE
ATTN: S TAIMUTY

LTV AEROSPACE & DEFENSE COMPANY
2 CYS ATTN: LIBRARY

MAGNAVOX ADVANCED PRODUCTS & SYS CO
ATTN: W HAGEMEIER

MARTIN MARIETTA CORP
ATTN: TIC/MP-30

MARTIN MARIETTA CORP
ATTN: S BUCHNER
ATTN: T DAVIS

MARTIN MARIETTA DENVER AEROSPACE
ATTN: RESEARCH LIBRARY

MARYLAND, UNIVERSITY OF
ATTN: H C LIN

MCDONNELL DOUGLAS CORP
ATTN: A P MUNIE
ATTN: D L DOHM
ATTN: R L KLOSTER

MCDONNELL DOUGLAS CORPORATION
ATTN: P ALBRECHT
ATTN: TECHNICAL LIBRARY

MESSENGER, GEORGE C
ATTN: G MESSENGER

MISSION RESEARCH CORP
ATTN: R PEASE

MISSION RESEARCH CORP
ATTN: J LUBELL
ATTN: R CURRY
ATTN: W WARE

MISSION RESEARCH CORP, SAN DIEGO
ATTN: J RAYMOND

MITRE CORPORATION
ATTN: J R SPURRIER
ATTN: M FITZGERALD

MOTOROLA, INC
ATTN: A CHRISTENSEN

MOTOROLA, INC
ATTN: L CLARK

NATIONAL SEMICONDUCTOR CORP
ATTN: F C JONES

NORDEN SYSTEMS, INC
ATTN: TECHNICAL LIBRARY

NORTHROP CORP
ATTN: A BAHRAMAN

NORTHROP ELECTRONICS SYSTEMS DIVISION
ATTN: E KING

PACIFIC-SIERRA RESEARCH CORP
ATTN: H BRODE

R & D ASSOCIATES
ATTN: D CARLSON

RAND CORP
ATTN: C CRAIN

RAND CORP
ATTN: B BENNETT

RAYTHEON CO
ATTN: H FLESCHER

RCA CORPORATION
ATTN: G BRUCKER

RESEARCH TRIANGLE INSTITUTE
ATTN: M SIMONS

ROCKWELL INTERNATIONAL CORP
ATTN: T YATES

ROCKWELL INTERNATIONAL CORP
ATTN: A BELL
2 CYS ATTN: A E WASKIEWICZ
ATTN: D KONO
ATTN. J BURSON
2 CYS ATTN: J W GRONINGER
ATTN: V DE MARTINO
ATTN: V STRAHAN
ATTN: 031-OA13, YIN-BUTE YU

S-CUBED
ATTN: J KNIGHTEN
ATTN: J M WILKENFELD
ATTN: M ROSE

SCIENCE APPLICATION INTL CORP
ATTN: P ZIELIE

SCIENCE APPLICATIONS INTL CORP
ATTN: D LONG
ATTN: D MILLWARD

SCIENCE APPLICATIONS INTL CORP
ATTN: J RETZLER

SCIENCE APPLICATIONS INTL CORP
ATTN: J SPRATT

SCIENCE APPLICATIONS INTL CORP
ATTN: W CHADSEY

SUNDSTRAND CORP
ATTN: C WHITE

SYSTRON-DONNER CORP
ATTN: J RAY

TELEDYNE BROWN ENGINEERING
ATTN: G R EZELL

TELEDYNE SYSTEMS CO
ATTN: R SUHRKE

TEXAS INSTRUMENTS, INC
ATTN: E JEFFREY
ATTN: F POBLENZ
ATTN: T CHEEK

TRW INC
ATTN: TECH INFO CTR

TRW SPACE & DEFENSE SYSTEMS
ATTN: D M LAYTON

TRW SPACE & DEFENSE, DEFENSE SYSTEMS
ATTN: C BLASNEK
ATTN: J GORMAN

UNISYS CORPORATION-DEFENSE SYSTEMS
ATTN: P MARROFFINO

VISIDYNE, INC
ATTN: C H HUMPHREY
ATTN: W P REIDY

WESTINGHOUSE ELECTRIC CORP
ATTN: S WOOD

FOREIGN

FOA 2
ATTN: B SJOHOLM

FOA 3
ATTN: T KARLSSON